

Option Pricing with Time-Varying Volatility Risk Aversion*

Peter Reinhard Hansen^a and Chen Tong^{b,c†}

^a*University of North Carolina & Copenhagen Business School*

^b*Department of Finance, School of Economics, Xiamen University*

^c*Wang Yanan Institute for Studies in Economics, Xiamen University*

March 11, 2025

Abstract

We introduce a pricing kernel with time-varying volatility risk aversion to explain observed time variations in the shape of the pricing kernel. When combined with the Heston-Nandi GARCH model, this framework yields a tractable option pricing model in which the variance risk ratio (VRR) emerges as a key variable. We show that the VRR is closely linked to economic fundamentals, as well as sentiment and uncertainty measures. A novel approximation method provides analytical option pricing formulas, and we demonstrate substantial reductions in pricing errors through an empirical application to the S&P 500 index, the CBOE VIX, and option prices.

*We are grateful to Szabolcs Blazsek, Stefano Giglio, Jens Jackwerth, Tobias Sichert, two anonymous reviewers, and conference participants at the SoFiE 2022 conference for valuable comments.

†Chen Tong acknowledges financial support from the National Natural Science Foundation of China (72301227) and the Ministry of Education of China, Humanities and Social Sciences Youth Fund (22YJC790117).

Introduction

The pricing kernel, which represents the ratio of risk-neutral to physical state probabilities, is a fundamental concept in economics with roots in Arrow-Debreu securities, see [Arrow and Debreu \(1954\)](#). A cornerstone of asset pricing theory, the [Lucas \(1978\)](#) tree model, implies a monotonically decreasing pricing kernel with respect to aggregate wealth, see [Hansen and Renault \(2010\)](#). However, empirical studies consistently find the pricing kernel to be non-monotonic and time-varying, giving rise to the so-called pricing kernel puzzles, see e.g. [Aït-Sahalia and Lo \(2000\)](#), [Jackwerth \(2000\)](#), and [Rosenberg and Engle \(2002\)](#).

In this paper, we propose a pricing kernel with time-varying volatility risk aversion to resolve these pricing kernel puzzles. Building on [Heston and Nandi \(2000\)](#) and [Christoffersen et al. \(2013\)](#), we develop a novel framework for derivatives pricing, in which the *variance risk ratio* (VRR) emerges as the key quantity. The VRR, defined as the ratio of risk-neutral to physical conditional variance, characterizes both the shape and time variation of the pricing kernel and it is closely related to the variance risk premium by [Carr and Wu \(2008\)](#). The dynamic pricing kernel introduces challenges for closed-form option pricing formulas, which we address through a novel analytical approximation method applicable to non-affine models. Our empirical implementation of the dynamic structure for VRR is based on the score-driven framework of [Creal et al. \(2013\)](#), which intuitively updates time-varying quantities in response to first-order conditions. In an empirical application to the S&P 500 index, the CBOE VIX, and option prices, we show that the new model substantially reduces pricing errors, both in-sample and out-of-sample.

The discrete-time Heston-Nandi GARCH (HNG) model, developed by [Heston and Nandi \(2000\)](#), conveniently yields closed-form expressions for option prices while allowing for time-varying volatility. However, it implies a monotonic pricing kernel. [Christoffersen et al. \(2013\)](#) extended the HNG model by introducing a variance-dependent pricing kernel, resulting in a non-monotonic shape. Their model remains tractable, retains closed-form option pricing expressions, and has become a benchmark in the option pricing literature. The shape of the pricing kernel in their framework is governed by the variance risk premium (VRP), where a negative VRP leads to a U-shaped pricing kernel, a pattern confirmed in their empirical

analysis, see also [Cuesdeanu and Jackwerth \(2018\)](#).

While [Christoffersen et al. \(2013\)](#) explain non-monotonicity, their framework cannot account for the time variation observed in the pricing kernel. When estimated over long sample periods, the pricing kernel is typically U-shaped, yet the shape differs distinctly in certain periods, such as the years leading up to the global financial crisis. The shape of the pricing kernel can be expressed in terms of the probability weighting function. If individuals overweight low-probability events and underweight high-probability events, the probability weighting function will have an inverse S-shape, which corresponds to a U-shaped pricing kernel. [Polkovnichenko and Zhao \(2013\)](#) estimated the probability weighting function non-parametrically and found it to be time-varying. Their estimate has an inverse S-shape during most of their sample periods but a regular S-shape during the years 2004–2006. Similar results were obtained by [Chabi-Yo and Song \(2013\)](#), and an inverted U-shape was also documented with DAX 30 options during the same years, 2004–2006, as reported by [Grith et al. \(2017\)](#). Further evidence comes from [Kiesel and Rahe \(2017\)](#) and [Beare and Schmidt \(2016\)](#). Interestingly, [Christoffersen et al. \(2013, figure 3\)](#) also contains evidence of time variations in empirical pricing kernels. For most calendar years, their estimated empirical pricing kernel is U-shaped; however, in some calendar years, it takes an inverted U-shape.¹

The derivative pricing model proposed in this paper combines a pricing kernel with time-varying volatility risk aversion and the GARCH model of [Heston and Nandi \(2000\)](#). The VRR, defined as the ratio of risk-neutral to physical conditional variance, $\eta_t = h_{t+1}^*/h_{t+1}$, governs the time variation in the pricing kernel and is functionally linked to the volatility risk aversion parameter, which captures the curvature of the pricing kernel. We demonstrate that this structure can generate the observed time variation in the empirical pricing kernel, including its different shapes. Our new model nests [Christoffersen et al. \(2013\)](#) as the special case where η_t is constant, which we denote as CHNG. The HNG option pricing model of [Heston and Nandi \(2000\)](#) is also nested by imposing $\eta_t = 1$. We refer to our new model as DHNG model, where “D” stands for dynamic, and highlight its key properties below.

We derive a closed-form CBOE VIX pricing formula for the DHNG model and develop an

¹The authors do not comment on this observation, but they estimate a more flexible structure, which is not based on a pricing kernel with a fixed shape, see [Christoffersen et al. \(2013, figure 6\)](#).

analytical option pricing formula, which constitutes a separate and important methodological contribution. When volatility risk aversion follows a stochastic process, the conditional moment-generating function (MGF) of future cumulative returns does not have an affine form, making it very challenging to derive option prices. However, we introduce a novel approximation method that is applicable to non-affine models. This approach constructs an auxiliary MGF for a simplified, related problem and then applies a Taylor expansion to obtain an analytical option pricing formula. The approximation method is shown to be highly accurate in an empirically relevant simulation design.

To implement the theoretical framework, we connect the model for η_t with observed data using an observation-driven approach, which is a natural choice since the GARCH model under the physical measure also follows an observation-driven formulation. Specifically, we propose a score-driven model following [Creal et al. \(2013\)](#), where the first-order conditions of the log-likelihood function define the innovations in the dynamic model for η_t . This design is intuitive because η_t is updated to minimize pricing errors. Conveniently, this structure also enhances robustness to model misspecification. Another advantage of the observation-driven model is its simplicity in estimation, which is particularly useful in applications involving long sample periods and large panels of option prices.

An empirical application using 32 years of daily S&P 500 returns, the CBOE VIX, and a large panel of option prices provides strong support for the model. The estimation incorporates information from both the physical and risk-neutral measures, as advocated by [Chernov and Ghysels \(2000\)](#). The results show that the pricing kernel with time-varying volatility risk aversion typically reduces pricing errors by 50% or more, as measured by the root mean square error. This reduction is achieved for both VIX and option prices, in both in-sample and out-of-sample comparisons. The estimated time variation in the shape of the pricing kernel aligns with previous studies, generally exhibiting a U-shape, but taking on an inverted U-shape during certain periods, including 2004–2007 and around 1993 and 2017.

Finally, having established the VRR as a fundamental quantity, it is natural to investigate its connection to key asset pricing variables, including those linked to pricing kernel puzzles. Theoretical and empirical studies suggest that heterogeneous beliefs and disagreements about the physical distribution can contribute to a U-shaped pricing kernel, see e.g. [Shefrin \(2001\)](#),

2008), [Bakshi and Madan \(2008\)](#), [Bakshi et al. \(2010\)](#). Similar arguments have been made about sentiment and uncertainty among investors, see e.g. [Han \(2008\)](#), [Polkovnichenko and Zhao \(2013\)](#), [Baker et al. \(2016\)](#), and [Bollerslev et al. \(2018\)](#). [Bali and Zhou \(2016\)](#) argue that market uncertainty can be approximated by the variance risk premium, see [Carr and Wu \(2008\)](#). The VRR is obviously related to the variance risk premium, which has been shown to predict stock returns, see [Bollerslev et al. \(2009\)](#). A straightforward explanation is that preferences are state-dependent, with market uncertainty being a possible state variable, see e.g. [Grith et al. \(2017\)](#). We connect our results to these studies by showing that the monthly average VRR is closely related to commonly used measures of sentiment, uncertainty, and disagreement, as well as other key economic indicators.

Our paper is related to and builds on a large body of literature, including studies that have sought to address pricing kernel puzzles by augmenting existing models with additional state variables, see e.g. [Chabi-Yo et al. \(2008\)](#), [Chabi-Yo \(2012\)](#), [Brown and Jackwerth \(2012\)](#) and [Song and Xiu \(2016\)](#). In our framework, the quantity VRR can be viewed as an additional state variable that emerges naturally from the model structure.

Our work is also related to [Barone-Adesi et al. \(2008\)](#), who estimated a GJR-GARCH model for returns under the physical measure. They did not specify a pricing kernel but simply assumed that the model under the risk-neutral measure is also a GJR-GARCH model, with time-varying parameters calibrated to minimize option pricing errors. While we also seek to minimize pricing errors, our approach is fundamentally different. Our starting point is a pricing kernel and a model for the physical probability measure, \mathbb{P} , and the two imply the model under the risk-neutral probability measure, \mathbb{Q} . An empirical comparison in [Christoffersen et al. \(2013\)](#) explores the same idea as in [Barone-Adesi et al. \(2008\)](#), as they estimate separate HNG models under both \mathbb{P} and \mathbb{Q} measures. They referred to this structure as an *ad-hoc model*, because it is not derived from their pricing kernel. However, we show that the pricing kernel with a time-varying VRR is incoherent with HNG models (with constant parameters) under both \mathbb{P} and \mathbb{Q} measures.

Additionally, our paper contributes to the literature on time-varying risk aversion, which relates to the local shape of the pricing kernel. A seminal paper by [Campbell and Cochrane \(1999\)](#) addresses this concept, while [Li \(2007\)](#) demonstrated how time-varying risk aversion

links to a time-varying risk premium. Moreover, [González et al. \(2018\)](#) identified risk aversion dynamics as a key determinant of stock market betas. More recently, [Bekaert et al. \(2020\)](#) introduced a no-arbitrage asset pricing model with time-varying risk aversion for pricing equities and corporate bonds, where risk aversion is driven by uncertainty shocks.

The rest of the paper is organized as follows. We present the theoretical model in Section 1 and derive closed-form pricing formula for the VIX and an option pricing formula, based on the new approximation method in Section 2. Section 3 introduces a dynamic model for the variance risk ratio using a score-driven approach. An empirical application with 32 years of S&P 500 returns, VIX, and option prices is presented in Section 4. We show that the variance risk ratio relates to well-known measures of sentiment, disagreement, and uncertainty in Section 5. A summary is presented in Section 6. All proofs are provided in the Appendix A and supplementary empirical results can be found in the Online Appendix.

1 The Model

This section introduces the new model with dynamic variance risk aversion (DHNG), building on the models by [Heston and Nandi \(2000\)](#) (HNG) and [Christoffersen et al. \(2013\)](#) (CHNG).

The observed variables include the daily returns, $R_t \equiv \log(S_t/S_{t-1})$, where S_t is the underlying asset price, and a vector of derivative prices, X_t . We will work with two filtrations, $\mathcal{F}_t = \sigma(\{R_j, X_j\}, j \leq t)$ and $\mathcal{G}_t = \sigma(\{R_j, X_{j-1}\}, j \leq t)$, where the latter arises naturally from a factorization of the joint likelihood function. Clearly, $\mathcal{F}_{t-1} \subset \mathcal{G}_t \subset \mathcal{F}_t$ for all t . Throughout this paper, we will use the notation $\mathbb{E}_t^{\mathbb{P}}(\cdot) \equiv \mathbb{E}^{\mathbb{P}}(\cdot|\mathcal{G}_t)$ and $\mathbb{E}_t^{\mathbb{Q}}(\cdot) \equiv \mathbb{E}_t^{\mathbb{Q}}(\cdot|\mathcal{G}_t)$ to denote the conditional expectations with respect to \mathcal{G}_t under \mathbb{P} and \mathbb{Q} measures, respectively.

We model returns in physical measure \mathbb{P} using the classical Heston-Nandi GARCH model (HNG), which has a convenient structure for derivatives pricing. This model is given by

$$R_{t+1} = r + (\lambda - \frac{1}{2})h_{t+1} + \sqrt{h_{t+1}}z_{t+1}, \quad (1)$$

$$h_{t+1} = \omega + \beta h_t + \alpha(z_t - \gamma\sqrt{h_t})^2, \quad (2)$$

where the return shock, z_{t+1} , is independent and identically distributed (iid) with a standard normal distribution, $N(0, 1)$; r is the risk-free rate; λ is the equity risk premium because the

expected return is given by $\mathbb{E}^{\mathbb{P}}(\exp(R_{t+1})|\mathcal{F}_t) = \exp(r + \lambda h_{t+1})$; and $h_{t+1} = \text{var}^{\mathbb{P}}(R_{t+1}|\mathcal{F}_t)$ is the daily conditional variance, see [Heston and Nandi \(2000\)](#). The HNG model captures time variation in the conditional variance, as is the case for ARCH and GARCH models, see [Engle \(1982\)](#) and [Bollerslev \(1986\)](#). However, the HNG model also allows for dependence between returns and volatility (leverage). It is straightforward to verify that $\text{cov}^{\mathbb{P}}(R_t, h_{t+1}|\mathcal{F}_{t-1}) = -2\gamma\alpha h_t$, which shows that the magnitude of the leverage effect is defined by γ . A leverage effect is required to generate the empirically important volatility smirk in option prices. The dynamic structure of the HNG model is carefully crafted to yield a closed-form solution for option valuation, and [Heston and Nandi \(2000\)](#) showed that the continuous limit of the HNG model (as the time interval between observations shrinks to zero) yields a variance process, h_t , that converges weakly to a continuous-time square-root variance process, see [Feller \(1951\)](#), [Cox et al. \(1985\)](#), and [Heston \(1993\)](#).

Option pricing with GARCH models can be achieved with a simple risk-neutralization by [Duan \(1995\)](#), known as the *locally risk-neutral valuation relationship* (LRNVR). This approach is equivalent to imposing a pricing kernel with a single risk premium for equity risk, see [Huang et al. \(2017\)](#). However, the LRNVR-based pricing kernel is inadequate for explaining many discrepancies between \mathbb{P} and \mathbb{Q} , including the variance risk premium, see [Hao and Zhang \(2013\)](#) and [Christoffersen et al. \(2013\)](#). We will review their model next and then proceed to introduce the new model with time-varying volatility risk aversion.

1.1 Pricing Kernel with Constant Parameters (CHNG)

The model in [Christoffersen et al. \(2013\)](#) (CHNG) generalizes the HNG model by [Heston and Nandi \(2000\)](#), to have a variance-dependent pricing kernel, which is given by,

$$\frac{M_{t+1}}{M_t} = \left(\frac{S_{t+1}}{S_t}\right)^\phi \exp[\delta + \pi h_{t+1} + \xi(h_{t+2} - h_{t+1})],$$

and [Corsi et al. \(2013\)](#) showed that it can be conveniently expressed as

$$M_{t+1,t} \equiv \frac{M_{t+1}}{\mathbb{E}^{\mathbb{P}}[M_{t+1}|\mathcal{F}_t^R]} = \frac{\exp(\phi R_{t+1} + \xi h_{t+2})}{\mathbb{E}^{\mathbb{P}}[\exp(\phi R_{t+1} + \xi h_{t+2})|\mathcal{F}_t^R]},$$

where $\mathcal{F}_t^R = \sigma(\{R_j\}, j \leq t)$ is the natural filtration for returns only. The pricing kernel above depends on both equity risk and variance risk, where the latter is typically characterized by

the parameter ξ . The equity risk is governed by ϕ , as well as ξ , because h_{t+2} depends on return R_{t+1} . This pricing kernel implies the following risk-neutral dynamics:

$$\begin{aligned} R_{t+1} &= r - \frac{1}{2}h_{t+1}^* + \sqrt{h_{t+1}^*}z_{t+1}^* \\ h_{t+1}^* &= \omega^* + \beta^*h_t^* + \alpha^*(z_t^* - \gamma^*\sqrt{h_t^*})^2, \end{aligned}$$

with $z_{t+1}^*|\mathcal{F}_t^R \stackrel{\mathbb{Q}}{\sim} iid N(0,1)$ and the following relations between \mathbb{P} and \mathbb{Q} parameters:

$$h_t^* = h_t\eta, \quad \omega^* = \omega\eta, \quad \beta^* = \beta, \quad \alpha^* = \alpha\eta^2, \quad \gamma^* = \frac{1}{\eta}(\gamma + \lambda - \frac{1}{2}) + \frac{1}{2}, \quad \eta \equiv (1 - 2\alpha\xi)^{-1}.$$

The logarithm of the pricing kernel is a quadratic function of the daily market return,

$$\log \frac{M_t}{M_{t-1}} = -\lambda(R_t - r) + \xi\alpha \frac{(R_t - r)^2}{h_t} + \kappa_0 + \kappa_1 h_t, \quad (3)$$

where $\kappa_0 = -\frac{1}{2}\log \eta$ and $\kappa_1 = \frac{1}{2}(\lambda - \frac{1}{2})^2 - \frac{1}{8}\eta$.² Expression (3) shows that λ and ξ define the linear and quadratic terms, respectively, with positive ξ leading to a U-shaped and negative ξ to an inverted U-shaped pricing kernel. Empirically, this relationship tends to be generally U-shaped, but it is unstable over time as seen in [Christoffersen et al. \(2013, figure 3\)](#). Figure 1 includes parts of figures 3 and 5 in [Christoffersen et al. \(2013\)](#); the four left panels are based on model-free market prices and the corresponding four right panels are based on model prices using their estimated CHNG model. There are periods where the relationship has an inverted U-shape, such as the years 2004–2007 (of which 2005 and 2006 are shown in Figure 1), which is incompatible with a static quadratic coefficient ξ .

These observations, and the fact that ξ defines the shape of the relationship between $\log M_t/M_{t-1}$ and returns, motivate us to develop a new model where ξ can be time-varying. This parameter, ξ , is directly tied to volatility risk aversion, as it is the coefficient to the state variable, h_{t+2} , in the pricing kernel. Moreover, ξ is also negatively related to the VRP, because $h_t - h_t^* = -\xi \times \frac{2\alpha h_t}{1-2\alpha\xi} \approx -\xi \times 2\alpha h_t$, where $2\alpha h_t > 0$.

²The expressions for κ_0 and κ_1 in [Christoffersen et al. \(2013\)](#) are $\kappa_0 = \delta + \xi\omega + \phi r$ and $\kappa_1 = \pi + \xi(\beta - 1 + \alpha(\lambda - \frac{1}{2} + \gamma)^2)$. It follows from our results in Lemma 1 that they are equivalent to those presented here.

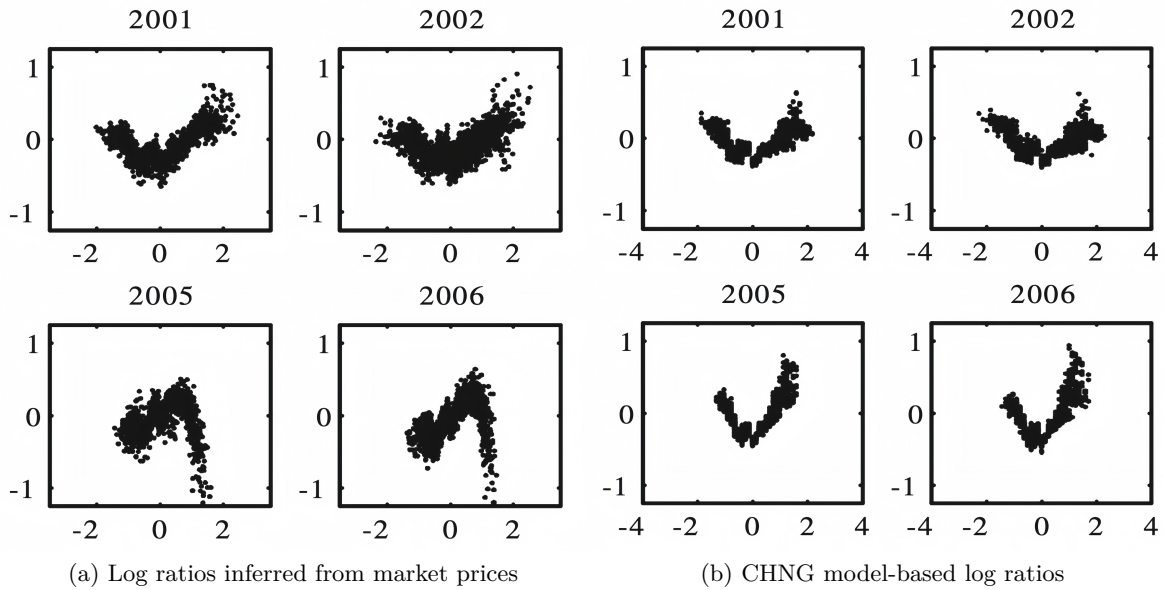


Figure 1: Log ratios of risk-neutral one-month densities and physical one-month histogram against log returns in monthly standard deviations. Panels (a) and (b) are subsets of figures 3 and 5, respectively, in [Christoffersen et al. \(2013\)](#). The former is based on empirical market prices and the latter has the corresponding CHNG model-based log ratios.

Alt text: The shape of the pricing kernel based on market prices and the CHNG model for four calendar years. The figure plots log ratios of risk-neutral to physical one-month densities against log returns. The shapes for 2001 and 2002 are similar, while those for 2005 and 2006 are distinctively different.

1.2 Dynamic Pricing Kernel by Means of Variance Risk Aversion

We seek a more flexible pricing kernel that is coherent with the observed variation over time. Next, we introduce a new dynamic pricing kernel while maintaining the Heston-Nandi GARCH structure (1)-(2) under physical measure, \mathbb{P} .

Assumption 1. Returns are given by the Heston-Nandi GARCH model, (1)-(2), under \mathbb{P} .

Assumption 2. The pricing kernel takes the following form:

$$M_{t+1,t} = \frac{\exp(\phi_t R_{t+1} + \xi_t h_{t+2})}{\mathbb{E}_t^{\mathbb{P}}[\exp(\phi_t R_{t+1} + \xi_t h_{t+2})]}, \quad (4)$$

where ϕ_t and ξ_t are \mathcal{G}_t -measurable.

Assumptions 1 and 2 induce the following dynamic properties under risk-neutral measure.

Theorem 1. Suppose Assumptions 1 and 2 hold and define $\eta_t \equiv (1 - 2\alpha\xi_t)^{-1}$.

(i) The risk aversion parameters satisfy

$$\xi_t = \frac{1}{2\alpha} \frac{\eta_t - 1}{\eta_t}, \quad \phi_t = \frac{\eta_t - 1}{\eta_t} (\gamma - \frac{1}{2}) - \frac{1}{\eta_t} \lambda,$$

such that their dynamic properties are defined by that of η_t .

(ii) The return dynamics under the risk-neutral measure \mathbb{Q} are given by:

$$\begin{aligned} R_{t+1} &= r - \frac{1}{2} h_{t+1}^* + \sqrt{h_{t+1}^*} z_{t+1}^*, \\ h_{t+1}^* &= \omega_t^* + \beta_t^* h_t^* + \alpha_t^* \left(z_t^* - \gamma_{t-1}^* \sqrt{h_t^*} \right)^2, \end{aligned}$$

where $z_{t+1}^* | \mathcal{G}_t \stackrel{\mathbb{Q}}{\sim} \text{iid } N(0, 1)$ and the following relations between \mathbb{P} and \mathbb{Q} parameters:

$$\omega_t^* = \omega \eta_t, \quad \beta_t^* = \beta \frac{\eta_t}{\eta_{t-1}}, \quad \alpha_t^* = \alpha \eta_t \eta_{t-1}, \quad \gamma_t^* = \frac{1}{\eta_t} (\gamma + \lambda - \frac{1}{2}) + \frac{1}{2}.$$

(iii) The dynamic parameter, η_t , equals the ratio of the conditional variances under \mathbb{Q} and \mathbb{P} ,

$$\eta_t = \frac{h_{t+1}^*}{h_{t+1}}.$$

Theorem 1 reveals the following six interesting properties of the risk-neutral probability measure and its dynamics.

First, $\eta_t = h_{t+1}^*/h_{t+1}$ emerges as a fundamental quantity³, which is termed the *variance risk ratio*. It is \mathcal{G}_t -measurable since η_t is a function of $\xi_t \in \mathcal{G}_t$ defined in Assumption 2. This variable appears in all expressions relating \mathbb{P} and \mathbb{Q} , and it has a straightforward interpretation. Its functional relationship with ξ_t shows that η_t is an indirect measure of volatility risk aversion. When η_t is large, agents demand a large compensation for taking on variance risk, while a small value of η_t corresponds to an appetite for variance risk. Moreover, η_t is obviously related to the VRP, where the latter concerns the expectation of future values of $h_{t+1} - h_{t+1}^*$. This follows from $h_{t+1} - h_{t+1}^* = (1 - \eta_t)h_{t+1}$. This relation could be used to construct a model-based measure of the VRP. Note that the VRP can be positive in the most general version of the model. A negative VRP can be guaranteed in the model design by restricting η_t to be greater than one.⁴ For comparison, the ratio, h_t^*/h_t , is constant in CHNG model, and the relation $h_t - h_t^* = (1 - \eta)h_t$ shows that CHNG model implicitly restricts the VRP to be proportional to the conditional variance under \mathbb{P} .

Second, the shape of the pricing kernel is time-varying, as shown by the following results.

Lemma 1 (Shape of Pricing Kernel). *The following expression*

$$\log M_{t+1,t} = -\lambda R_{t+1} + \xi_t \alpha \frac{(R_{t+1} - r)^2}{h_{t+1}} + \kappa_{0,t} + \kappa_{1,t} h_{t+1},$$

is equivalent to (4), where $\kappa_{0,t} = -\frac{1}{2} \log \eta_t$, and $\kappa_{1,t} = \frac{1}{2}(\lambda - \frac{1}{2})^2 - \frac{1}{8}\eta_t$.

The expression in Lemma 1 is the generalization of (3) to the case with time-varying preference parameter, ϕ_t and ξ_t . The quadratic coefficient can be time-varying, because it depends on ξ_t , which makes it clear that ξ_t influences the shape of the pricing kernels. Or, equivalently, η_t governs the shape. We have a U-shape if $\xi_t > 0$ ($\Leftrightarrow \eta_t > 1$) and an inverted U-shape if $\xi_t < 0$ ($\Leftrightarrow \eta_t < 1$).⁵ Thus, this framework can generate a variety of shapes of the pricing kernel. This is illustrated in the upper left panel of Figure 2, where the pricing kernel for cumulated returns over one month is presented for two levels of η . The design is based on the empirical estimates of the model in Section 4, where $\eta_{\text{low}} = 0.70$ and $\eta_{\text{high}} = 1.70$ correspond to the 10% and 90% quantiles of the unconditional distribution of η_t , respectively. The low value of η

³Parameterize the model with the inverse ratio, $\theta_t = h_{t+1}/h_{t+1}^*$, simplifies several expressions, such as $\xi_t = \frac{1}{2\alpha}(1 - \theta_t)$ and $\phi_t = (1 - \theta_t)(\gamma - \frac{1}{2}) - \theta_t\lambda$. We adopt η_t , because it is more common in the literature.

⁴This can be achieved by specifying a dynamic model for $\log(\eta_t - 1)$. We do not impose this restriction in our analysis, as we specify a model for $\log \eta_t$.

⁵We have $\alpha > 0$ in the Heston-Nandi GARCH model.

produce an inverted U-shape similar to that observed during the years 2004 to 2007, whereas the high value of η results in a shape with a pronounced U-shape.

Third, the equity risk premium, λ , is constant, despite ϕ_t and ξ_t being time-varying. This is an implication of the no-arbitrage condition, that ties the linear coefficient to λ , which is determined under the physical measure in the Heston-Nandi GARCH model.

Fourth, an important reason for permitting η_t to be time-varying is that it enables h_t^* to incorporate information from derivative prices. In conventional GARCH models, the conditional variance depends only on lagged returns, such that $h_{t+1} \in \mathcal{F}_t^R$. A restrictive implication of a constant VRR is that it requires the two conditional variances to be proportional to each other. Consequently, h_{t+1}^* is driven solely by lagged returns, leaving no room for derivative prices to influence its dynamic properties. Allowing η to be time-varying eliminates this rigidity and enables the model to incorporate information from derivative prices into the dynamic model of h_{t+1}^* . We take advantage of this feature in our empirical implementation.

Fifth, the structure in Theorem 1 nests the CHNG model of Christoffersen et al. (2013) and the HNG model, which corresponds to $\eta_t = \eta$ and $\eta_t = 1$, respectively. If h_t is constant and $\eta_t = 1$, then it leads to the pricing kernel given by the power utility function, see Rubinstein (1976). So the famous Black-Scholes model is also nested as the special case. Interestingly, when η_t is time-varying, there is time variation in the risk aversion parameters, which is similar to the habit formation models, see Campbell and Cochrane (1999).

Sixth, the structure introduced in Theorem 1 generates time-varying leverage under \mathbb{Q} , which manifests itself in a number of ways. A time-varying leverage effect will impact the distribution of cumulative returns, and the lower panels of Figure 2 show the skewness and kurtosis of cumulative returns under \mathbb{Q} as a function of the number of days that returns are cumulated over (the x -axis). Skewness and kurtosis are shown for the two levels of the VRR, η_{low} and η_{high} , and these result in distinctively different levels of skewness and kurtosis under \mathbb{Q} . Both skewness and kurtosis are far more pronounced for the large value of η . Another way to illustrate the leverage effect is with the news impact curve by Engle and Ng (1993). The news impact curve under \mathbb{Q} is defined by $\text{NIC}(z^*) = \mathbb{E}_t^{\mathbb{Q}}(h_{t+1}^* | z_t^* = z^*) - \mathbb{E}_t^{\mathbb{Q}}(h_{t+1}^* | z_t^* = 0)$, and from Theorem 1 it follows that $\text{NIC}(z^*) = \alpha\eta_t\eta_{t-1}z^{*2} - 2\alpha\gamma\eta_t\sqrt{h_t^*}z^*$, whose shape depends on the VRR. The upper right panel of Figure 2 presents the news impact curve, with h_t^* equal

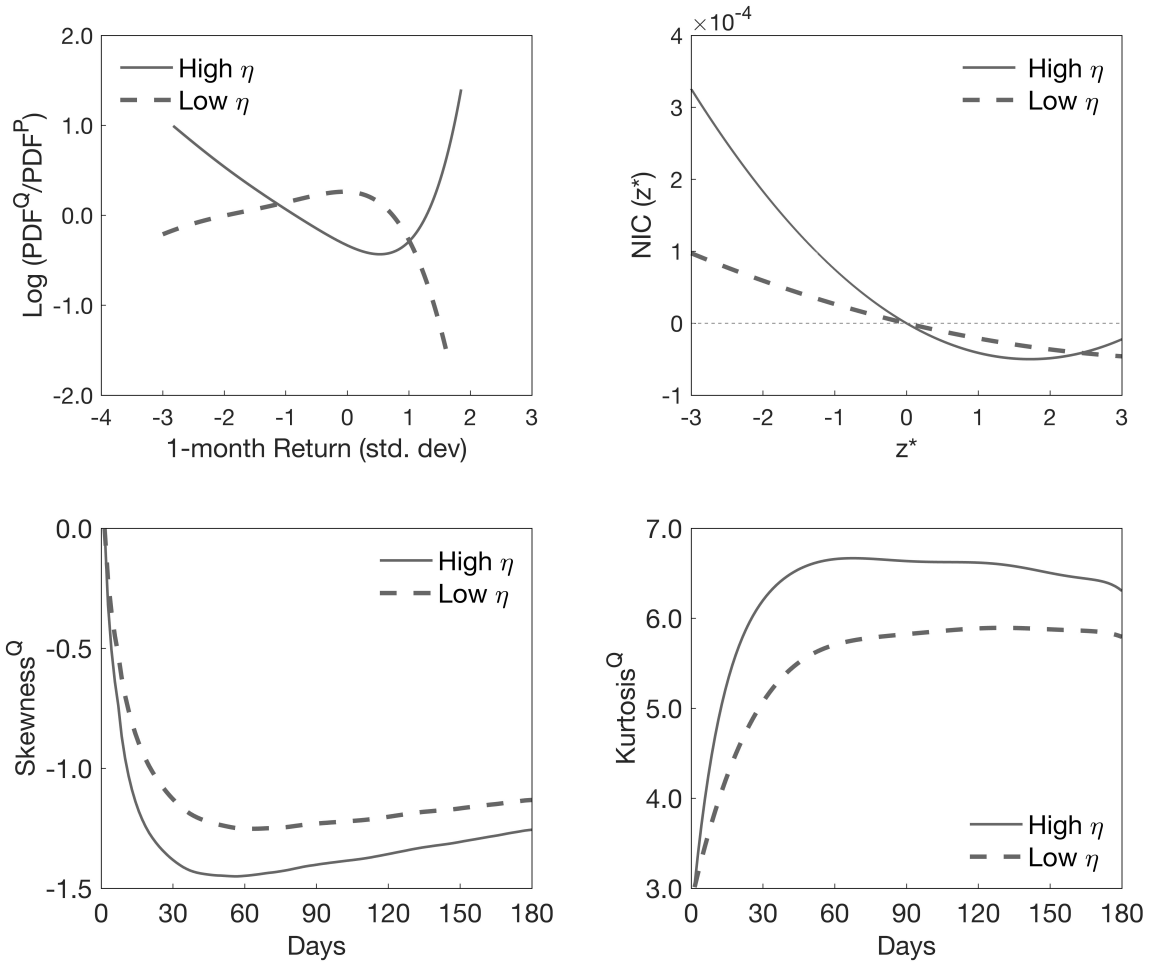


Figure 2: Properties of cumulative returns for two levels of variance risk ratio, $\eta_{\text{low}} = 0.70$ (dashed lines) and $\eta_{\text{high}} = 1.70$ (solid lines). The upper left panel presents the log-ratios of the \mathbb{Q} -to- \mathbb{P} densities for cumulative returns over one month, the corresponding news impact curves under \mathbb{Q} are shown in the upper right panel, and skewness and kurtosis of multi-period cumulative returns under the risk-neutral measure \mathbb{Q} are shown in the two lower panels. These results are based on 1 million simulations using a design based on our model estimates (last column in Table 3), where $\eta_{\text{low}} = 0.70$ and $\eta_{\text{high}} = 1.70$ correspond to the 10% and 90% quantiles of the unconditional distribution of η_t , respectively.

Alt text: Properties of cumulative returns for two levels of the variance risk ratio: low and high. The figure consists of four panels displaying (1) the log-ratio of risk-neutral to physical densities, (2) news impact curves, (3) skewness under the risk-neutral measure, and (4) kurtosis under the risk-neutral measure.

to its unconditional mean under \mathbb{Q} , as estimated in Section 4, and with $\eta = \eta_t = \eta_{t-1}$ equal to either η_{low} (dashed line) or η_{high} (solid line). We observe the asymmetric shape of the news impact curve, see e.g. [Chen and Ghysels \(2011\)](#). However, the level of asymmetry depends on the level of η , such that volatility is more responsive to negative return shocks when η is large, than when η is small.

2 Derivatives Pricing with Dynamic Volatility Risk Aversion

In this section, we consider cases where η_t is time-varying and stochastic. We derive a closed-form expression for the VIX under the assumption that $\log \eta_t$ follows an autoregressive moving average process, ARMA(p, q). We also obtain analytical expressions for option prices under the same assumptions. The option pricing formula is obtained with a novel approximation method based on a Taylor expansion of the MGF for cumulative returns.

2.1 VIX Pricing

It is relatively straightforward to obtain closed-form expressions for VIX pricing, once the dynamic properties of η_t under \mathbb{Q} are known. This only requires expressions for $\mathbb{E}_t^{\mathbb{Q}}(h_{t+k}^*)$, $k = 1, \dots, M$, because the risk-neutral dynamics of returns under Theorem 1 implies the following M -period ahead VIX pricing formula

$$\text{VIX}_t = A \times \sqrt{\frac{1}{M} \sum_{k=1}^M \mathbb{E}_t^{\mathbb{Q}}(h_{t+k}^*)}, \quad (5)$$

where $A = 100\sqrt{252}$ is the annualizing factor.

Assumption 3. *Suppose that the logarithm of variance risk ratio, $\log \eta_t$, follows an autoregressive moving average process of orders (p, q) ,*

$$\varphi(L)(\log \eta_t - \zeta) = \theta(L)\varepsilon_t, \quad (6)$$

where $\varphi(x) = 0 \Rightarrow |x| > 1$, $\theta(x)$ and $\varphi(x)$ have no common roots. The innovation ε_t is \mathcal{G}_t -measurable, and $\varepsilon_{t+1}|\mathcal{G}_t$ follows an iid distribution with $\mathbb{E}_t^{\mathbb{Q}}(\varepsilon_{t+1}) = 0$, $\text{var}_t^{\mathbb{Q}}(\varepsilon_{t+1}) = \sigma^2$, and a MGF satisfying $\text{mgf}_\varepsilon(s) \equiv \mathbb{E}_t^{\mathbb{Q}}[\exp(s\varepsilon_{t+1})] < \infty$ a.s. for $s \in \mathbb{R}$. Additionally, ε_t is independent of the return shock z_τ for all τ .

Assumption 3 is explicit about the first two conditional moments of ε_t , but does not impose restrictive distributional assumptions. However, the exact distribution is important for VIX and option prices, as these depend on $\text{mgf}_\varepsilon(s)$. That ε_t is \mathcal{G}_t -measurable follows from Assumption 2 and therefore not a new assumption.

Theorem 2 (VIX pricing). *Suppose that Assumptions 1-3 hold, then the analytical expression for M -period ahead VIX in (5) is given by*

$$\text{VIX}(M, \sigma^2, h_{t+1}^*) = \sqrt{a_1(M, \sigma^2) + a_2(M, \sigma^2)h_{t+1}^*}, \quad (7)$$

where $a_1(M, \sigma^2)$ and $a_2(M, \sigma^2)$ both depend on $(\eta_t, \dots, \eta_{t-p+1})$, $(\varepsilon_t, \dots, \varepsilon_{t-q+1})$, and $\text{mgf}_\varepsilon(s)$. See Appendix A.3 for their exact expressions.⁶

2.2 Option Pricing: A Novel Analytical Approximation

In this section, we derive the European option pricing formula for the case where the variance risk aversion is time-varying.

The European call option price at time t is given by the conditional risk-neutral expectation $C_t = e^{-r(T-t)}\mathbb{E}_t^{\mathbb{Q}}[\max(S_T - K, 0)]$, where T is the maturity date, K is the strike price, and S_T is the terminal price of underlying asset. Let $M = T - t$ be the number of periods to maturity, it is well-known that an affine structure of the MGF of future cumulative returns,

$$g_{t,M}(s) = \mathbb{E}_t^{\mathbb{Q}} \left[\exp \left(s \sum_{i=1}^M R_{t+i} \right) \right], \quad s \in \mathbb{R}$$

is the key to closed-form option pricing formula, see [Heston and Nandi \(2000\)](#). Unfortunately, $g_{t,M}(s)$ does not have an affine structure when the variance risk aversion follows a stochastic process. We propose a novel approximation method that extrapolates from the solution to a simpler auxiliary problem, leading to an approximation of $g_{t,M}(s)$.

The future values of $\log \eta_t$ that are relevant for pricing an option with M periods to maturity are the elements of the vector, $\boldsymbol{\eta}_{t,M} = (\log \eta_{t+1}, \dots, \log \eta_{t+M})'$. Under Assumption 3, this is a random vector. For later use, we use the notation, $\bar{\boldsymbol{\eta}}_{t,M}$, to represent a predetermined path (i.e. $\bar{\boldsymbol{\eta}}_{t,M} \in \mathcal{G}_t$), where the prime example is the conditionally expected trajectory, given

⁶We have suppressed the terms dependence on φ , ζ , and the parameters of the HNG model and (7) suppresses an approximation term that is negligible in practice (see Lemma A.1).

by $\bar{\boldsymbol{\eta}}_{t,M}^e = \mathbb{E}_t^{\mathbb{Q}}(\boldsymbol{\eta}_{t,M}) \in \mathbb{R}^{M \times 1}$.

2.2.1 MGF with Predetermined Path

The assumption that $\log \eta_t$ will follow a deterministic trajectory, $\bar{\boldsymbol{\eta}}_{t,M}$, implies that ϕ_{t+j} and ξ_{t+j} are also predetermined for $j = 1, \dots, M$, and similarly, ω_{t+j}^* , α_{t+j}^* , β_{t+j}^* , and γ_{t+j}^* (the GARCH parameters under \mathbb{Q}) are also predetermined for $j = 1, \dots, M$. This is a direct consequence of Theorem 1. We show that the affine structure is preserved in this case with the following closed-form expression for the MGF of cumulative returns.

Lemma 2. *Suppose that Assumptions 1-2 hold and that $\log \eta_t$ take the predetermined path, $\bar{\boldsymbol{\eta}}_{t,M}$. Then the MGF for future cumulative returns under \mathbb{Q} has the affine form,*

$$g_{t,M}(s|\bar{\boldsymbol{\eta}}_{t,M}) = \exp(A_T(s, M) + B_T(s, M)h_{t+1}^*), \quad T = t + M,$$

where the expressions for $A_T(s, M)$ and $B_T(s, M)$ depend on $\bar{\boldsymbol{\eta}}_{t,M}$, and both are given from simple recursive expressions, see Appendix A.4.

The expression for the MGF in Lemma 2 simplifies to that in Christoffersen et al. (2013) if $\bar{\boldsymbol{\eta}}_{t,M} = (\log \eta, \dots, \log \eta)'$, and it simplifies further to that in Heston and Nandi (2000) when $\bar{\boldsymbol{\eta}}_{t,M} = 0_{M \times 1}$. Aside from these two special cases, this naive approach does not constitute a coherent model for option pricing. However, it serves as an important auxiliary “model” with the desired affine structure.

2.2.2 Option Pricing with Stochastic Variance Risk Aversion

We now turn to the more challenging problem where $\boldsymbol{\eta}_{t,M}$ is stochastic. The lack of an affine structure thwarts the standard approach to obtaining closed-form option pricing formula, and it is common to resort to simulation methods in this case.

The idea behind our approximation method is simply to extrapolate from the simple case, $g_{t,M}(s|\bar{\boldsymbol{\eta}}_{t,M}^e)$, and apply a second-order Taylor expansion about $\bar{\boldsymbol{\eta}}_{t,M}^e$. This leads to a quadratic expression in the M -dimensional vector, $\boldsymbol{\varepsilon}_{t,M} = \boldsymbol{\eta}_{t,M} - \bar{\boldsymbol{\eta}}_{t,M}^e$. After taking the conditional expectation, we arrive at the approximate MGF, which is a perturbation of $g_{t,M}(s|\bar{\boldsymbol{\eta}}_{t,M}^e)$ to account for the randomness in $\boldsymbol{\eta}_{t,M}$. The adjustment of $g_{t,M}(s|\bar{\boldsymbol{\eta}}_{t,M}^e)$ is simple, because

Assumption 3 implies that $\mathbb{E}_t^{\mathbb{Q}}[\boldsymbol{\varepsilon}_{t,M}] = 0$ and makes it simple to evaluate $\mathbb{E}_t^{\mathbb{Q}}[\boldsymbol{\varepsilon}_{t,M}\boldsymbol{\varepsilon}'_{t,M}] = \Sigma_M$.

Theorem 3. *Suppose that Assumptions 1-3 hold, then the approximate model-implied MGF, based on a second-order Taylor expansion, is given by*

$$\hat{g}_{t,M}(s) = g_{t,M}(s|\bar{\boldsymbol{\eta}}_{t,M}^e) \left[1 + \frac{1}{2} \text{tr}\{H_{t,M}(s)\Sigma_M\} \right],$$

where $H_{t,M}(s) \in \mathbb{R}^{M \times M}$ is the Hessian from the Taylor expansion and $\Sigma_M = \text{var}_t^{\mathbb{Q}}(\boldsymbol{\varepsilon}_{t,M})$, see Appendix A.5 for details.⁷ The corresponding European call option price is given by

$$\hat{C}(S_t, M, K, r; h_{t+1}^*) = S_t P_{1,t} - K \exp(-rM) P_{2,t},$$

where

$$\begin{aligned} P_{1,t} &= \frac{1}{2} + \frac{\exp(-rM)}{\pi} \int_0^\infty \text{Re} \left[\frac{K^{-iu} \hat{g}_{t,M}(iu + 1)}{iu S_t} \right] du, \\ P_{2,t} &= \frac{1}{2} + \frac{1}{\pi} \int_0^\infty \text{Re} \left[\frac{K^{-iu} \hat{g}_{t,M}(iu)}{iu} \right] du. \end{aligned}$$

Theorem 3 clarifies how random variation in η_t impacts the MGF.⁸ The core principle behind the proposed approximation method is akin to perturbation methods used to find approximate solutions to Schrödinger equations for which standard methods are not applicable. Perturbation methods also starts from an exact solution of a simpler, related problem, from which an approximate solution to the actual problem is deduced. Our approximation is based on a Taylor expansion about an M -dimensional vector, where the conditional moments of the terms in the expansion are deduced from Assumption 3. Next, we evaluate the accuracy of the approximation.

2.3 Accuracy of Analytical Approximation

The option pricing formula in Theorem 3 involves a second-order approximation that accounts for the first two conditional moments of $\boldsymbol{\eta}_{t,M}$.⁹ A first-order approximation is equivalent to assuming that η_t will take the path of its conditional expectation, $\bar{\boldsymbol{\eta}}_{t,M}^e$. Thus, $g_{t,M}(\cdot|\bar{\boldsymbol{\eta}}_{t,M}^e)$ is the MGF for the first-order approximation, which we previously labeled ‘‘Auxiliary’’, because

⁷While $g_{t,M}(s)$ is a MGF, the approximation, $\hat{g}_{t,M}(s)$, need not be one, because there may not exist a density for which $\hat{g}_{t,M}(s)$ is the corresponding MGF.

⁸The integrations in Theorem 3 can be numerically evaluated through the method in Appendix A.9.

⁹If the distribution of $\boldsymbol{\varepsilon}_{t,M}$ is symmetric, (e.g. Gaussian), then it is an approximation to third-order.

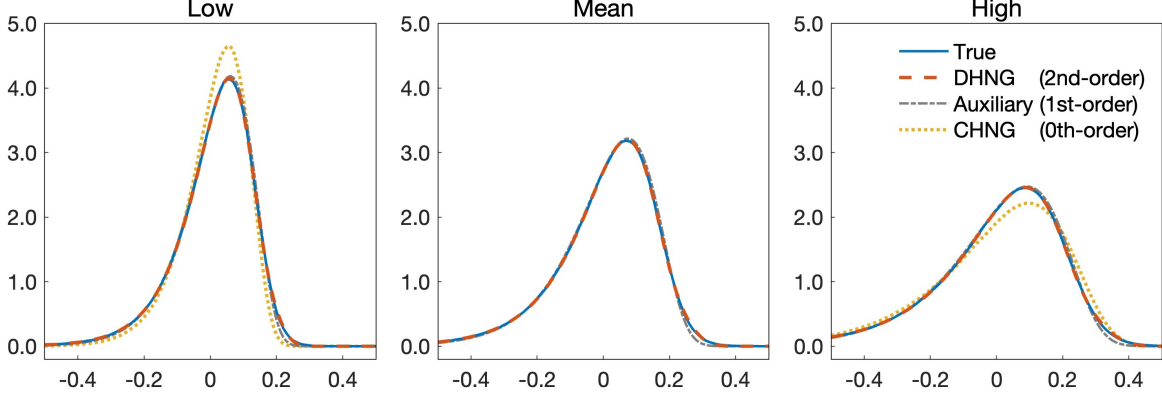


Figure 3: Risk-neutral densities of (six months) cumulative return, for different initial values of variance risk ratio, $\eta_0 = 0.70$ (left panel), $\eta_0 = 1.11$ (middle panel), and $\eta_0 = 1.70$ (right panel). The blue solid line represents the true density from 1 million simulations, the red dashed line is the (2nd-order) approximate density by DHNG, the gray dash-dotted line is the auxiliary model based on $\bar{\eta}_{t,M}^e$ (1st-order), and the yellow dotted line is the (0th-order) density by CHNG with constant η_t . The model parameters are based on the estimates with option prices (the last column in Table 3).

Alt text: Risk-neutral densities for cumulative six-month returns, shown for three initial levels of the variance risk ratio: low, middle, and high. Each density is compared with three approximations—CHNG, the auxiliary model, and DHNG. DHNG provides the most accurate approximation.

it was used as an intermediate step towards our preferred approximation, $\hat{g}_{t,M}(\cdot)$. Taking $\eta_t = \eta_0$ to be constant, $\bar{\eta}_{t,M}^c = (\log \eta_0, \dots, \log \eta_0)'$, is a characteristic of CHNG, and this case can be interpreted as the zero-order “approximation”.

We first consider the risk-neutral density of cumulative returns. The blue solid lines in Figure 3 present the true risk-neutral densities for cumulative returns over six months for three initial values, $\eta_0 = 0.70$ (left panel), $\eta_0 = 1.11$ (middle panel), and $\eta_0 = 1.70$ (right panel), based on 1 million simulations. The data generation process is based on the structure in Theorem 1, using the parameter estimates from our empirical analysis of option prices with $\log \eta_t \sim \text{AR}(1)$, normally distributed innovations, and h_1 initialized at its unconditional mean. In this design, the exponential of unconditional mean, $\exp(\mathbb{E} \log \eta_t) = \exp(\zeta)$, is used as the initial value η_0 in the middle panel.

The red dashed lines are the risk-neutral densities of DHNG implied by $\hat{g}_{t,M}(\cdot)$, the gray dot-dashed lines are based on the auxiliary, $g_{t,M}(\cdot | \bar{\eta}_{t,M}^e)$, and the yellow dotted line is the risk-neutral density for CHNG, i.e. $g_{t,M}(\cdot | \bar{\eta}_{t,M}^c)$. DHNG, which is based on the second-order approximation of Theorem 3, is accurate, whereas the Auxiliary structure fails to match the

upper tail of the densities. The CHNG is the worst approximation of the true density in all cases. It is tied with Auxiliary in the middle panel, because the two are identical when $\log \eta_0$ is set to have its unconditional mean ζ .

The accuracy of the densities can also be assessed by the moments of cumulative returns under \mathbb{Q} . We plot the variance, skewness and kurtosis of multi-period cumulative returns in Figure 4. The variance is presented in annualized units and scaled by 100, such that 4 corresponds to $\sqrt{0.04} = 20\%$ annualized volatility. The k -th moment of cumulative returns can be computed by evaluating the k -th derivative of the MGF in Theorem 3 at zero. However, Theorem 4, presented below, provides a much simpler and more direct method for evaluating moments. Figure 4 shows that neglecting the random variation in η_t yields moments that are far from their true values, whereas the second-order approximation is quite accurate, especially for the second and third moment. Both CHNG and Auxiliary are far less accurate, with CHNG being the least accurate, except in the middle column of panels, where $\bar{\eta}_{t,M}^c = \bar{\eta}_{t,M}^e$.

Theorem 4. *The conditional risk-neutral k -th moment for $k \in \mathbb{N}$ of the M -period ahead cumulative returns can be expressed as*

$$\mathbb{E}_t^{\mathbb{Q}} \left(R_{t,M}^k \right) = \frac{1}{\pi} \int_0^\infty \operatorname{Re} \left[\frac{k!}{v^{k+1}} g_{t,M}(v) - \frac{k!}{u^{k+1}} g_{t,M}(u) \right] ds,$$

where $R_{t,M} = \sum_{i=1}^M R_{t+i}$, and u, v are two complex numbers denoted by $u = u_R + is$ and $v = v_R + is$, with $u_R < 0$, $v_R > 0$ and $s \in \mathbb{R}$. The function, $g_{t,M}(u) = \mathbb{E}_t^{\mathbb{Q}} [\exp(uR_{t,M})]$, is the conditional MGF of the cumulated returns over M periods.

The expression for the conditional moments in Theorem 4 is, to the best of our knowledge, a new result, and it is applicable to any dynamic process with a well-defined MGF.

As a third way to assess the accuracy, we compare the (model) implied volatilities with the true implied volatilities for options with different levels of moneyness (Black-Scholes Delta) and days-to-maturity (DTM). Table 1 reports the percentage errors, $e_i \equiv 100 \times [\log IV_i^{\text{model}} - \log IV_i^{\text{true}}]$, where the implied volatilities are deduced from option prices by the Black-Scholes formula. The data generating process is the same as that used in Figures 3 and 4. We consider three initial values of η_0 over a two-dimensional grid for Delta and DTM.

Table 1 shows that the DHNG option pricing formula of Theorem 3 is far more accurate

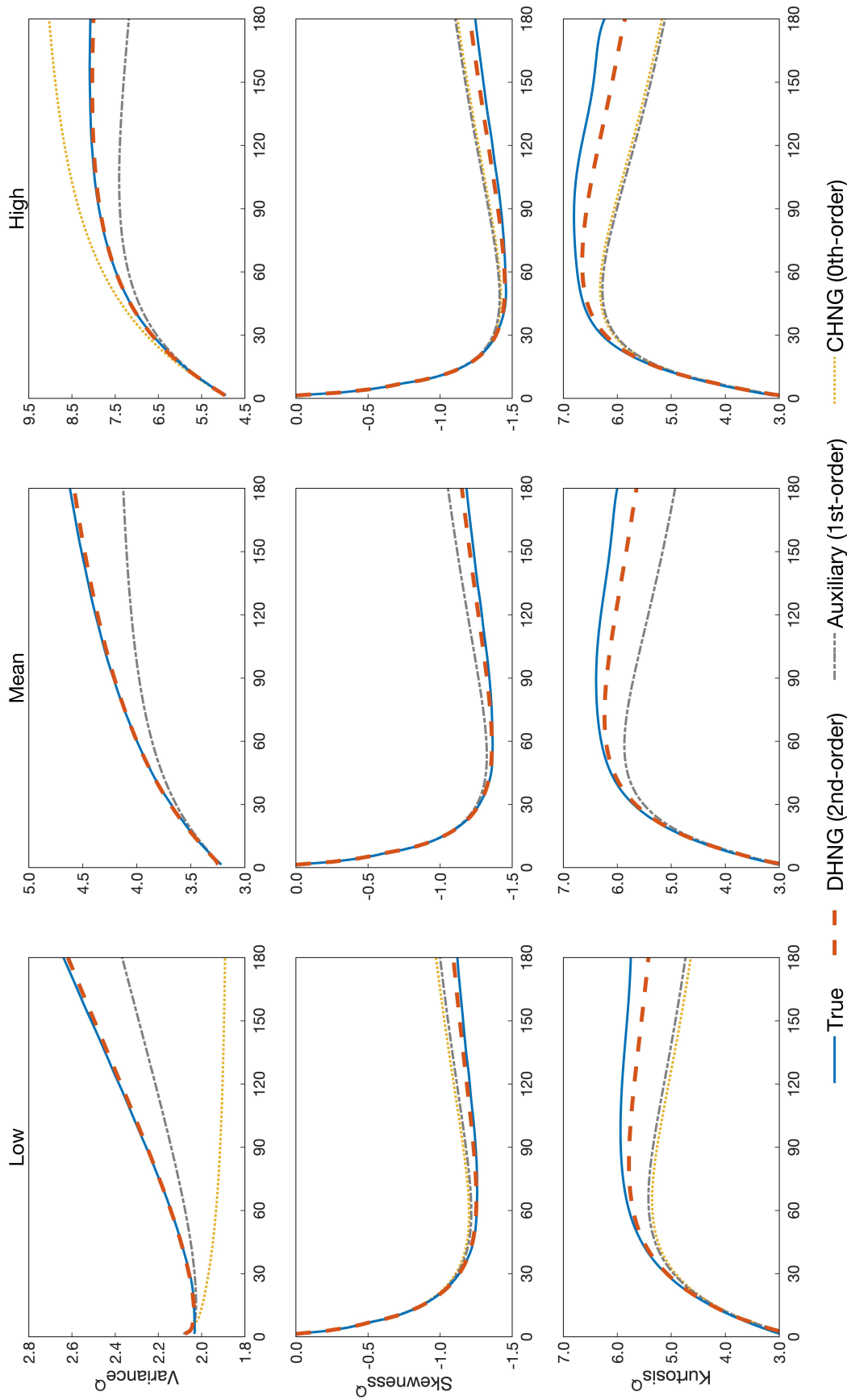


Figure 4: Annualized variance, $\frac{252}{M} \text{var}_t^Q(\sum_{i=1}^M R_{t+i}) \times 100\%$, skewness, and kurtosis of cumulative returns over M days, are shown with three different initial variance risk ratios, $\eta_0 = 0.70$ (left panels), $\eta_0 = 1.11$ (middle panels), and $\eta_0 = 1.70$ (right panels). Blue lines represent true population moments, red dashed lines are those of DHNG, yellow dotted lines are those for CHNG, and the gray dash-dotted lines are those for the auxiliary “model”. Population moments were obtained from 1 million simulated trajectories, using a design based on the parameter estimates obtained with option prices (the last column in Table 3).

Alt text: Variance, skewness, and kurtosis of cumulative returns for three initial levels of the variance risk ratio: low, middle, and high. The figure compares the term structure of true moments with those estimated using CHNG, the auxiliary model, and DHNG, with DHNG providing the most accurate approximation.

than those of Auxiliary and CHNG. This is true across all types of options and initial values of η_0 . The absolute approximation error (MAE) is just 0.08% on average over all designs in Table 1, and the average error (ME) is -0.05%. Unsurprisingly, CHNG is the least accurate option pricing model. The assumptions that η_t is constant leads to underpricing of options when η_0 is small and overpricing when η_0 is large. The option pricing formula for the Auxiliary structure systematically underprices options, and we observe that the pricing error is increasing in DTM. This is consistent with the results in Figure 4, where the predicted values of $h_{t+1}^*, \dots, h_{t+M}^*$ for the Auxiliary structure are downward-biased and increasingly so as M increases. This has implications for empirical estimations under the Auxiliary structure. To rationalize the observed option prices, the Auxiliary structure will need to exaggerate the predicted values of $\log \eta_t$, such that Auxiliary is expected to yield larger predictions of $\log \eta_t$ than those based on DHNG when estimated with option prices. This is indeed what we find in the supplementary results, see Table S.3 in Appendix S.3.

3 Observation-Driven Model for Variance Risk Aversion

In this section, we develop an observation-driven model for η_t , which facilitates an implementation of the results from the previous section. In practice, this requires inferring the current value of η_t and estimate its dynamic model. To this end, we adopt an intuitive observation-driven model for η_t , inspired by the score-driven framework of Creal et al. (2013). We use the first-order conditions for minimizing pricing errors to define innovations to η_t , ensuring that η_t is adjusted to reduce pricing errors on average.¹⁰ The first-order condition of the log-likelihood function is presented in the empirical section. For now, it suffices to express the log-likelihood function in its generic form, $\sum_{t=1}^T \ell(R_t, X_t | \mathcal{F}_{t-1})$, where T is the sample size, and we should emphasize that it relies on information from both \mathbb{P} and \mathbb{Q} . We factorize $\ell(R_t, X_t | \mathcal{F}_{t-1}) = \ell(R_t | \mathcal{F}_{t-1}) + \ell(X_t | R_t, \mathcal{F}_{t-1})$, where the latter can be expressed as $\ell(X_t | \mathcal{G}_t)$. This likelihood term measures how well the observed derivative prices are explained by the statistical model for returns and the pricing kernel.

¹⁰Alternatively, one could adopt state space approach. This is computationally more complicated without necessarily providing any benefit. Even when the true model is a state space model, the score-driven models are typically found to be competitive, see Koopman et al. (2016).

Table 1: Approximation Errors by Logarithm of Implied Volatility (in percentage)

Delta	DTM	Low η			Mean η		High η		
		CHNG	Auxiliary	DHNG	Auxiliary DHNG		CHNG	Auxiliary	DHNG
0.3	30	-2.09	-0.41	0.10	-0.48	0.11	1.16	-0.72	-0.02
	60	-5.06	-1.30	0.02	-1.55	-0.04	2.55	-1.69	-0.05
	90	-8.26	-2.23	-0.06	-2.41	-0.07	3.93	-2.56	-0.06
	120	-11.21	-2.99	-0.07	-3.15	-0.06	5.26	-3.28	-0.06
	150	-13.99	-3.70	-0.09	-3.84	-0.09	6.50	-3.93	-0.09
0.4	30	-1.62	-0.02	0.41	-0.49	0.04	1.12	-0.68	-0.07
	60	-4.88	-1.23	-0.04	-1.34	-0.05	2.61	-1.44	-0.05
	90	-7.83	-1.96	-0.07	-2.08	-0.06	4.03	-2.18	-0.06
	120	-10.64	-2.62	-0.05	-2.72	-0.05	5.41	-2.80	-0.05
	150	-13.34	-3.26	-0.07	-3.33	-0.07	6.69	-3.37	-0.07
0.5	30	-1.74	-0.20	0.22	-0.69	-0.18	1.11	-0.63	-0.09
	60	-4.83	-1.21	-0.10	-1.23	-0.05	2.56	-1.32	-0.05
	90	-7.59	-1.82	-0.06	-1.92	-0.06	3.98	-1.99	-0.06
	120	-10.38	-2.46	-0.04	-2.53	-0.04	5.37	-2.57	-0.04
	150	-13.07	-3.07	-0.06	-3.10	-0.06	6.66	-3.11	-0.05
0.6	30	-2.32	-0.76	-0.30	-0.65	-0.17	1.13	-0.55	-0.03
	60	-4.72	-1.11	-0.05	-1.22	-0.05	2.46	-1.29	-0.06
	90	-7.57	-1.82	-0.04	-1.89	-0.05	3.85	-1.94	-0.05
	120	-10.40	-2.46	-0.04	-2.50	-0.03	5.22	-2.51	-0.03
	150	-13.16	-3.09	-0.05	-3.08	-0.05	6.50	-3.05	-0.05
0.7	30	-2.70	-1.05	-0.56	-0.38	0.10	0.99	-0.65	-0.10
	60	-4.74	-1.14	-0.01	-1.28	-0.08	2.31	-1.34	-0.07
	90	-7.82	-1.94	-0.06	-1.98	-0.05	3.66	-2.01	-0.05
	120	-10.81	-2.65	-0.04	-2.65	-0.04	4.97	-2.62	-0.04
	150	-13.78	-3.32	-0.04	-3.26	-0.04	6.25	-3.19	-0.04
MAE		7.78	1.91	0.11	1.99	0.07	3.85	2.06	0.06
ME		-7.78	-1.91	-0.05	-1.99	-0.05	3.85	-2.06	-0.06

Note: This table reports the approximation errors, $e_i = \left[\log IV_i^{\text{model}} - \log IV_i^{\text{true}} \right] \times 100$ for options with different Moneyness (Delta), days to maturity (DTM), and initial value of η . The true option prices are obtained with 10 million simulated paths from the true model, and the implied volatilities are computed using Black-Scholes formula. The column-wise averages for the mean absolute error (MAE) and the mean error (ME), are presented in the last two rows. CHNG, Auxiliary, and DHNG correspond to zero-, first-, and second-order approximations, respectively. The model parameters are based on the empirical estimates obtained with option prices (the last column in Table 3).

A score-driven model updates a parameter in the direction dictated by the first-order conditions of the log-likelihood function, known as the score.¹¹ In our model, the relevant score is $\partial\ell(X_t|\mathcal{G}_t)/\partial\log\eta_t$, because $\ell(R_t|\mathcal{F}_{t-1})$ does not depend on η_t . The required structure for ε_t , as specified in Assumption 3, motivates the choice

$$\varepsilon_{t+1} = \sigma s_t, \tag{8}$$

where the normalized score is defined by

$$s_t = \frac{\nabla_t}{\sqrt{\mathbb{E}_t^{\mathbb{P}}(\nabla_t^2)}}, \quad \text{with} \quad \nabla_t = \frac{\partial\ell(X_t|\mathcal{G}_t)}{\partial\log\eta_t}. \tag{9}$$

Since s_t is \mathcal{F}_t -measurable, we have $\varepsilon_{t+1} \in \mathcal{F}_t \subset \mathcal{G}_{t+1}$ as required by Assumption 3. Additionally, when the score is evaluated at the true parameters we have

$$\mathbb{E}_t^{\mathbb{P}}(s_t) = 0, \quad \text{and} \quad \text{var}_t^{\mathbb{P}}(s_t) = 1,$$

such that $\mathbb{E}_t^{\mathbb{P}}(\varepsilon_{t+1}) = 0$ and $\text{var}_t^{\mathbb{P}}(\varepsilon_{t+1}) = \sigma^2$. Note that this definition of the score does not ensure that $\{s_t\}$ is a sequence of iid random variables with zero mean and unit variance under \mathbb{Q} , as needed by Assumption 3. This requires additional distributional assumptions about the pricing errors. For instance, we will make assumptions about the pricing errors that imply $s_t|\mathcal{G}_t \sim iid N(0,1)$ under both in \mathbb{P} and \mathbb{Q} measures (see Theorem 5 below), in which case the score satisfies all the requirements in Assumption 3. From (6) and the specifications (8)-(9), it follows that our constructed η_t is \mathcal{F}_{t-1} -measurable, which ensures that the information about current derivative prices are not used to price themselves.

This approach to modeling $\log\eta_t$ is analogous to the way the conditional variance is modeled in GARCH models. For instance, the GARCH(1,1) model by Bollerslev (1986) implies that $h_t = c + bh_{t-1} + a(r_{t-1}^2 - h_{t-1})$, such that $h_t \sim \text{AR}(1)$ and changes in h_t are driven by discrepancies between squared returns and the conditional variance. The score model invokes a similar self-adjusting property, where $\log\eta_t$ is updated in response to derivative prices that indicate that pricing errors can be reduced by revising the value of $\log\eta_t$.

In our empirical analysis, we will adopt a score-driven model with an AR(1) structure for $\log\eta_t$. Theorem 3 can accommodate the case where $\log\eta_t \sim \text{ARMA}(p, q)$, whereas more gen-

¹¹The score-driven approach is locally optimal in the Kullback-Leibler sense, see Blasques et al. (2015).

eral models for $\log \eta_t$, such as exogenous/endogenous explanatory variables and long-memory specifications, would require analogous option pricing results to be established first.

3.1 The Log-Likelihood Function and the Form of Score

Next, we turn to the log-likelihood function used to estimate model parameters. Our observed data consist of returns, R_t , and a vector of derivative prices, X_t . Without loss of generality, we can factorize the log-likelihood function as follows:

$$\ell(R_1, \dots, R_T, X_1, \dots, X_T, \mathcal{F}_0) = \sum_{t=1}^T \ell(R_t, X_t | \mathcal{F}_{t-1}) = \sum_{t=1}^T \ell(R_t | \mathcal{F}_{t-1}) + \ell(X_t | R_t, \mathcal{F}_{t-1}).$$

This decomposition was also used by [Christoffersen et al. \(2013\)](#). The log-likelihood function for returns, $\ell(R_t | \mathcal{F}_{t-1})$, is that of the HNG model in (1)-(2),

$$\ell(R_t | \mathcal{F}_{t-1}) = -\frac{1}{2} \left[\log(2\pi) + \log h_t + (R_t - r - (\lambda - \frac{1}{2})h_t)^2 / h_t \right],$$

which assumes that $z_t \stackrel{\mathbb{P}}{\sim} iid N(0, 1)$. To complete the model, we need to specify the log-likelihood function for the vector of derivative prices, $\ell(X_t | R_t, \mathcal{F}_{t-1}) = \ell(X_t | \mathcal{G}_t)$. To this end, we let $X_t^m \in \mathcal{G}_t$ denote the vector of model-based derivative prices and make the following assumption for pricing errors.

Assumption 4. *The derivative pricing errors follow an iid multivariate normal distribution*

$$e_t = X_t - X_t^m | \mathcal{G}_t \stackrel{\mathbb{P}}{\sim} iid N \left(0, \sigma_e^2 \Omega_{N_t} \right),$$

with correlation matrix Ω_{N_t} , where N_t is the number of derivative prices at time t . Additionally, e_t is independent of the return shock z_τ for all τ .

The vector of derivative “prices”, X_t , can be defined in several ways. [Wang et al. \(2017\)](#) measured X_t in the unit of volatility (the level of VIX), [Christoffersen et al. \(2013\)](#) used the Vega-weighted option price, and [Feunou and Okou \(2019\)](#) used the Black-Scholes implied volatility. In our empirical analysis, we use the logarithmically transformed VIX and the logarithmically transformed Black-Scholes implied volatilities for options, which are natural choices because we specify a model for $\log \eta_t$. Moreover, the logarithmic transformation reduces the risk of severe model misspecification, because the distribution of log-volatilities is

often well-approximated by a Gaussian distribution, see [Andersen et al. \(2003\)](#).

The existing empirical studies that used derivative pricing errors in this manner, all assumed that the pricing errors were uncorrelated, i.e. $\Omega_{N_t} = I_{N_t}$ where I_{N_t} is the N_t -dimensional identity matrix. This is unrealistic, because contemporaneous pricing errors tend to be positively correlated. We will therefore allow for a non-zero common correlation, which is important for the statistical properties of the score, see [Theorem 5](#) below. For instance, if we impose $\Omega_{N_t} = I_{N_t}$ in our empirical analysis with option prices, then it would result in a type of misspecification that induces an upward bias in the estimated variance of s_t .

Assumption 5. *The correlation matrix for pricing errors has the form: $\Omega_{N_t} = (1 - \rho)I_{N_t} + \rho U_{N_t}$, where $I_{N_t} \in \mathbb{R}^{N_t \times N_t}$ is the identity matrix and $U_{N_t} \in \mathbb{R}^{N_t \times N_t}$ is a matrix of ones.*

The correlation matrix in [Assumption 5](#), Ω_{N_t} , is known as an equicorrelation matrix. Having a common correlation for all pairs of pricing errors is particularly useful in applications where the panel of derivative prices is unbalanced over time. In this case, the dimension of Ω_{N_t} will be time-varying, but this is not problematic if an equicorrelation structure is assumed. A common correlation can be motivated by the assumption that pricing errors, $e_{i,t} = u_t + v_{i,t}$, have a common component, u_t , and uncorrelated idiosyncratic components, $v_{i,t}$, $i = 1, \dots, N_t$. This will bring about the structure in [Assumption 5](#) with $\rho = \sigma_u^2 / \sigma_e^2$ and $\sigma_e^2 = \sigma_u^2 + \sigma_v^2$.

Under [Assumption 4](#), the part of log-likelihood function that relates to derivative prices is

$$\ell(X_t | \mathcal{G}_t) = \ell(e_t | \mathcal{G}_t) = -\frac{1}{2} \left(N_t \log(2\pi\sigma_e^2) + \log |\Omega_{N_t}| + \sigma_e^{-2} e_t' \Omega_{N_t}^{-1} e_t \right).$$

The model for returns under \mathbb{P} continues to be a time-homogeneous Heston-GARCH model, which does not depend on derivative prices. This is also true in the DHNG model, despite the time variations in the pricing kernel. For this reason, the model parameters can (if needed) be estimated by a two-stage estimation method, where the parameters in the GARCH model is estimated from returns in the first stage, followed by the remaining parameters being estimated in the second stage with derivative prices.¹²

¹²In our empirical application we estimated the model by maximizing the full log-likelihood function, which was straightforward and did not cause computational issues. If needed, two-stage estimation can be adopted to reduce the computational burden, and the approach to estimation is not uncommon in this setting, see e.g. [Broadie et al. \(2007\)](#), [Corsi et al. \(2013\)](#), [Christoffersen et al. \(2013\)](#), and [Majewski et al. \(2015\)](#).

Theorem 5. *Suppose that Assumption 4 holds. Then the score, (9), is given by*

$$\nabla_t = \frac{1}{\sigma_e^2} \left(\frac{\partial X_t^m}{\partial \log \eta_t} \right)' \Omega_{N_t}^{-1} e_t,$$

which has zero conditional mean, $\mathbb{E}_t^{\mathbb{P}}(\nabla_t) = 0$, and conditional variance:

$$\mathbb{E}_t^{\mathbb{P}}(\nabla_t^2) = \frac{1}{\sigma_e^2} \left(\frac{\partial X_t^m}{\partial \log \eta_t} \right)' \Omega_{N_t}^{-1} \left(\frac{\partial X_t^m}{\partial \log \eta_t} \right).$$

Moreover, the scaled score is \mathcal{F}_t -measurable and satisfies $s_t | \mathcal{G}_t \sim iid N(0, 1)$, under \mathbb{P} and \mathbb{Q} measures.

To obtain the score, we need to derive $\partial X_t^m / \partial \log \eta_t$, and this must be done separately for the VIX and option prices. These terms are derived in Appendix A.8. Note that if X_t^m is univariate (the case with a single derivative), then the scaled score simplifies to

$$s_t = \frac{1}{\sigma_e} \text{sign} \left(\frac{\partial X_t^m}{\partial \log \eta_t} \right) e_t.$$

From this expression, it is evident that the score will indicate the direction of change for η_t , which is expected to reduce pricing errors.

4 Empirical Analysis

4.1 Data

Our empirical analysis is based on daily returns for the S&P 500 index, the CBOE VIX, and the panel of SPX option prices based on the S&P 500 index. Our sample period spans 32 years from January 2nd, 1990, to December 31, 2021, with 8,064 trading days. Returns are defined from cum-dividend logarithmic transformed closing prices, which were downloaded from the CRSP of Wharton Research Data Services (WRDS). Daily VIX prices were obtained from the Chicago Board Options Exchange (CBOE) website. The SPX option prices were obtained from two sources. Prices for the first six years (1990–1995) are the so-called Optsum data, which were purchased from CBOE website. Option prices for the remaining 26 years are OptionMetrics data downloaded from the WRDS database.

Option prices were primarily preprocessed following [Christoffersen et al. \(2014\)](#) and [Bakshi et al. \(1997\)](#). Specifically, we include out-of-the-money put and call option prices with positive

trading volume and maturities between two weeks and six months. Options with missing implied volatilities or prices below one dollar are excluded. Put option prices are converted to call options using the put-call parity. Very deep out-of-the-money options with deltas larger than 0.85 or less than 0.15 are discarded. Much of the existing literature uses weekly data, and a panel of option prices is typically sampled on Wednesdays, because liquidity tends to be highest on Wednesdays. However, in our analysis, we use daily option prices, because a daily score, s_t , is needed to update η_t . The number of available options has grown rapidly over the sample period, both in terms of available maturities and the range of moneyness at each maturity.¹³ From the pool of available options, we select up to six options per trading day. The inclusion criteria are as follows: we first determine the most liquid option for each maturity on day t , as measured by daily trading volume. We sort these options by maturity in ascending order and index these by $j = 1, \dots, \tilde{N}_t$, where \tilde{N}_t is the number of distinct maturities on day t . From this set, we include all options if $\tilde{N}_t \leq 6$; the first six options if $7 \leq \tilde{N}_t \leq 10$; options $\{1, 3, 5, 7, 9, 11\}$ if $11 \leq \tilde{N}_t \leq 15$; and options $\{1, 4, 7, 10, 13, 16\}$ if $16 \leq \tilde{N}_t \leq 20$; and so forth. This resulting set of options will be representative for the range of available maturities, and we have $N_t = 6$ on most days. The total number of option prices in our full sample period is 37,152.

Table 2 contains descriptive statistics for our S&P 500 returns and the CBOE VIX in Panel A, and option prices in Panel B. As expected, the sample average of the VIX (19.48%) is larger than the standard deviation for annualized returns (18.11%). This difference reflects the (average) negative volatility risk premium. The S&P 500 returns exhibit slight negative skewness and a high degree of kurtosis, whereas the VIX has positive skewness and slightly lower kurtosis. We also report summary statistics for option prices partitioned by moneyness, maturity, and the contemporaneous level of VIX. Options with deltas below 0.5 are out-of-the-money call options, and options with deltas above 0.5 are based on out-of-the-money put options. Deep out-of-the-money put options (i.e., deltas greater than 0.7) are expensive relative to out-of-the-money call options, reflecting the well-known volatility smirk. The implied volatility has a relatively flat term structure with respect to time to maturity. Unsurprisingly,

¹³The number of available option prices has increased almost 50-fold over our sample period, initially from about 38 daily option prices to well over 1,700.

Table 2: Summary Statistics

<i>A: S&P 500 returns and the CBOE VIX</i>					
	Mean(%)	Std(%)	Skewness	Kurtosis	Obs.
Returns (annualized)	8.13	18.11	-0.41	14.37	8,064
VIX	19.48	8.01	2.21	11.49	8,064
 <i>B: Option Price Data</i>					
	Implied Volatility (%)	Average price (\$)	Observations		
All options	18.47	63.63	37,152		
 <i>Partitioned by Moneyness</i>					
Delta<0.3	14.18	11.04	5,452		
0.3≤Delta<0.4	15.52	20.92	2,955		
0.4≤Delta<0.5	16.76	33.92	3,912		
0.5≤Delta<0.6	18.94	48.78	7,091		
0.6≤Delta<0.7	19.40	64.86	6,098		
0.7≤Delta	21.02	117.47	11,644		
 <i>Partitioned by Maturity</i>					
DTM<30	16.89	41.41	9,614		
30≤DTM<60	17.91	52.29	9,696		
60≤DTM<90	19.00	65.63	7,465		
90≤DTM<120	20.25	87.43	4,421		
120≤DTM<150	20.22	98.51	2,931		
150≤DTM	19.68	97.06	3,025		
 <i>Partitioned by the level of VIX</i>					
VIX<15	12.15	44.77	12,638		
15≤VIX<20	16.70	62.49	10,788		
20≤VIX<25	21.45	74.72	7,143		
25≤VIX<30	25.43	84.16	3,395		
30≤VIX<35	29.61	88.12	1,456		
35≤VIX	40.23	101.70	1,732		

Note: Summary statistics for close-to-close S&P 500 index log returns, CBOE VIX, and SPX option prices from January 1990 to December 2021. We report the sample mean (Mean), standard deviation (Std), skewness (Skew), kurtosis (Kurt), number of observations (Obs), for returns and the VIX. Option prices are based on closing prices of out-of-the-money call and put options. We report the average Black-Scholes implied volatility (IV), average price, and the number of option prices for different ranges of Moneyness, days to maturity (DTM), and VIX levels. Data sources: S&P 500 returns from CRSP, VIX from CBOE's website. Option prices from Optsum data (1990–1995) and OptionMetrics (1996–2021).

the implied volatility increases with the VIX level, as shown at the bottom of Table 2, where option prices are partitioned by the contemporaneous level of the VIX.

4.2 Parameter estimation

We estimate the model with both constant and time-varying variance risk aversion, CHNG and DHNG, respectively.¹⁴ Both specifications are estimated using two types of derivative prices, VIX data and the panel of option prices. Parameters are estimated by maximizing the joint log-likelihood function for the full sample period from January 1990 to December 2021. Each column reports the parameter estimates for the specification listed in the first row of Table 3. The type of derivatives, VIX or option prices, used in the estimation is indicated with [VIX] and [Opt], respectively. Robust standard errors are given in parentheses below the estimates.¹⁵ We also report the implied persistence of volatility under both \mathbb{P} and \mathbb{Q} . These are given by $\pi^{\mathbb{P}} = \beta + \alpha\gamma^2$ and $\pi^{\mathbb{Q}} = \mathbb{E}^{\mathbb{Q}}[\beta_t^* + \alpha_t^*\gamma_{t-1}^{*2}]$, respectively, where the latter simplifies to $\pi^{\mathbb{Q}} = \beta^* + \alpha^*\gamma^{*2}$ for the CHNG model with constant parameters. We also report the different terms of the log-likelihood (for returns and different sets of derivative prices). Some of these likelihood terms can be interpreted as pseudo out-of-sample log-likelihood values, indicated in *italic*. For instance, the CHNG[VIX] model is estimated using returns and the VIX, but the estimated model also yields model-based option prices that can be compared with actual option prices. The reported pseudo log-likelihood for option prices is evaluated with the resulting option pricing errors that are implicitly used to obtain estimates of ρ and σ_e for option prices. Similarly, we evaluate the log-likelihood for VIX pricing errors for the specifications estimated with option prices. In this case, we compute the implied estimate of σ_e for VIX prices. The largest log-likelihood within each row is highlighted in bold.

There are several interesting observations to be made from Table 3. First, the volatility process is found to be highly persistent across all specifications, and the persistence is larger under \mathbb{Q} than under \mathbb{P} , which is consistent with the existing literature. Second, the estimate of the equity risk premium, λ , is positive and significant in all specification. Third, the VRR, η , is significantly larger than one in both CHNG specifications. Similarly, for the DHNG model

¹⁴The corresponding results for the Auxiliary structure are presented in the Appendix S.3.

¹⁵Following Christoffersen et al. (2013), we impose $\omega = 0$ in estimation when the non-negativity constraint, which ensures positive variances, is binding.

Table 3: Joint Estimation Results

Model	CHNG [VIX]	CHNG [Opt]	DHNG [VIX]	DHNG [Opt]
λ	3.377 (0.662)	2.828 (0.022)	3.398 (1.281)	3.088 (0.644)
β	0.902 (0.001)	0.713 (0.008)	0.720 (0.018)	0.570 (0.015)
$\alpha(\times 10^{-6})$	1.166 (0.206)	2.495 (0.012)	4.428 (0.416)	5.833 (0.256)
γ	272.45 (23.81)	327.49 (3.81)	220.45 (9.474)	249.59 (10.28)
ζ			0.192 (0.057)	0.102 (0.011)
φ			0.988 (0.002)	0.994 (0.001)
σ			0.061 (0.002)	0.042 (0.010)
ρ		0.822 (0.015)		0.087 (0.010)
σ_e	0.175 (0.071)	0.229 (0.024)	0.043 (0.001)	0.091 (0.006)
$\eta, \mathbb{E}\eta$	1.371 (0.041)	1.252 (0.013)	1.314	1.190
$\widehat{\text{var}}(s_t)$			1.000	1.007
$\pi^{\mathbb{P}}$	0.989	0.981	0.935	0.934
$\pi^{\mathbb{Q}}$	0.991	0.985	0.944	0.944
LogL				
$\ell(\text{R})$	26,324	26,438	26,450	26,419
$\ell(\text{VIX})$	2,619	<i>1,602</i>	13,917	<i>7,932</i>
$\ell(\text{Opt})$	<i>15,177</i>	21,647	<i>27,857</i>	36,682
$\ell(\text{R}, \text{VIX})$	28,944	<i>28,041</i>	40,367	<i>34,351</i>
$\ell(\text{R}, \text{Opt})$	<i>41,501</i>	48,085	<i>54,307</i>	63,101

Note: Estimation results for the full sample period, January 1990 to December 2021. CHNG is the model by [Christoffersen et al. \(2013\)](#) and DHNG is the model introduced in this paper. The type of derivatives used to estimate each model, VIX or option prices, is indicated with [VIX] and [Opt], respectively. Estimates are reported with robust standard errors (in parentheses), and $\pi^{\mathbb{P}}$ and $\pi^{\mathbb{Q}}$ refer to the persistence of volatility under \mathbb{P} and \mathbb{Q} , respectively. The components of the maximized log-likelihood function are reported at the bottom of the table, and bold is used to highlight the largest log-likelihood in each row. Italic font is used to highlight pseudo out-of-sample log-likelihoods.

the expected value of $\log \eta_t$, ζ , is significantly positive in both DHNG specifications. Their corresponding expected η_t (denoted $\mathbb{E}\eta$) inferred from the AR(1) model for $\log \eta_t$ are both notably larger than one. This implies that the risk-neutral volatility, h^* , is (on average) larger than the physical volatility, h . Fourth, the parameter that defines the leverage effects, γ , is also found to be significant across all specification. Fifth, for the DHNG specification we note that, η_t , is highly persistent, as φ is estimated to be close to one. In fact, it is estimated to be more persistent than h_t and h_t^* across all DHNG specifications. Sixth, the coefficient, σ , which measures the impact of s_{t-1} on η_t , is estimated to be positive and significant.¹⁶ The implied unconditional variance for η_t is similar for the two DHNG specifications, $\text{var}(\eta_t) = 0.29$ when estimated with VIX and $\text{var}(\eta_t) = 0.23$ when estimated with option prices.¹⁷ Seventh, all specifications yield similar likelihood values for the returns. This is to be expected because they all rely on the same Heston-Nandi GARCH model for returns under physical measure.

Eighth, the key difference between the CHNG and DHNG models is the enhanced flexibility in DHNG's pricing kernel. This generalization leads to large improvements in the likelihood for derivative prices. The reason is that the adaptive pricing kernel with time-varying variance risk aversion yields model-implied derivative prices that are much closer to observed prices, and the substantial reduction in the pricing errors translates to much higher values of the log-likelihood for derivative prices. Ninth, estimating the models with VIX or option prices results in some differences across the estimated parameters. This is to be expected, as the vector of option prices contains more information about the distribution of future returns than the VIX. For instance, the leverage parameter, γ , is estimated to be larger with option prices than with the VIX. Tenth, the correlation among option pricing errors, ρ , is estimated to be positive and significant for both models. The estimate has the staggering large value of 82.2% for the CHNG model and a more moderate value of 8.7% for DHNG model. Ignoring this correlation (assuming it to be zero) would greatly underestimate the condition variance of ∇_t , which makes the variance of s_t larger than one.

Figure 5 presents the estimated daily time series of the VRR, $\eta_t = h_{t+1}^*/h_{t+1}$, based on the VIX (blue line) and option prices (red line). The two have a high degree of comovement

¹⁶In principle, σ could be negative, but $\text{var}(\sigma s_t) = \sigma^2$ is non-negative.

¹⁷The variance for η_t is computed from AR(1) parameters for $\log \eta_t$ and the assumptions imply that the unconditional distribution for η_t is log-normal.

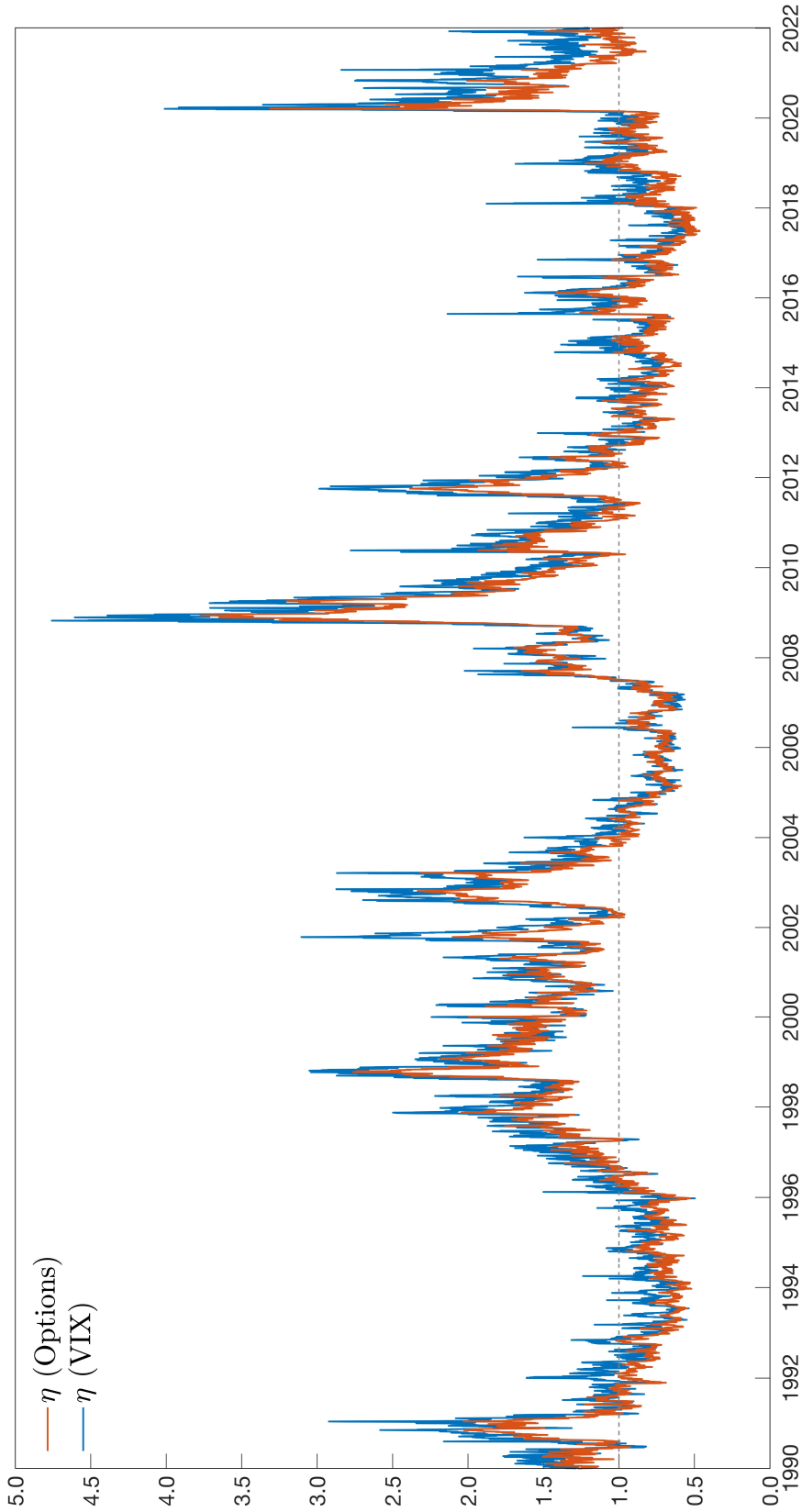


Figure 5: This figure displays the full-sample time series of the daily estimated variance risk ratio, η_t , from January 1990 to December 2021. The blue line is based on the VIX and the red line on option prices. The two time series are very similar, albeit the η_t based on the VIX tend to be slightly larger than that based on option prices.

Alt text: Time series of the variance risk ratio from 1990 to 2021, estimated using VIX data and option prices. The two series follow similar trends, with occasional level differences, particularly during financial crises and market stress periods.

and, as we discussed earlier, the unconditional variance of the two series is very similar. Importantly, the VRR occasionally falls below one, as is seen during the years 1993–1995, 2004–2007, and around 2017. A value below one ($\eta_t < 1$) indicates that investors have an increased appetite for variance risk, whereas a large value of η implies that investors demand additional compensation for variance risk. The latter was particularly the case during financial crises, such as the immediate aftermath of the Lehman collapse and the recent COVID-19 pandemic. The observed conditional variance was unusually high during these episodes, and the large value of η_t implies that h_t^* increased to far higher levels and was, briefly, more than three times larger than h_t .

The level of η_t based on the VIX tend to be slightly larger than that based on option prices. This discrepancy can be attributed to the fact that the VIX is based on options with 30 days to maturity, whereas the options have maturities up to 180 days. A possible explanation is that short-term investors demand larger compensation for variance risk than long-term investors, which would be consistent with the findings in [Eisenbach and Schmalz \(2016\)](#) and [Andries et al. \(2018\)](#).

4.3 In-Sample VIX and Option Pricing Performance

We evaluate the performance of the models in terms of their ability to accurately price the VIX and options. We report the root mean squared errors (RMSE) for the logarithm of VIX and the logarithmically transformed implied volatilities.¹⁸ The RMSE multiplied by 100 can be interpreted as the (absolute) relative pricing errors in percent. This loss function is coherent with our log-likelihood function, where the term that involves derivative prices is given in Assumption 4. A similar loss function was adopted in [Ornthanalai \(2014\)](#), who used the relative implied volatility to prevent days with high volatility from being given a disproportionately large weight in the comparisons. For each of the specifications listed in Table 3, we report their (in-sample) RMSEs in Table 4.

¹⁸As a robustness check, we also computed the RMSE for the level of VIX and implied volatilities. These results are reported in Appendix S.1.

Table 4: VIX and Option Pricing Performance

Model	CHNG [VIX]	CHNG [Opt]	DHNG [VIX]	DHNG [Opt]
<i>A: RMSE for VIX Pricing</i>				
Full Sample	17.49	19.81	4.308	9.049
<i>B: RMSE for Option Pricing</i>				
Full Sample	23.06	22.88	13.34	9.191
<i>Partitioned by moneyness</i>				
Delta<0.3	33.05	29.80	21.11	12.77
0.3≤Delta<0.4	27.84	26.59	17.86	11.28
0.4≤Delta<0.5	23.29	23.87	14.68	9.375
0.5≤Delta<0.6	19.74	21.49	11.41	7.271
0.6≤Delta<0.7	18.83	20.62	9.72	6.859
0.7≤Delta	19.50	19.48	8.78	8.634
<i>Partitioned by maturity</i>				
DTM<30	25.48	23.51	13.72	12.19
30≤DTM<60	23.48	23.27	12.80	7.848
60≤DTM<90	21.78	22.30	12.75	6.914
90≤DTM<120	20.47	21.81	13.51	7.963
120≤DTM<150	20.74	21.68	13.84	8.622
150≤DTM	22.18	23.58	14.45	9.226
<i>Partitioned by the level of VIX</i>				
VIX<15	29.25	28.06	15.60	10.02
15≤VIX<20	18.47	19.72	13.16	9.021
20≤VIX<25	18.23	19.51	10.89	8.224
25≤VIX<30	18.74	18.52	11.02	8.518
30≤VIX<35	19.48	19.23	10.97	8.542
35≤VIX	25.36	22.41	11.57	9.508

Note: This table presents the full-sample VIX and option pricing performance from January 1990 to December 2021 for each model listed in 3. We evaluate the model's VIX and option pricing ability through the root mean square error for log VIX and log implied volatility (log IV), respectively, see (10) and (11). Results for option pricing are presented for different ranges of moneyness (Black-Scholes Delta), days-to-maturity (DTM), and the VIX levels.

We present the in-sample RMSEs for the VIX in Panel A. These are defined by

$$\text{RMSE}_{\text{VIX}} = \sqrt{\frac{1}{T} \sum_{t=1}^T [\log \text{VIX}_t^m - \log \text{VIX}_t]^2} \times 100, \quad (10)$$

where VIX_t^m is the model-based quantity and VIX_t is the observed market VIX value. Panel A of Table 4 shows that a time-varying VRR, η_t , results in substantially smaller average pricing errors, relative to a constant η , which is a characteristic of CHNG. The improved VIX pricing is substantial and impressive. The most accurate VIX pricing is achieved with by the DHNG model, when it is estimated with VIX data. This reduces the RMSE by a factor of four relative to both CHNG specifications. Even the DHNG model that is estimated solely with option prices, has a much smaller RMSE for VIX prices than the CHNG specification that uses VIX prices as part of the objective in the estimation. This is impressive, because the DHNG model estimated with option prices is based on an objective that simultaneously seeks to price options with maturities ranging from one to six months. This entails a trade-off across maturities, unlike models estimated with solely with VIX, that specifically targets the one-month maturity.

Panel B of Table 4 reports the in-sample performance for option pricing. We follow the literature and convert option prices to their corresponding Black-Scholes implied volatilities. We compare the model-based implied volatility, IV^m , with the market-based implied volatility, IV , where the latter is defined by the observed option price. The resulting RMSE,

$$\text{RMSE}_{\text{IV}} = \sqrt{\frac{1}{\sum_{t=1}^T N_t} \sum_{t=1}^T \sum_{i=1}^{N_t} [\log \text{IV}_{t,i}^m - \log \text{IV}_{t,i}]^2} \times 100, \quad (11)$$

is reported in the first row of Panel B. We also compute the RMSE_{IV} for options partitioned by moneyness, time to maturity, and the contemporaneous VIX level. The resulting RMSEs can be used to identify shortcomings in a model, such as its inability to generate sufficient leverage effect, capture the dynamic properties, and generate a proper variance risk premium.

The DHNG specifications clearly dominate the CHNG specifications in terms of option pricing. The average option pricing errors are substantially smaller for DHNG models than for CHNG models, and the smallest RMSE is obtained by the DHNG model estimated with option prices. Its RMSE is less than half that of any of the CHNG specifications. Impressively, the

DHNG specifications uniformly dominate all CHNG specifications for both VIX and option pricing across all partitions. This further supports the advantage of having a dynamic variance risk aversion in the model. Note that the largest gains in pricing accuracy are found during periods with low volatility and for out-of-the-money call options, which tend to be options with low variance risk premia.

Figure 6 displays the model-based VIX and implied volatility (red lines) alongside the corresponding market-based quantities (blue lines). The upper panels show the model-based VIX for CHNG and DHNG, with both models estimated using VIX data. The lower panels present the daily average of model-based implied volatilities for CHNG and DHNG, estimated with option prices. For CHNG, we see larger discrepancies between model-based and market-based quantities as evident in Figure 6. Specifically, CHNG underprices when volatility is high and overprices when volatility is low, whereas no such patterns are observed for DHNG.

Interestingly, Christoffersen et al. (2013) also estimated an ad-hoc model where the ratio of volatility under \mathbb{P} and \mathbb{Q} is not held constant. This model was used as a benchmark for the CHNG model. The ad-hoc model consisted of two separate HNGs: one fitted to returns under \mathbb{P} , and one that was estimated with option prices under \mathbb{Q} . This model is referred to as ad-hoc, because it makes no attempt to uncover a pricing kernel that explains the differences between \mathbb{P} and \mathbb{Q} . Their ad-hoc model did not improve option pricing accuracy relative to CHNG. Theorem 1 provides a theoretical explanation for the poor performance of their ad-hoc model, as it shows that any time variation in ξ_t (or, equivalently, in η_t) makes it impossible to have HNGs with time-invariant parameters under both \mathbb{P} and \mathbb{Q} measures.¹⁹

In the next section, we evaluate if the substantial in-sample improvements in derivatives pricing also holds out-of-sample.

4.4 Out-of-Sample Pricing Performance

In this section, we shift our focus to out-of-sample comparisons. Since the DHNG model nests the CHNG model as a special case, it naturally achieves a higher in-sample log-likelihood. Out-of-sample comparisons are crucial to determine whether the improved in-sample performance

¹⁹The ad-hoc model is therefore internally inconsistent. Additionally, the ad-hoc model only leads to a minuscule improvement in the empirical fit, as the log-likelihood for option prices improves by only about 0.1 units.

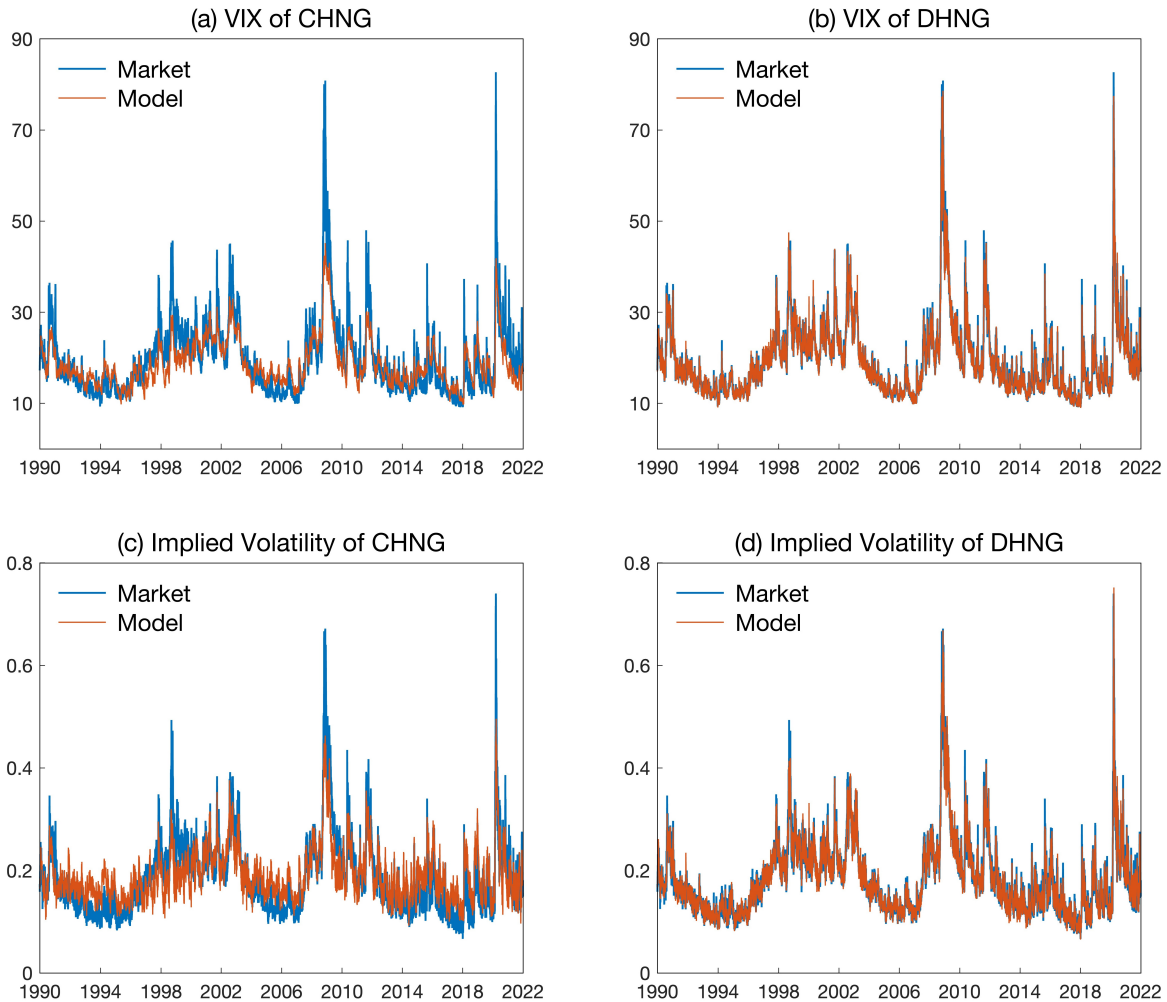


Figure 6: This figure displays the full-sample time series of the daily model-based (red lines) and market-based (blue lines) VIX and average implied volatility. The CHNG and DHNG models are estimated with VIX data in the upper panels and option prices in the lower panels. Model parameters are based on the Table 3.

Alt text: Comparison of model-based and market-based values for the VIX and average implied volatility over time. The figure presents results for both the CHNG and DHNG models, estimated using VIX data in the upper panels and option prices in the lower panels. DHNG provides a closer match to market values.

Table 5: Out-of-sample VIX and Option Pricing

Model	CHNG [VIX]	CHNG [Opt]	DHNG [VIX]	DHNG [Opt]
<i>A: RMSE for VIX Pricing</i>				
Out-of-Sample	18.33	19.60	4.782	10.03
<i>B: RMSE for Option Pricing</i>				
Out-of-Sample	24.33	20.98	15.52	9.815
<i>Partitioned by moneyness</i>				
Delta<0.3	36.55	29.30	25.22	13.58
0.3≤Delta<0.4	31.16	25.64	21.19	11.66
0.4≤Delta<0.5	25.81	22.17	17.05	9.540
0.5≤Delta<0.6	20.56	19.05	12.62	7.145
0.6≤Delta<0.7	18.51	17.39	9.373	6.883
0.7≤Delta	16.81	15.81	8.670	9.381
<i>Partitioned by maturity</i>				
DTM<30	28.51	22.73	16.86	11.92
30≤DTM<60	25.27	21.61	15.64	8.372
60≤DTM<90	20.23	18.80	14.07	7.737
90≤DTM<120	19.73	19.22	14.34	8.809
120≤DTM<150	18.02	17.64	14.11	9.539
150≤DTM	21.33	21.02	15.27	10.62
<i>Partitioned by the level of VIX</i>				
VIX<15	32.40	24.86	17.71	10.82
15≤VIX<20	19.31	18.82	15.62	9.580
20≤VIX<25	14.41	18.11	12.99	8.233
25≤VIX<30	16.27	17.42	13.20	9.281
30≤VIX<35	18.40	17.24	13.32	9.569
35≤VIX	27.69	21.02	12.43	9.924

Note: Each model is estimated once, using data from the years 1990–2007 (in-sample). The pricing accuracy of each estimated model is evaluated out-of-sample using the remaining 14 years of data, 2008–2021, in terms of the RMSE for log prices. We also present results for subsets of options, partitioning them by moneyness (Black-Scholes Delta), days-to-maturity (DTM), and the VIX levels.

is due to overfitting or reflects the true quality of the DHNG model. We investigate whether the DHNG model also produces more accurate derivative prices in out-of-sample comparisons. The full dataset is divided into two subsamples: data from the years 1990–2007 (in-sample) are used to estimate each of the four specifications, while data from the period 2008–2021 (out-of-sample) are used to evaluate the estimated models. Similar to the in-sample comparisons, we assess and compare the models based on their root mean squared pricing errors.

We find that the out-of-sample performance of the DHNG model is just as impressive as its in-sample performance. The most accurate VIX pricing is once again achieved with the DHNG model estimated using VIX data, while the best option pricing is similarly achieved by the DHNG model estimated with option prices. Although these two specifications have similar point estimates and produce very similar paths for η_t , the small differences between the two estimated model do affect derivative pricing. Overall, the out-of-sample results are very encouraging and align closely with the in-sample findings.

Next, we turn our attention to the autocorrelations of the pricing errors.

4.5 Key Insight from Autocorrelations of Pricing Error

The autocorrelations of pricing errors offer valuable insights into the improved derivative pricing achieved by the DHNG model. The estimated DHNG models reveal substantial time variation in η_t . In contrast, the CHNG model, which relies on a constant η , tends to produce positive pricing errors when η_t is small and negative pricing errors when η_t is large. Given the high persistence of η_t , this is expected to induce autocorrelation in the pricing errors for the CHNG model, which is indeed what we observe.

Figure 7 displays the autocorrelation functions (ACF) for VIX pricing errors in the upper panels and ACFs for average option pricing errors in the lower panels, covering the full sample period. The very high and persistent ACFs for CHNG indicate that a constant η induces a high degree of predictability in the pricing errors. In stark contrast, the results for DHNG, shown in the right panels, reveal autocorrelations that are substantially closer to zero. The horizontal lines in each plot represent two standard deviations from zero. For DHNG, the autocorrelations are largely insignificant, with the exception of the first few autocorrelations in the lower-right panel.

The remarkable reduction in these autocorrelations is a clear demonstration of the adaptive nature of score-driven models. The DHNG model continuously adjusts η_t to minimize pricing errors, using the latest first-order conditions (and curvature) to determine the direction and magnitude of each adjustment. As a result, the first-order conditions are more consistently satisfied throughout the sample. In contrast, models with static parameters, such as CHNG, focus only on the average first-order condition. This approach allows for large pricing errors, as long as the positive errors are offset by negative errors. This explains why the CHNG model exhibits much larger RMSE and significant autocorrelations in its pricing errors.

4.6 Adaptive Compensation for Misspecification

The adaptive nature of the DHNG model, where parameters are adjusted according to the first-order conditions, enhances the robustness of the derivative pricing formulae against model misspecification. This robustness arises because η_t is automatically adjusted to compensate for any misspecification that would otherwise lead to increased pricing errors. While this adaptive feature is a strength of the model, it also reveals a potential drawback: misspecification can undermine the interpretation of η_t as the variance risk ratio.

Expected volatility under \mathbb{Q} can be measured accurately using observed derivative prices. However, the situation differs under \mathbb{P} , where we must rely on a model to estimate expected volatility. If the model is misspecified, the resulting model-based expected volatility may be biased. One common form of misspecification is parameter instability. [Sichert \(2022\)](#) demonstrates that a GARCH model with structural breaks can resolve the pricing kernel puzzle related to the inverted U-shape. This explanation is further explored in the empirical analysis by [Tong et al. \(2022\)](#), where they estimate a Markov switching Realized GARCH model with two states. Their findings show significant U-shaped pricing kernels in the high-volatility regime, which aligns with our results. However, the positive variance risk premium (associated with the inverted U-shaped pricing kernel) they observed in the low-volatility regime is close to zero and statistically insignificant.

If the model-based expected volatility is biased, this bias will affect η_t , meaning η_t may not accurately reflect the true variance risk ratio. For example, a small η_t might not indicate an investor's appetite for variance risk; instead, it could be an artifact of the Heston-Nandi

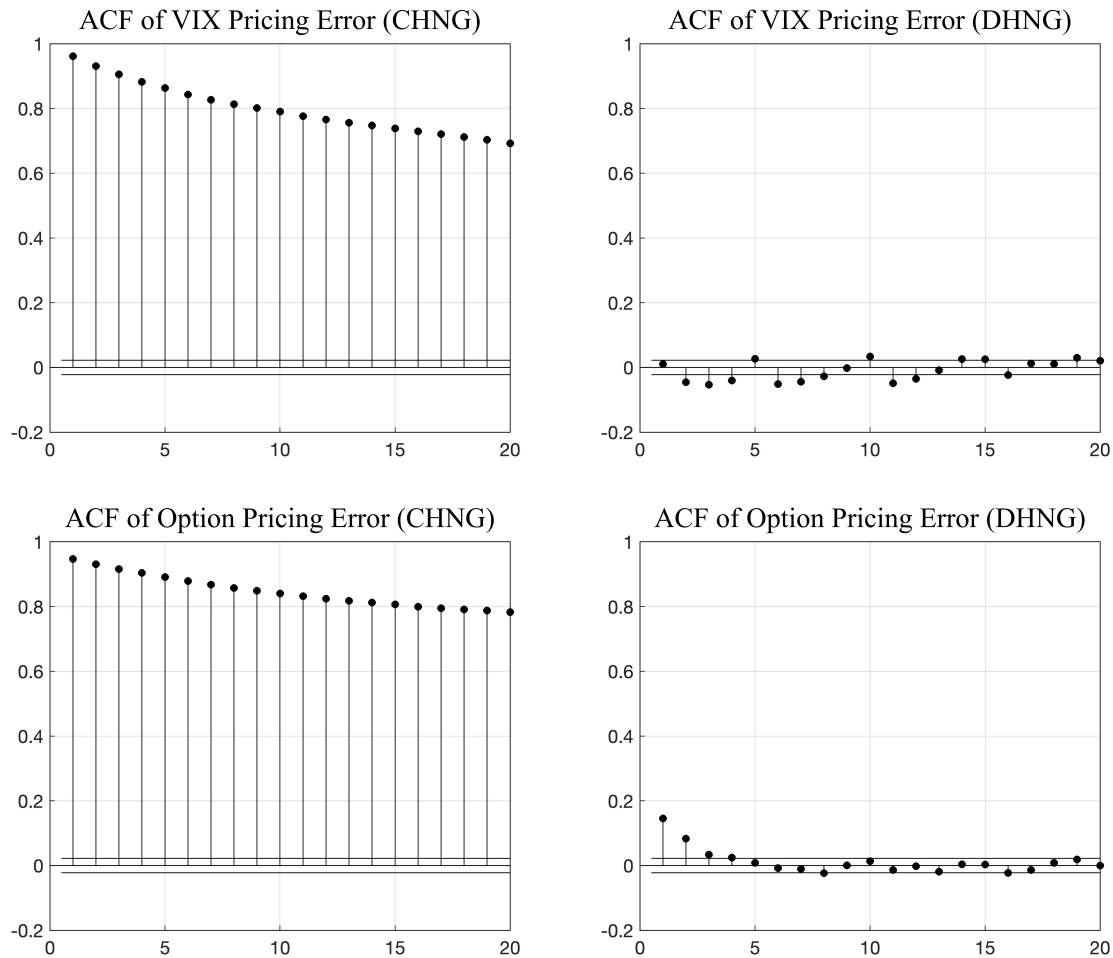


Figure 7: The autocorrelation function (ACF) for derivative pricing errors over the full sample period (January 1990 to December 2021). The ACFs for the VIX are shown in the upper panels, and the ACFs for the average option pricing errors are shown in the lower panels. The CHNG and DHNG models are estimated with VIX data in the upper panels and option prices in the lower panels. Model parameters are based on the Table 3.

Alt text: Autocorrelation functions (ACFs) of derivative pricing errors over the full sample period (1990–2021) for the CHNG and DHNG models. DHNG exhibits vastly smaller autocorrelations for both VIX pricing errors and average option pricing errors, consistent with improved pricing accuracy.

model overestimating future volatility relative to actual expectations under \mathbb{P} .

As a robustness check, we computed an alternative VRR that does not rely on the Heston-Nandi GARCH model. This alternative measure is based on model-free realized variances and uses a simple AR(1) model to define expected variance under \mathbb{P} . The resulting time series of this alternative VRR, reported in Appendix S.2, closely resembles that of η_t in Figure 5. This similarity suggests that the observed fluctuations in η_t are not driven by a flaw specific to the GARCH model (1)-(2). However, an oversimplified description of how expected volatility evolves can be the cause. The AR(1) model and standard GARCH models both produce volatility forecasts with mean-reverting characteristics.

Regarding misspecification as a potential source of time variation in η_t , we generated scatterplots of pricing errors against η_t . These scatterplots do not suggest a systematic relationship between pricing errors and η_t ; see Figure S.2 in Appendix S.2.

5 Variance Risk Aversion and Economic Fundamentals

Time variation in volatility risk aversion is the key characteristic of the new pricing kernel. In this section, we relate the time variation in η_t to economic fundamentals and several other variables that are widely used in the asset pricing literature.

We focus on seven core measures of uncertainty, disagreement, and sentiment. The first set of variables is related to investor disagreements. Following [Bollerslev et al. \(2018\)](#), we use two types of proxies for disagreement. The first concerns macroeconomic fundamentals, for which we use the forecast dispersion for both the unemployment rate and GDP growth from the Survey of Professional Forecasters.²⁰ The second proxy is disagreement about economic policy, for which we adopt the *Economic Policy Uncertainty* index by [Baker et al. \(2016\)](#).

We also include the *variance risk premium* (VRP) by [Carr and Wu \(2008\)](#), which [Grith et al. \(2017\)](#) suggest serves as a proxy for market uncertainty. Additionally, we incorporate three uncertainty measures from existing literature: the *Economic Uncertainty Index* by [Bali et al. \(2014\)](#), the *Survey-based Uncertainty Index* by [Ozturk and Sheng \(2018\)](#);²¹ and the

²⁰[Bollerslev et al. \(2018\)](#) only use the forecast dispersion for the one-quarter-ahead unemployment rate.

²¹This index is constructed from the Consensus Forecasts publication by Consensus Economics Inc. The authors provide data up to October 2021, and we fill in the values for the last two months using a simple predictive regression on all our explanatory variables.

well-known *Sentiment* variable by [Baker and Wurgler \(2006\)](#).

In addition to these seven core variables, we include the economic variables previously used in [Baker and Wurgler \(2006\)](#) and [Welch and Goyal \(2007\)](#), which we label as “control variables”. Most variables are available at a monthly frequency. Therefore, we take the monthly average of η_t and regress the logarithmically transformed average on the variables listed above, as well as subsets of these variables.

The full-sample monthly regression results are presented in [Table 6](#). The seven core variables are listed at the top of the table, followed by the six control variables that contributed the most to explaining variation in η_t . There are eleven additional control variables, labeled “Other Controls”, which were largely insignificant.²² To conserve space, the results for all control variables (along with their labels) are presented in the [Appendix S.4](#).

The first column in [Table 6](#) corresponds to the specification that includes only the control variables, which explain 70.9% of the variation in the monthly average of η . The six most significant control variables are stock market volatility, the dividend-price ratio, and four variables related to interest rates and credit risk.

Columns two through eight present the results for specifications that include a single core variable in addition to the control variables. Every core variable is significant in these regressions, and the signs of their estimated coefficients align with expectations. The sentiment variable has a negative coefficient, indicating that low sentiment is associated with high volatility risk aversion. The five uncertainty-related variables all have positive coefficients, suggesting that high uncertainty is associated with high volatility aversion.

Finally, the variance risk premium is an empirical measure of the difference between volatility under \mathbb{Q} and \mathbb{P} . As expected, this variable has a positive coefficient and contributes the most to the increase in R^2 . The last column shows the results for a “kitchen sink regression” that includes all explanatory variables. Most of the variables in [Table 6](#) remain significant in this regression, and the R^2 increases to nearly 87%. However, three core variables—Forecast Dispersion of Unemployment, Forecast Dispersion of GDP Growth, and the Economic Uncer-

²²We follow [Welch and Goyal \(2007\)](#) in the definitions of these variables. For instance, the yield spread is the difference between BAA- and AAA-rated corporate bond yields, and the default return spread is the difference between the return on long-term corporate bonds and government bonds. See [Welch and Goyal \(2007\)](#) for more details.

Table 6: Economic Explanation for Time-Varying Variance Risk Aversion

	Log Variance Risk Ratio (Monthly Average)								
	(1)	(2)	(3)	(4)	(5)	(6)	(7)	(8)	(9)
Sentiment		-0.095*** (0.026)							-0.093*** (0.020)
Dispersion-UNEMP			0.139*** (0.052)						0.008 (0.044)
Dispersion-GDP				0.176*** (0.040)					0.050 (0.049)
Economic Policy Uncertainty					0.380*** (0.060)				0.208*** (0.045)
Survey-based Uncertainty						0.148*** (0.026)			0.078*** (0.025)
Economic Uncertainty Index							0.071*** (0.009)		0.013 (0.009)
Variance Risk Premium								0.120*** (0.014)	0.096*** (0.012)
Stock Market Volatility	0.394*** (0.042)	0.395*** (0.041)	0.368*** (0.043)	0.356*** (0.043)	0.294*** (0.039)	0.363*** (0.042)	0.354*** (0.041)	0.395*** (0.029)	0.306*** (0.029)
Default Yield Spread	0.385*** (0.090)	0.358*** (0.091)	0.372*** (0.088)	0.365*** (0.087)	0.393*** (0.078)	0.282*** (0.087)	0.246*** (0.081)	0.285*** (0.067)	0.196*** (0.058)
Default Return Spread	0.026*** (0.008)	0.027*** (0.008)	0.025*** (0.007)	0.025*** (0.007)	0.019*** (0.007)	0.024*** (0.007)	0.021*** (0.007)	0.026*** (0.006)	0.020*** (0.005)
Long Term Yield	0.028** (0.013)	0.030** (0.013)	0.040*** (0.013)	0.043*** (0.012)	0.077*** (0.012)	0.016 (0.011)	0.045*** (0.010)	0.035*** (0.010)	0.063*** (0.010)
Dividend Price Ratio	-0.457*** (0.132)	-0.435*** (0.127)	-0.525*** (0.130)	-0.529*** (0.129)	-0.638*** (0.117)	-0.463*** (0.133)	-0.403*** (0.122)	-0.354*** (0.091)	-0.471*** (0.085)
Term Spread	-0.031* (0.018)	-0.040** (0.017)	-0.020 (0.018)	-0.018 (0.018)	-0.035** (0.015)	-0.031* (0.018)	-0.030* (0.016)	-0.011 (0.012)	-0.022* (0.012)
Other Controls	YES	YES	YES	YES	YES	YES	YES	YES	YES
R^2	0.709	0.722	0.722	0.732	0.756	0.741	0.761	0.817	0.866
$\rho(1)$	0.607	0.579	0.620	0.628	0.612	0.626	0.584	0.326	0.383

Note: The full-sample monthly regression results from January 1990 to December 2021, and the dependent variable is logarithm of monthly averaged variance risk ratio estimated by option prices (the last column of Table 3). The control variables are from Welch and Goyal (2007) and Baker and Wurgler (2006). "Other Controls" refer to six macro variables that control for macroeconomic conditions (monthly growth rate of industrial production, real durables consumption, real nondurables consumption, real services consumption, employment, and the NBER recession indicator) and five financial variables (earnings-to-price ratio, book-to-market ratio, net equity expansion, long-term rate of return, and the consumer price index). Most of these additional control variables are insignificant. Newey-West standard errors are reported in parentheses. $\rho(1)$ the first-order autocorrelation for residuals.

tainty Index—become insignificant in the kitchen sink regression, possibly due to collinearity, as the first two and the last two variables exhibit the highest correlations among all core variables (88.6% and 54.8%), respectively.

6 Summary

We have introduced a novel option pricing model based on a flexible pricing kernel with time-varying risk aversion. This model, denoted DHNG, offers an elegant and tractable framework when combined with the Heston-Nandi GARCH model. The variance risk ratio, η_t , emerges as the fundamental variable that captures all time variation in the pricing kernel. This ratio is functionally linked to the variance risk aversion parameter, which defines the curvature of the pricing kernel, and the framework can generate the empirically observed shapes of the pricing kernel. Additionally, η_t is closely related to a range of well-known measures of sentiment, disagreement, uncertainty, and other key economic variables.

Under the assumptions characterizing the DHNG model, we derived a closed-form expression for the VIX and an approximate option pricing formula. This formula is based on a novel approximation method that can yield affine-type pricing formulae for non-affine models. The method has proven to be highly accurate in simulation studies. Our comprehensive empirical analysis demonstrated that DHNG significantly reduces derivative pricing errors. Specifically, DHNG typically reduces the root mean square error of pricing errors by more than 50% compared to the CHNG models where η_t is constant. This substantial reduction in pricing errors is observed both in-sample and out-of-sample.

The time-varying pricing kernel can also be combined with other GARCH models, such as EGARCH, GJR-GARCH, and NGARCH, see [Nelson \(1991\)](#), [Glosten et al. \(1993\)](#), and [Engle and Ng \(1993\)](#), as well as volatility models that utilize realized measures of volatility, such as Realized GARCH models by [Hansen et al. \(2012\)](#) and [Hansen and Huang \(2016\)](#), the GARV model by [Christoffersen et al. \(2014\)](#), and the LHARG, see [Majewski et al. \(2015\)](#). For some of these models, such as GARV and LHARG, it is possible to define an Auxiliary models with an affine MGF, and it may be possible to establish closed-form option pricing expressions with the approximation method we have proposed in this paper. Other approximation methods,

such as that by [Duan et al. \(1999\)](#), may be applicable to the non-affine models.

Analytical results are generally easier to establish in continuous-time models, such as those by [Heston \(1993\)](#) and [Cox et al. \(1985\)](#), which partly explains their popularity among practitioners. However, the discrete-time HNG model also offers an analytical option pricing formula, and we successfully derived an analytical option pricing formula for our discrete-time model using the new approximation method. In contrast, obtaining analytical results in a continuous-time framework with a time-varying VRR would be highly challenging due to the non-affine structure. Additionally, the estimation process would be further complicated by the presence of the latent variable η_t . The key advantage of discrete-time GARCH models over stochastic volatility models lies in their relative ease of estimation. This is particularly beneficial in empirical studies involving a large number of options. Our empirical implementation of the DHNG model retains a straightforward analytical log-likelihood function, which greatly simplifies the estimation process.

References

- Aït-Sahalia, Y. and Lo, A. W. (2000). Nonparametric risk management and implied risk aversion. *Journal of Econometrics*, 94:9–51.
- Andersen, T. G., Bollerslev, T., Diebold, F. X., and Labys, P. (2003). Modeling and Forecasting Realized Volatility. *Econometrica*, 71:579–625.
- Andries, M., Eisenbach, T. M., and Schmalz, M. C. (2018). Horizon-dependent risk aversion and the timing and pricing of uncertainty. *FRB of New York Staff Report*, (703).
- Arrow, K. J. and Debreu, G. (1954). Existence of an equilibrium for a competitive economy. *Econometrica*, 22:265–290.
- Baker, M. and Wurgler, J. (2006). Investor sentiment and the cross-section of stock returns. *The journal of Finance*, 61:1645–1680.
- Baker, S. R., Bloom, N., and Davis, S. J. (2016). Measuring economic policy uncertainty. *The quarterly journal of economics*, 131:1593–1636.

- Bakshi, G., Cao, C., and Chen, Z. (1997). Empirical performance of alternative option pricing models. *The Journal of Finance*, 52:2003–2049.
- Bakshi, G. and Madan, D. (2008). Investor heterogeneity and the non-monotonicity of the aggregate marginal rate of substitution in the market index. *Unpublished working paper, University of Maryland*.
- Bakshi, G., Madan, D., and Panayotov, G. (2010). Returns of claims on the upside and the viability of u-shaped pricing kernels. *Journal of Financial Economics*, 97:130–154.
- Bali, T. G., Brown, S. J., and Caglayan, M. O. (2014). Macroeconomic risk and hedge fund returns. *Journal of Financial Economics*, 114:1–19.
- Bali, T. G. and Zhou, H. (2016). Risk, uncertainty, and expected returns. *Journal of Financial and Quantitative Analysis*, 51:707–735.
- Barone-Adesi, G., Engle, R. F., and Mancini, L. (2008). A GARCH option pricing model with filtered historical simulation. *Review of Financial Studies*, 21:1223–1258.
- Beare, B. K. and Schmidt, L. D. (2016). An empirical test of pricing kernel monotonicity. *Journal of Applied Econometrics*, 31:338–356.
- Bekaert, G., Engstrom, E. C., and Xu, N. R. (2020). The time variation in risk appetite and uncertainty. *NBER*.
- Blasques, F., Koopman, S. J., and Lucas, A. (2015). Information-theoretic optimality of observation-driven time series models for continuous responses. *Biometrika*, 102:325–343.
- Bollerslev, T. (1986). Generalized autoregressive heteroskedasticity. *Journal of Econometrics*, 31:307–327.
- Bollerslev, T., Li, J., and Xue, Y. (2018). Volume, volatility, and public news announcements. *The Review of Economic Studies*, 85:2005–2041.
- Bollerslev, T., Tauchen, G., and Zhou, H. (2009). Expected Stock Returns and Variance Risk Premia. *The Review of Financial Studies*, 22:4463–4492.

- Broadie, M., Chernov, M., and Johannes, M. (2007). Model specification and risk premia: Evidence from futures options. *The Journal of Finance*, 62:1453–1490.
- Brown, D. P. and Jackwerth, J. C. (2012). The pricing kernel puzzle: Reconciling index option data and economic theory. In *Derivative Securities Pricing and Modelling*, pages 155–183. Emerald Group Publishing Limited.
- Campbell, J. Y. and Cochrane, J. H. (1999). By force of habit: A consumption-based explanation of aggregate stock market behavior. *Journal of political Economy*, 107:205–251.
- Carr, P. and Wu, L. (2008). Variance Risk Premiums. *The Review of Financial Studies*, 22:1311–1341.
- Chabi-Yo, F. (2012). Pricing kernels with stochastic skewness and volatility risk. *Management Science*, 58:624–640.
- Chabi-Yo, F., Garcia, R., and Renault, E. (2008). State dependence can explain the risk aversion puzzle. *Review of Financial Studies*, 21:973–1011.
- Chabi-Yo, F. and Song, Z. (2013). Recovering the probability weights of tail events with volatility risk from option prices. Technical report, Working Paper, Ohio State University.
- Chen, X. and Ghysels, E. (2011). News – good or bad – and its impact on volatility predictions over multiple horizons. *Review of Financial Studies*, 24:46–81.
- Chernov, M. and Ghysels, E. (2000). A study towards a unified approach to the joint estimation of objective and risk neutral measures for the purpose of options valuation. *Journal of Financial Economics*, 56:407–458.
- Christoffersen, P., Feunou, B., Jacobs, K., and Meddahi, N. (2014). The economic value of realized volatility: Using high-frequency returns for option valuation. *Journal of Financial and Quantitative Analysis*, 49:663–697.
- Christoffersen, P., Heston, S. L., and Jacobs, K. (2013). Capturing option anomalies with a variance-dependent pricing kernel. *Review of Financial Studies*, 26:1963–2006.

- Corsi, F., Fusari, N., and Vecchia, D. L. (2013). Realizing smiles: Options pricing with realized volatility. *Journal of Financial Economics*, 107:284–304.
- Cox, J. C., Ingersoll, J. E., and Ross, S. A. (1985). A theory of the term structure of interest rates. *Econometrica*, 53:385–408.
- Creal, D., Koopman, S. J., and Lucas, A. (2013). Generalized autoregressive score models with applications. *Journal of Applied Econometrics*, 28:777–795.
- Cuesdeanu, H. and Jackwerth, J. C. (2018). The pricing kernel puzzle in forward looking data. *Review of Derivatives Research*, 21:253–276.
- Duan, J.-C. (1995). The GARCH option pricing model. *Mathematical finance*, 5:13–32.
- Duan, J.-C., Gauthier, G., and Simonato, J. (1999). An analytical approximation for the GARCH option pricing model. *Journal of Computational Finance*, 2:75–116.
- Eisenbach, T. M. and Schmalz, M. C. (2016). Anxiety in the face of risk. *Journal of Financial Economics*, 121:414–426.
- Engle, R. F. (1982). Autoregressive conditional heteroskedasticity with estimates of the variance of U.K. inflation. *Econometrica*, 45:987–1007.
- Engle, R. F. and Ng, V. K. (1993). Measuring and Testing the Impact of News on Volatility. *Journal of Finance*, 48:1749–78.
- Feller, W. (1951). Two singular diffusion problems. *Annals of mathematics*, pages 173–182.
- Feunou, B. and Okou, C. (2019). Good volatility, bad volatility, and option pricing. *Journal of Financial and Quantitative Analysis*, 54:695–727.
- Glosten, L. R., Jagannathan, R., and Runkle, D. E. (1993). On the Relation between the Expected Value and the Volatility of the Nominal Excess Return on Stocks. *Journal of Finance*, 48:1779–1801.
- González, M., Nave, J., and Rubio, G. (2018). Macroeconomic determinants of stock market betas. *Journal of Empirical Finance*, 45:26–44.

- Grith, M., Härdle, W. K., and Krätschmer, V. (2017). Reference-dependent preferences and the empirical pricing kernel puzzle. *Review of Finance*, 21:269–298.
- Han, B. (2008). Investor sentiment and option prices. *The Review of Financial Studies*, 21:387–414.
- Hansen, L. P. and Renault, E. (2010). Pricing kernels. In *Encyclopedia of Quantitative Finance*, volume 3, pages 1418–1428. John Wiley & Sons, Ltd.
- Hansen, P. R. and Huang, Z. (2016). Exponential GARCH modeling with realized measures of volatility. *Journal of Business and Economic Statistics*, 34:269–287.
- Hansen, P. R., Huang, Z., and Shek, H. (2012). Realized GARCH: A joint model of returns and realized measures of volatility. *Journal of Applied Econometrics*, 27:877–906.
- Hansen, P. R. and Tong, C. (2024). Moments by integrating the moment-generating function. *arXiv:2410.23587*, [econ.EM].
- Hao, J. and Zhang, J. E. (2013). GARCH option pricing models, the CBOE VIX, and variance risk premium. *Journal of Financial Econometrics*, 11:556–580.
- Heston, S. L. (1993). A closed-form solution for options with stochastic volatility with applications to bond and currency options. *Review of Financial Studies*, 6:327–343.
- Heston, S. L. and Nandi, S. (2000). A closed-form GARCH option valuation model. *Review of Financial Studies*, 13:585–625.
- Huang, Z., Wang, T., and Hansen, P. R. (2017). Option pricing with the realized GARCH model: An analytical approximation approach. *Journal of Futures Markets*, 37:328–358.
- Jackwerth, J. C. (2000). Recovering risk aversion from option prices and realized returns. *The Review of Financial Studies*, 13:433–451.
- Kiesel, R. and Rahe, F. (2017). Option pricing under time-varying risk-aversion with applications to risk forecasting. *Journal of Banking & Finance*, 76:120–138.

- Koopman, S. J., Lucas, A., and Scharth, M. (2016). Predicting time-varying parameters with parameter-driven and observation-driven models. *Review of Economics and Statistics*, 98:97–110.
- Li, G. (2007). Time-varying risk aversion and asset prices. *Journal of Banking & Finance*, 31:243–257.
- Lucas, R. E. (1978). Asset prices in an exchange economy. *Econometrica*, 46:1429–1445.
- Majewski, A. A., Bormetti, G., and Corsi, F. (2015). Smile from the past: A general option pricing framework with multiple volatility and leverage components. *Journal of Econometrics*, 187:521–531.
- Nelson, D. B. (1991). Conditional heteroskedasticity in asset returns: A new approach. *Econometrica*, 59:347–370.
- Ornthanalai, C. (2014). Levy jump risk: Evidence from options and returns. *Journal of Financial Economics*, 112:69–90.
- Ozturk, E. O. and Sheng, X. S. (2018). Measuring global and country-specific uncertainty. *Journal of International Money and Finance*, 88:276–295.
- Polkovnichenko, V. and Zhao, F. (2013). Probability weighting functions implied in options prices. *Journal of Financial Economics*, 107:580–609.
- Rosenberg, J. V. and Engle, R. F. (2002). Empirical pricing kernels. *Journal of Financial Economics*, 64:341–372.
- Rubinstein, M. (1976). The valuation of uncertain income streams and the pricing of options. *Bell Journal of Economics*, 7:407–425.
- Shefrin, H. (2001). On kernels and sentiment. *Available at SSRN 288258*.
- Shefrin, H. (2008). Risk and return in behavioral SDF-based asset pricing models. *Journal of Investment Management*, 6:1–18.
- Sichert, T. (2022). The pricing kernel is U-shaped. *Working Paper*.

- Song, Z. and Xiu, D. (2016). A tale of two option markets: Pricing kernels and volatility risk. *Journal of Econometrics*, 190:176–196.
- Tong, C., Hansen, P. R., and Huang, Z. (2022). Option pricing with state-dependent pricing kernel. *Journal of Futures Prices*, 42:1409–1433.
- Wang, T., Shen, Y., Jiang, Y., and Huang, Z. (2017). Pricing the CBOE VIX futures with the Heston–Nandi GARCH model. *Journal of Futures Markets*, 37(7):641–659.
- Welch, I. and Goyal, A. (2007). A comprehensive look at the empirical performance of equity premium prediction. *The Review of Financial Studies*, 21:1455–1508.

A Appendix of Proofs

A.1 Proof of Theorem 1

The pricing kernel with dynamic risk parameters takes the form

$$M_{t+1,t} = \frac{\exp(\phi_t R_{t+1} + \xi_t h_{t+2})}{\mathbb{E}_t^{\mathbb{P}}[\exp(\phi_t R_{t+1} + \xi_t h_{t+2})]},$$

where the parameters ϕ_t and ξ_t are \mathcal{G}_t -measurable. The pricing kernel implies some dynamic properties in risk-neutral measure satisfying the no-arbitrage conditions: $\mathbb{E}_t^{\mathbb{P}}[M_{t+1,t}] = 1$ and $\mathbb{E}_t^{\mathbb{P}}[M_{t+1,t} \exp(R_{t+1})] = \exp(r)$. The first is trivial, whereas the second condition reads

$$\frac{\mathbb{E}_t^{\mathbb{P}}[\exp\{(\phi_t + 1)R_{t+1} + \xi_t h_{t+2}\}]}{\mathbb{E}_t^{\mathbb{P}}[\exp(\phi_t R_{t+1} + \xi_t h_{t+2})]} = \exp(r). \quad (\text{A.1})$$

The MGF of (R_{t+1}, h_{t+2}) under \mathbb{P} is

$$\begin{aligned} & \mathbb{E}_t^{\mathbb{P}}[\exp(v_1 R_{t+1} + v_2 h_{t+2})] \\ &= \exp\left[v_1 r + v_2 \omega + \left[v_1\left(\lambda - \frac{1}{2}\right) + v_2(\beta + \alpha\gamma^2)\right]h_{t+1}\right] \times \mathbb{E}_t^{\mathbb{P}}\left[\exp\left(v_2 \alpha z_{t+1}^2 + (v_1 - 2v_2 \alpha \gamma)\sqrt{h_{t+1}} z_{t+1}\right)\right] \\ &= \exp\left[v_1 r + v_2 \omega + \left[v_1\left(\lambda - \frac{1}{2}\right) + v_2(\beta + \alpha\gamma^2)\right]h_{t+1} - \frac{1}{2} \log(1 - 2v_2 \alpha) + \frac{(v_1 - 2v_2 \alpha \gamma)^2}{2(1 - 2v_2 \alpha)} h_{t+1}\right] \\ &= \exp\left[v_1 r + v_2 \omega - \frac{1}{2} \log(1 - 2v_2 \alpha) + \left(v_1\left(\lambda - \frac{1}{2}\right) + v_2(\beta + \alpha\gamma^2) + \frac{(v_1 - 2v_2 \alpha \gamma)^2}{2(1 - 2v_2 \alpha)}\right) h_{t+1}\right] \quad (\text{A.2}) \end{aligned}$$

Substituting $(\phi_{t+1} + 1, \xi_t)$ and (ϕ_{t+1}, ξ_t) for (v_1, v_2) and taking their ratio, reveals that (A.1) simplifies to $[\lambda - \frac{1}{2} + \frac{1+2\phi_t-4\xi_t\alpha\gamma}{2(1-2\xi_t\alpha)}]h_{t+1} = 0$. Next, solving for λ yields

$$\lambda = \eta_t \left(\gamma - \phi_t - \frac{1}{2}\right) - \gamma + \frac{1}{2}, \quad \text{where } \eta_t \equiv \frac{1}{1 - 2\alpha\xi_t}, \quad (\text{A.3})$$

and the results stated in part (i) of Theorem 1 are established.

The risk-neutral dynamic is deduced from the MGF of z_{t+1} under the \mathbb{Q} measure is:

$$\begin{aligned} \mathbb{E}_t^{\mathbb{Q}}[\exp(v_1 z_{t+1})] &= \exp\left[\left(\frac{\phi_t - 2\xi_t \alpha \gamma}{1 - 2\xi_t \alpha} \sqrt{h_{t+1}}\right) v_1 + \frac{1}{2(1 - 2\xi_t \alpha)} v_1^2\right] \\ &= \exp\left[\left[-\left(\lambda + \frac{1}{2}\eta_t - \frac{1}{2}\right) \sqrt{h_{t+1}}\right] v_1 + \frac{1}{2}\eta_t v_1^2\right] \quad (\text{A.4}) \end{aligned}$$

The last equality comes from (A.3). The expression (A.4) shows that z_{t+1} is also normally distributed under \mathbb{Q} , but with a different mean and a different variance (than under \mathbb{P}). So

we define

$$z_{t+1}^* = \frac{z_{t+1} - \mathbb{E}_t^{\mathbb{Q}}(z_{t+1})}{\sqrt{\text{var}_t^{\mathbb{Q}}(z_{t+1})}} = \frac{1}{\sqrt{\eta_t}} \left(z_{t+1} + \left(\lambda + \frac{1}{2}\eta_t - \frac{1}{2} \right) \sqrt{h_{t+1}} \right),$$

such that $z_t^* | \mathcal{G}_t \sim iid N(0, 1)$ under \mathbb{Q} . Substituting the risk-neutralized quantities, z_{t+1}^* and $h_{t+1}^* = \eta_t h_{t+1}$ into (1), we arrive at the expressions stated in part (ii). Finally, part (iii) is an implication of the MGF for z_{t+1} under \mathbb{Q} , see (A.4). \square

A.2 Proof of Lemma 1

Using (A.2), the pricing kernel in (4) can be expressed as

$$\log M_{t+1,t} = \delta_t + \phi_t (R_{t+1} - r) + \theta_t h_{t+1} + \xi_t h_{t+2},$$

where $\theta_t = - \left(\phi_t \left(\lambda - \frac{1}{2} \right) + \xi_t (\beta + \alpha \gamma^2) + \frac{(\phi_t - 2\xi_t \alpha \gamma)^2}{2(1 - 2\xi_t \alpha)} \right)$ and $\delta_t = -\xi_t \omega + \frac{1}{2} \log(1 - 2\xi_t \alpha)$.

Using the expression of h_{t+2} , we have

$$\begin{aligned} \log M_{t+1,t} &= \delta_t + \phi_t (R_{t+1} - r) + \theta_t h_{t+1} + \xi_t \left(\omega + \beta h_{t+1} + \alpha \left(z_{t+1} - \gamma \sqrt{h_{t+1}} \right)^2 \right) \\ &= [\delta_t + \xi_t \omega] + \phi_t (R_{t+1} - r) + (\theta_t + \xi_t \beta) h_{t+1} + \frac{\xi_t \alpha}{h_{t+1}} \left(R_{t+1} - r - \left(\lambda - \frac{1}{2} + \gamma \right) h_{t+1} \right)^2 \\ &= [\delta_t + \xi_t \omega] + \phi_t (R_{t+1} - r) + (\theta_t + \xi_t \beta) h_{t+1} + \frac{\xi_t \alpha}{h_{t+1}} (R_{t+1} - r)^2 \\ &\quad + \frac{\xi_t \alpha}{h_{t+1}} \left(\lambda - \frac{1}{2} + \gamma \right)^2 h_{t+1}^2 - 2 \frac{\xi_t \alpha}{h_{t+1}} (R_{t+1} - r) \left(\lambda - \frac{1}{2} + \gamma \right) h_{t+1} \\ &= \kappa_{0,t} + \kappa_{1,t} h_{t+1} + \kappa_{2,t} (R_{t+1} - r) + \frac{\xi_t \alpha}{h_{t+1}} (R_{t+1} - r)^2, \end{aligned}$$

where $\kappa_{0,t} = \delta_t + \xi_t \omega = \frac{1}{2} \log(1 - 2\xi_t \alpha) = -\frac{1}{2} \log \eta_t$, and $\kappa_{2,t} = \phi_t - 2\alpha \xi_t \left(\lambda - \frac{1}{2} + \gamma \right) = -\lambda$, where we used that $\lambda = \frac{1}{1 - 2\alpha \xi_t} \left(\gamma - \phi_t - \frac{1}{2} \right) - \gamma + \frac{1}{2}$, see (A.3), and

$$\begin{aligned} \kappa_{1,t} &= \theta_t + \xi_t \beta + \xi_t \alpha \left(\lambda - \frac{1}{2} + \gamma \right)^2 \\ &= \theta_t + \xi_t \left(\beta + \alpha \gamma^2 \right) + \xi_t \alpha \left(\lambda - \frac{1}{2} \right)^2 + 2\xi_t \alpha \gamma \left(\lambda - \frac{1}{2} \right) \\ &= -\phi_t \left(\lambda - \frac{1}{2} \right) + \xi_t \alpha \left(\lambda - \frac{1}{2} \right)^2 + 2\xi_t \alpha \gamma \left(\lambda - \frac{1}{2} \right) - \frac{(\phi_t - 2\xi_t \alpha \gamma)^2}{2(1 - 2\xi_t \alpha)} \\ &= -\alpha \xi_t \left(\lambda - \frac{1}{2} \right)^2 + \lambda \left(\lambda - \frac{1}{2} \right) - \frac{\left(\lambda - 2\xi_t \alpha \left(\lambda - \frac{1}{2} \right) \right)^2}{2(1 - 2\xi_t \alpha)} \\ &= \frac{1}{2} (1 - 2\alpha \xi_t) \left(\lambda - \frac{1}{2} \right)^2 - \frac{1}{2} \left(\lambda - \frac{1}{2} \right)^2 + \lambda \left(\lambda - \frac{1}{2} \right) - \frac{1}{2} \left[\frac{1}{\eta_t} \left(\lambda - \frac{1}{2} \right)^2 + \frac{1}{4} \eta_t + \left(\lambda - \frac{1}{2} \right) \right] \\ &= -\frac{1}{8} \eta_t + \frac{1}{2} \left(\lambda - \frac{1}{2} \right)^2. \end{aligned}$$

A.3 Proof of Theorem 2

We rewrite the volatility dynamic under \mathbb{Q} measure as

$$h_{t+1}^* = (\omega_t^* + \alpha_t^*) + (\beta_t^* + \alpha_t^* \gamma_{t-1}^{*2}) h_t^* + \nu_t,$$

where $\nu_t = \alpha_t^* ((z_t^*)^2 - 1 - 2\gamma_{t-1}^* z_t^* \sqrt{h_t^*})$ is a zero-mean variation condition on \mathcal{G}_{t-1} due to the facts that $z_t^* | \mathcal{G}_{t-1} \stackrel{\mathbb{Q}}{\sim} iid N(0, 1)$, and the independence between ε_t and z_t .

We denote $A_t \equiv \omega_t^* + \alpha_t^*$ and $B_t \equiv \beta_t^* + \alpha_t^* \gamma_{t-1}^{*2}$, then we have

$$\begin{aligned} h_{t+k}^* &= A_{t+k-1} + B_{t+k-1} h_{t+k-1}^* + \nu_{t+k-1} \\ &= A_{t+k-1} + B_{t+k-1} A_{t+k-2} + B_{t+k-1} B_{t+k-2} h_{t+k-2}^* + B_{t+k-1} \nu_{t+k-2} + \nu_{t+k-1} \\ &= A_{t+k-1} + B_{t+k-1} A_{t+k-2} + \cdots + B_{t+k-1} \cdots B_{t+2} A_{t+1} + B_{t+k-1} \cdots B_{t+1} h_{t+1}^* \\ &\quad + \sum_{i=1}^{k-2} B_{t+k-1} B_{t+k-2} \cdots B_{t+i+1} \nu_{t+i} + \nu_{t+k-1}. \end{aligned}$$

In order to get its analytical formula, we replace B_t with $\tilde{B}_t \equiv \beta_t^* + \alpha_t^* \tilde{\gamma}_{t-1}^{*2}$ where $\tilde{\gamma}_t^* = \frac{1}{\eta_t}(\gamma + \lambda)$. Empirically $\tilde{\gamma}_t^*$ is indistinguishable from $\gamma_t^* = \frac{1}{\eta_t}(\gamma + \lambda + \frac{1}{2}(\eta_t - 1))$ because the magnitude of $\gamma + \lambda$ is much larger than $\frac{1}{2}(\eta_t - 1)$. Empirically we have $\gamma + \lambda \approx 253$ whereas $\frac{1}{2}(\eta_t - 1)$ ranges between -0.27 and 1.39 , with an average value of about 0.07 . Then it follows that²³

$$\tilde{B}_t = \beta_t^* + \alpha_t^* \tilde{\gamma}_{t-1}^{*2} = \beta \frac{\eta_t}{\eta_{t-1}} + \alpha \eta_t \eta_{t-1} \left(\frac{\gamma + \lambda}{\eta_{t-1}} \right)^2 = \tilde{\beta} \frac{\eta_t}{\eta_{t-1}},$$

where $\tilde{\beta} \equiv \beta + \alpha(\gamma + \lambda)^2$, so that $\tilde{B}_{t+k} \tilde{B}_{t+k-1} \cdots \tilde{B}_{t+i} = \tilde{\beta}^{k-i+1} \frac{\eta_{t+k}}{\eta_{t+i-1}}$, and

$$\tilde{B}_{t+k} \cdots \tilde{B}_{t+i+1} A_{t+i} = \tilde{\beta}^{k-i} \frac{\eta_{t+k}}{\eta_{t+i}} (\omega \eta_{t+i} + \alpha \eta_{t+i} \eta_{t+i-1}) = \tilde{\beta}^{k-i} (\omega \eta_{t+k} + \alpha \eta_{t+k} \eta_{t+i-1}).$$

Using these results, we have

$$\mathbb{E}_t^{\mathbb{Q}}(h_{t+k}^*) = \sum_{i=2}^k \tilde{\beta}^{k-i} \mathbb{E}_t^{\mathbb{Q}}(\omega \eta_{t+k-1} + \alpha \eta_{t+k-1} \eta_{t+i-2}) + \tilde{\beta}^{k-1} \mathbb{E}_t^{\mathbb{Q}}\left(\frac{\eta_{t+k-1}}{\eta_t}\right) h_{t+1}^* + \delta_k,$$

where δ_k is the term that arises from the substitution of \tilde{B}_t for B_t .

The M -days ahead VIX can be calculated as the annualized arithmetic average of the

²³Recall that $\alpha_t^* = \alpha \eta_t \eta_{t-1}$ and $\beta_t^* = \beta \frac{\eta_t}{\eta_{t-1}}$.

expected daily variance over the following month under the risk-neutral measure, i.e.,

$$\text{VIX}_t = A \times \sqrt{\frac{1}{M} \sum_{k=1}^M \mathbb{E}_t^{\mathbb{Q}}(h_{t+k}^*)}.$$

Where $A = 100\sqrt{252}$ is the annualizing factor. The model-implied squared VIX is given by,

$$\begin{aligned} \frac{A^2}{M} \sum_{k=1}^M \mathbb{E}_t^{\mathbb{Q}}(h_{t+k}^*) &= \underbrace{\frac{A^2}{M} \sum_{k=2}^M \sum_{i=2}^k \tilde{\beta}^{k-i} \mathbb{E}_t^{\mathbb{Q}}(\omega \eta_{t+k-1} + \alpha \eta_{t+k-1} \eta_{t+i-2})}_{a_1(M, \sigma^2)} \\ &+ \underbrace{\frac{A^2}{M} \sum_{k=1}^M \tilde{\beta}^{k-1} \mathbb{E}_t^{\mathbb{Q}} \left(\frac{\eta_{t+k-1}}{\eta_t} \right) h_{t+1}^*}_{a_2(M, \sigma^2)} + \Delta, \end{aligned} \quad (\text{A.5})$$

where $\Delta = \frac{A^2}{M} \sum \delta_k$. We provide bounds for the approximation error term Δ in Lemma A.1, and show that this term is negligible in practice.

For the ARMA(p, q) structure, $\log \eta_t = (1 - \sum_{i=1}^p \varphi_i) \zeta + \sum_{i=1}^p \varphi_i \log \eta_{t-i} + \sum_{j=1}^q \theta_j \varepsilon_{t-j} + \varepsilon_t$, we will show that

$$\log \eta_{t+k} = A_k + \sum_{i=1}^p B_{k,i} \log \eta_{t+1-i} + \sum_{j=1}^q C_{k,j} \varepsilon_{t+1-j} + \sum_{l=1}^k D_{k,l} \varepsilon_{t+l}, \quad (\text{A.6})$$

for $k \geq 1$, for suitable constants, A_k , $B_{k,i}$, $C_{k,j}$ and $D_{k,l}$. We show this by induction. For $k = 1$ it is easy to verify that $A_1 = (1 - \sum_{i=1}^p \varphi_i) \zeta$, $B_{1,i} = \varphi_i$, $C_{1,j} = \theta_j$ and $D_{1,1} = 1$. Suppose that (A.6) holds for $k \geq 1$, then for $k + 1$ we have

$$\begin{aligned} \log \eta_{t+k+1} &= A_k + \sum_{i=1}^p B_{k,i} \log \eta_{t+2-i} + \sum_{j=1}^q C_{k,j} \varepsilon_{t+2-j} + \sum_{l=1}^k D_{k,l} \varepsilon_{t+1+l} \\ &= A_k + B_{k,1} \log \eta_{t+1} + \sum_{i=1}^{p-1} B_{k,i+1} \log \eta_{t+1-i} + C_{k,1} \varepsilon_{t+1} + \sum_{j=1}^{q-1} C_{k,j+1} \varepsilon_{t+1-j} + \sum_{l=2}^{k+1} D_{k,l-1} \varepsilon_{t+l} \\ &= A_k + \sum_{i=1}^{p-1} B_{k,i+1} \log \eta_{t+1-i} + C_{k,1} \varepsilon_{t+1} + \sum_{j=1}^{q-1} C_{k,j+1} \varepsilon_{t+1-j} + \sum_{l=2}^{k+1} D_{k,l-1} \varepsilon_{t+l} \\ &\quad + B_{k,1} \left[\left(1 - \sum_{i=1}^p \varphi_i \right) \zeta + \sum_{i=1}^p \varphi_i \log \eta_{t+1-i} + \sum_{j=1}^q \theta_j \varepsilon_{t+1-j} + \varepsilon_{t+1} \right] \\ &= A_{k+1} + \sum_{i=1}^p B_{k+1,i} \log \eta_{t+1-i} + \sum_{j=1}^q C_{k+1,j} \varepsilon_{t+1-j} + \sum_{l=1}^{k+1} D_{k+1,l} \varepsilon_{t+l}, \end{aligned}$$

where

$$A_{k+1} = A_k + B_{k,1} \left(1 - \sum_{i=1}^p \varphi_i \right) \zeta, \quad B_{k+1,i} = \begin{cases} \varphi_i B_{k,1} + B_{k,i+1} & 1 \leq i \leq p-1, \\ \varphi_i B_{k,1} & i = p, \end{cases}$$

$$C_{k+1,j} = \begin{cases} \theta_j B_{k,1} + C_{k,j+1} & 1 \leq j \leq q-1, \\ \theta_j B_{k,1} & j = q, \end{cases} \quad D_{k+1,l} = \begin{cases} C_{k,1} + B_{k,1} & l = 1, \\ D_{k,l-1} & 2 \leq l \leq k+1. \end{cases}$$

This completes the proof of (A.6).

Suppose that ε_t is iid and let $\Psi(s) \equiv \log \mathbb{E}[\exp(s\varepsilon_t)]$ denote its log-MGF. Then we have

$$\mathbb{E}_t(\eta_{t+k}) = \exp \left\{ A_k + \sum_{i=1}^p B_{k,i} \log \eta_{t+1-i} + \sum_{j=1}^q C_{k,j} \varepsilon_{t+1-j} + \sum_{l=1}^k \Psi(D_{k,l}) \right\},$$

and for $i < k$, we have

$$\begin{aligned} \log(\eta_{t+k}\eta_{t+i}) &= A_k + A_i + \sum_{i'=1}^p (B_{k,i'} + B_{i,i'}) \log \eta_{t+1-i'} + \sum_{j=1}^q (C_{k,j} + C_{i,j}) \varepsilon_{t+1-j} \\ &\quad + \sum_{l=1}^i (D_{k,l} + D_{i,l}) \varepsilon_{t+l} + \sum_{l=i+1}^k D_{k,l} \varepsilon_{t+l}, \\ \mathbb{E}_t(\eta_{t+k}\eta_{t+i}) &= \exp \left\{ A_k + A_i + \sum_{i'=1}^p (B_{k,i'} + B_{i,i'}) \log \eta_{t+1-i'} + \sum_{j=1}^q (C_{k,j} + C_{i,j}) \varepsilon_{t+1-j} \right. \\ &\quad \left. + \sum_{l=1}^i \Psi(D_{k,l} + D_{i,l}) + \sum_{l=i+1}^k \Psi(D_{k,l}) \right\}. \end{aligned}$$

We can now compute the two key terms in (A.5).

The expression simplify in the special case with an AR(1) structure, $\log \eta_t = (1 - \varphi)\zeta + \varphi \log \eta_{t-1} + \varepsilon_t$, where $|\varphi| < 1$. It follows that $\log \eta_{t+k} = (1 - \varphi^k) \zeta + \varphi^k \log \eta_t + \sum_{j=1}^k \varphi^{k-j} \varepsilon_{t+j}$, such that, for $i < k$, we have

$$\log(\eta_{t+k}\eta_{t+i}) = (2 - \varphi^k - \varphi^i) \zeta + (\varphi^k + \varphi^i) \log \eta_t + \sum_{j=1}^i (\varphi^{k-j} + \varphi^{i-j}) \varepsilon_{t+j} + \sum_{j'=i+1}^k \varphi^{k-j'} \varepsilon_{t+j'},$$

$$\mathbb{E}_t(\eta_{t+k}) = \exp \left\{ (1 - \varphi^k) \zeta + \varphi^k \log \eta_t + \sum_{j=0}^{k-1} \Psi(\varphi^j) \right\}, \text{ and}$$

$$\mathbb{E}_t(\eta_{t+k}\eta_{t+i}) = \exp \left\{ (2 - \varphi^k - \varphi^i) \zeta + (\varphi^k + \varphi^i) \log \eta_t + \sum_{j=1}^i \Psi(\varphi^{k-j} + \varphi^{i-j}) + \sum_{j'=i+1}^k \Psi(\varphi^{k-j'}) \right\}.$$

We can therefore express the two key terms in (A.5) as,

$$a_1(M, \sigma^2) = \frac{A^2}{M} \sum_{k=2}^M \sum_{i=2}^k \tilde{\beta}^{k-i} \left[\omega \Lambda_1(k) \eta_t^{\varphi^{k-1}} + \alpha \Lambda_2(k, i) \eta_t^{\varphi^{k-1} + \varphi^{i-2}} \right],$$

and $a_2(M, \sigma^2) = \frac{A^2}{M} \sum_{k=1}^M \tilde{\beta}^{k-1} \Lambda_1(k) \eta_t^{\varphi^{k-1}-1}$, respectively, where

$$\Lambda_1(k) = \exp \left\{ \left(1 - \varphi^{k-1} \right) \zeta + \sum_{j=0}^{k-2} \Psi(\varphi^j) \right\},$$

$$\Lambda_2(k, i) = \exp \left\{ \left(2 - \varphi^{k-1} - \varphi^{i-2} \right) \zeta + \sum_{j=1}^{i-2} \Psi(\varphi^{k-1-j} + \varphi^{i-2-j}) + \sum_{j'=i-1}^{k-1} \Psi(\varphi^{k-1-j'}) \right\}.$$

If ε_t is normally distributed with zero mean and variance σ^2 , we have $\Psi(\phi) = \frac{1}{2} \sigma^2 \phi^2$. \square

Lemma A.1 (Bound for Δ). *Suppose that $\eta_t \in [\eta_L, \eta_H]$ is bounded where $\eta_L, \eta_H > 0$. Then $\Delta \leq \delta(\tilde{\beta}_{\max}) - \delta(\tilde{\beta}_{\min})$, where*

$$\delta(x) = A \times \sqrt{\frac{1}{M} \left[\sum_{k=2}^M \sum_{i=2}^k x^{k-i} \mathbb{E}_t^{\mathbb{Q}}(\omega \eta_{t+k-1} + \alpha \eta_{t+k-1} \eta_{t+i-2}) + \sum_{k=1}^M x^{k-1} \mathbb{E}_t^{\mathbb{Q}} \left(\frac{\eta_{t+k-1}}{\eta_t} \right) h_{t+1}^* \right]},$$

and $\tilde{\beta}_{\min} = \beta + \alpha(\gamma + \lambda + \frac{1}{2}(\eta_L - 1))^2$ and $\tilde{\beta}_{\max} = \beta + \alpha(\gamma + \lambda + \frac{1}{2}(\eta_H - 1))^2$.

Proof. We have $B_t = \beta_t^* + \alpha_t^* \gamma_{t-1}^{*2} \in [\tilde{\beta}_{\min}, \tilde{\beta}_{\max}] \frac{\eta_t}{\eta_{t-1}}$. Since $\delta(x)$ is a monotone function in x , there exists an $\bar{\beta} \in [\tilde{\beta}_{\min}, \tilde{\beta}_{\max}]$, such that $\delta(\bar{\beta}) = A \times \sqrt{\frac{1}{M} \sum_{k=1}^M \mathbb{E}_t^{\mathbb{Q}}(h_{t+k}^*)}$ (i.e., true value of VIX), and $\Delta = |\delta(\bar{\beta}) - \delta(\tilde{\beta})|$, then we have $\Delta \leq \delta(\tilde{\beta}_{\max}) - \delta(\tilde{\beta}_{\min})$. Note that $\delta(x)$ can be expressed in terms of $a_1(\eta_t, M, \sigma^2)$ and $a_2(\eta_t, M, \sigma^2)$. \square

A.4 Proof of Lemma 2

Lemma A.2 (Full Version of Lemma 2). *In the predetermined case with path $\bar{\eta}_{t,M}$, the conditional MGF for future cumulative returns has the following exponentially affine form:*

$$g_{t,M}(s | \bar{\eta}_{t,M}) = \mathbb{E}_t^{\mathbb{Q}}(\exp(s \sum_{\tau=t+1}^T R_\tau)) = \exp(A_T(s, M) + B_T(s, M) h_{t+1}^*),$$

where $M = T - t$, $A_T(s, m)$ and $B_T(s, m)$ are recursively given by

$$A_T(s, m+1) = A_T(s, m) + sr + B_T(s, m) \omega_{T-m}^* - \frac{1}{2} \log(1 - 2\alpha_{T-m}^* B_T(s, m)), \quad (\text{A.7})$$

$$B_T(s, m+1) = s(\gamma_{T-m-1}^* - \frac{1}{2}) - \frac{1}{2} \gamma_{T-m-1}^{*2} + \beta_{T-m}^* B_T(s, m) + \frac{(s - \gamma_{T-m-1}^*)^2}{2(1 - 2\alpha_{T-m}^* B_T(s, m))}, \quad (\text{A.8})$$

with initial values $A_T(s, 1) = sr$ and $B_T(s, 1) = \frac{1}{2}(s^2 - s)$, where all terms in (A.7) and (A.8) are predetermined.

Proof. For later use, we note that the MGF for (R_{t+1}, h_{t+2}^*) is given by

$$\begin{aligned} \mathbb{E}_t^{\mathbb{Q}}(\exp(sR_{t+1} + uh_{t+2}^*)) &= \exp\left[sr + u\omega_{t+1}^* - \frac{1}{2}\log(1 - 2u\alpha_{t+1}^*) \right. \\ &\quad \left. + \left(s(\gamma_t^* - \frac{1}{2}) + u\beta_{t+1}^* - \frac{1}{2}\gamma_t^{*2} + \frac{(s-\gamma_t^*)^2}{2(1-2u\alpha_{t+1}^*)} \right) h_{t+1}^* \right], \end{aligned} \quad (\text{A.9})$$

where we used Theorem 1. Next, we will establish the exponentially affine form,

$$\mathbb{E}_t^{\mathbb{Q}}(\exp(s \sum_{\tau=t+1}^T R_{\tau})) = \exp(A_T(s, M) + B_T(s, M)h_{t+1}^*)$$

where $M = T - t$. This is proven by backwards induction. First, for $t = T - 1$ we have

$$\mathbb{E}_{T-1}^{\mathbb{Q}}(\exp(sR_T)) = \exp[sr + \frac{1}{2}(s^2 - s)h_T^*].$$

So $A_T(s, 1) = sr$ and $B_T(s, 1) = \frac{1}{2}(s^2 - s)$ define the initial values for A_T and B_T . Next, we establish the recursions for A_T and B_T , by showing that the exponentially affine form holds for $t = T - m$, whenever it holds for $t = T - (m - 1)$. Thus, consider

$$\begin{aligned} \mathbb{E}_{T-m}^{\mathbb{Q}} \left[\exp \left(s \sum_{\tau=T-m+1}^T R_{\tau} \right) \right] &= \mathbb{E}_{T-m}^{\mathbb{Q}} \left[\exp \left(sR_{T-m+1} + s \sum_{\tau=T-m+2}^T R_{\tau} \right) \right] \\ &= \mathbb{E}_{T-m}^{\mathbb{Q}} \left[\mathbb{E}_{T-m+1}^{\mathbb{Q}} \left[\exp \left(sR_{T-m+1} + s \sum_{\tau=T-m+2}^T R_{\tau} \right) \right] \right] \\ &= \mathbb{E}_{T-m}^{\mathbb{Q}} \left[\exp(sR_{T-m+1}) \mathbb{E}_{T-m+1}^{\mathbb{Q}} \left(s \sum_{\tau=T-m+2}^T R_{\tau} \right) \right] \\ &= \mathbb{E}_{T-m}^{\mathbb{Q}} [\exp(sR_{T-m+1} + A_T(s, m-1) + B_T(s, m-1)h_{T-m+2}^*)]. \end{aligned}$$

Now substitute $B_T(s, m - 1)$ for u in (A.9) with $t = T - m$. The exponentially affine form now follows if we set

$$\begin{aligned} A_T(s, m) &= A_T(s, m - 1) + sr + B_T(s, m - 1)\omega_{T-m+1}^* - \frac{1}{2}\log(1 - 2\alpha_{T-m+1}^*B_T(s, m - 1)), \\ B_T(s, m) &= s(\gamma_{T-m}^* - \frac{1}{2}) - \frac{1}{2}\gamma_{T-m}^{*2} + \beta_{T-m+1}^*B_T(s, m - 1) + \frac{(s-\gamma_{T-m}^*)^2}{2(1-2\alpha_{T-m+1}^*B_T(s, m-1))}. \end{aligned}$$

There are some interesting differences between the new expressions and the original expressions. Our expressions for $A_T(s, m)$ and $B_T(s, m)$ depend s (the argument of the MGF) and

m (days to maturity), but unlike the original expressions it also depends on T (the maturity date). The reason is that the coefficients, ω^* , α^* , β^* , and γ^* , are time-varying under \mathbb{Q} due to their relation to η_t . \square

A.5 Proof of Theorem 3

Let $\boldsymbol{\eta}_{t,M} = (\log \eta_{t+1}, \dots, \log \eta_{t+M})'$ and $\bar{\boldsymbol{\eta}}_{t,M}^e = \mathbb{E}_t^{\mathbb{Q}}(\boldsymbol{\eta}_{t,M})$ which embeds the expected path of $\log \eta_t$. The MGF for M -period cumulative returns $R_{t,M}$ can be expressed as

$$g_{t,M}(s) \equiv \mathbb{E}_t^{\mathbb{Q}}[\exp(sR_{t,M})] = \mathbb{E}_t^{\mathbb{Q}}\{\mathbb{E}_t^{\mathbb{Q}}[\exp(sR_{t,T}) \mid \boldsymbol{\eta}_{t,M}]\} = \mathbb{E}_t^{\mathbb{Q}}[f(\boldsymbol{\eta}_{t,M})],$$

where $f(\boldsymbol{\eta}_{t,M}) \equiv \mathbb{E}_t^{\mathbb{Q}}[\exp(sR_{t,T}) \mid \boldsymbol{\eta}_{t,M}]$. A second-order Taylor expansion of $f(\boldsymbol{\eta}_{t,M})$ around $\bar{\boldsymbol{\eta}}_{t,M}^e$ gives us,

$$\begin{aligned} f(\boldsymbol{\eta}_{t,M}) &\approx f(\bar{\boldsymbol{\eta}}_{t,M}^e) + \nabla'(\boldsymbol{\eta}_{t,M} - \bar{\boldsymbol{\eta}}_{t,M}^e) + \frac{1}{2}(\boldsymbol{\eta}_{t,M} - \bar{\boldsymbol{\eta}}_{t,M}^e)' \tilde{H}_{t,M}(s)(\boldsymbol{\eta}_{t,M} - \bar{\boldsymbol{\eta}}_{t,M}^e) \\ &= f(\bar{\boldsymbol{\eta}}_{t,M}^e) + \nabla'(\boldsymbol{\eta}_{t,M} - \bar{\boldsymbol{\eta}}_{t,M}^e) + \frac{1}{2} \text{tr} \left\{ \tilde{H}_{t,M}(s) \boldsymbol{\varepsilon}_{t,M} \boldsymbol{\varepsilon}_{t,M}' \right\}, \end{aligned}$$

where

$$\tilde{H}_{t,M}(s) = \frac{\partial^2 f(\boldsymbol{\eta}_{t,M})}{\partial \boldsymbol{\eta}_{t,M} \partial \boldsymbol{\eta}_{t,M}'} \bigg|_{\boldsymbol{\eta}_{t,M} = \bar{\boldsymbol{\eta}}_{t,M}^e}$$

is the Hessian, ∇ is the Jacobian, and $\boldsymbol{\varepsilon}_{t,M} = \boldsymbol{\eta}_{t,M} - \bar{\boldsymbol{\eta}}_{t,M}^e$. Since $\bar{\boldsymbol{\eta}}_{t,M}^e \in \mathcal{G}_t$ and $f(\bar{\boldsymbol{\eta}}_{t,M}^e) = g_{t,M}(s \mid \bar{\boldsymbol{\eta}}_{t,M}^e)$, by taking conditional expectations on both sides, we arrive

$$g_{t,M}(s) \approx g_{t,M}(s \mid \bar{\boldsymbol{\eta}}_{t,M}^e) + \frac{1}{2} \text{tr} \left\{ \tilde{H}_{t,M}(s) \Sigma_M \right\},$$

where $\Sigma_M = \mathbb{E}_t^{\mathbb{Q}}[\boldsymbol{\varepsilon}_{t,M} \boldsymbol{\varepsilon}_{t,M}']$. From the AR(1) structure it follows that the m -th element of $\boldsymbol{\varepsilon}_{t,M}$ is given by, $[\boldsymbol{\varepsilon}_{t,M}]_m = \log \eta_{t+m} - \mathbb{E}_t^{\mathbb{Q}} \log \eta_{t+m} = \sum_{j=0}^{m-1} \varphi^j \varepsilon_{t+m-j}$, $m = 1, \dots, M$, such that

$$\Sigma_M = \text{var}_t^{\mathbb{Q}} \left[\boldsymbol{\eta}_{t,M} - \bar{\boldsymbol{\eta}}_{t,M}^e \right] = \text{var}_t^{\mathbb{Q}} (A_M \boldsymbol{\varepsilon}_{t,M}) = \sigma^2 A_M A_M',$$

where

$$[A_M]_{i,j} = \begin{cases} \varphi^{i-j} & \text{for } i \geq j \\ 0 & \text{otherwise.} \end{cases}$$

The results above is for the AR(1) case. With an ARMA structure, $\varphi(L) (\log \eta_t - \zeta) =$

$\theta(L)\varepsilon_t$, we have

$$\log \eta_t - \zeta = \frac{\theta(L)}{\varphi(L)}\varepsilon_t = \sum_{j=0}^{\infty} \psi_j \varepsilon_{t-j},$$

such that

$$[\varepsilon_{t,M}]_m = \log \eta_{t+m} - \mathbb{E} \log \eta_{t+m} = \sum_{j=0}^{m-1} \psi_j \varepsilon_{t+m-j} = \sum_{j=1}^m \psi_{m-j} \varepsilon_{t+j}.$$

So in the more general ARMA case we have

$$[A_M]_{i,j} = \begin{cases} \psi_{i-j} & \text{for } i \geq j \\ 0 & \text{otherwise.} \end{cases}$$

After obtaining the analytical approximated MGF, the closed-form formula for the price of a European call option can be simply adapted from [Heston and Nandi \(2000\)](#).

A.5.1 The Hessian Matrix $\tilde{H}_{t,M}(s)$

First, to simplify the notations, we suppress the dependence on T and s for most terms and write,

$$\begin{aligned} \omega_m &\equiv \omega_{T-m}^* = \omega \eta_{T-m}, \\ \alpha_m &\equiv \alpha_{T-m}^* = \alpha \eta_{T-m} \eta_{T-m-1}, \\ \beta_m &\equiv \beta_{T-m}^* = \beta \eta_{T-m} / \eta_{T-m-1}, \\ \gamma_m &\equiv \gamma_{T-m-1}^* = (\gamma + \lambda - \frac{1}{2}) / \eta_{T-m-1} + \frac{1}{2}, \end{aligned}$$

and $A(M) \equiv A_T(s, M)$, $B(M) \equiv B_T(s, M)$. For derivatives of a variable Y we write

$$Y^{(i)} \equiv \frac{\partial Y}{\partial \log \eta_{t+i}} \quad \text{and} \quad Y^{(i,j)} \equiv \frac{\partial^2 Y}{\partial \log \eta_{t+i} \partial \log \eta_{t+j}}.$$

From [Theorem 2](#), we have $f(\boldsymbol{\eta}_{t,M}) = \exp [A(M) + B(M)h_{t+1}^*]$ with first and second derivatives given by

$$f^{(i)} = f(\boldsymbol{\eta}_{t,M})[A^{(i)}(M) + B^{(i)}(M)h_{t+1}^*],$$

and

$$\begin{aligned} f^{(i,j)} &= f(\boldsymbol{\eta}_{t,M})[A^{(i)}(M) + B^{(i)}(M)h_{t+1}^*][A^{(j)}(M) + B^{(j)}(M)h_{t+1}^*] \\ &\quad + f(\boldsymbol{\eta}_{t,M})[A^{(i,j)}(M) + B^{(i,j)}(M)h_{t+1}^*], \end{aligned}$$

respectively. From the expression for $A(M)$ and $B(M)$ in Theorem 2, we find (for the first derivatives)

$$A^{(i)}(m+1) = A^{(i)}(m) + \omega_m^{(i)} B(m) + \omega_m B^{(i)}(m) + \frac{\alpha_m^{(i)} B(m) + \alpha_m B^{(i)}(m)}{1 - 2\alpha_m B(m)}, \quad (\text{A.10})$$

$$\begin{aligned} B^{(i)}(m+1) &= (s - \gamma_m) \gamma_m^{(i)} + \beta_m B^{(i)}(m) + \beta_m^{(i)} B(m) \\ &\quad + (s - \gamma_m)^2 \frac{\alpha_m^{(i)} B(m) + \alpha_m B^{(i)}(m)}{[1 - 2\alpha_m B(m)]^2} + (\gamma_m - s) \frac{\gamma_m^{(i)}}{[1 - 2\alpha_m B(m)]}, \end{aligned} \quad (\text{A.11})$$

with $A^{(i)}(1) = B^{(i)}(1) = 0$. Similarly, for the second derivatives we find

$$\begin{aligned} A^{(i,j)}(m+1) &= A^{(i,j)}(m) + \omega_m^{(i,j)} B(m) + \omega_m^{(i)} B^{(j)}(m) + B^{(i)}(m) \omega_m^{(j)} + \omega_m B^{(i,j)}(m) \\ &\quad + \frac{1}{[1 - 2\alpha_m B(m)]} \left(\alpha_m^{(i,j)} B(m) + \alpha_m^{(i)} B^{(j)}(m) + B^{(i)}(m) \alpha_m^{(j)} + \alpha_m B^{(i,j)}(m) \right) \\ &\quad + \frac{2}{[1 - 2\alpha_m B(m)]^2} \left(\alpha_m^{(i)} B(m) + \alpha_m B^{(i)}(m) \right) \left(\alpha_m^{(j)} B(m) + \alpha_m B^{(j)}(m) \right), \\ B^{(i,j)}(m+1) &= \beta_m^{(i,j)} B(m) + \beta_m^{(i)} B^{(j)}(m) + B^{(i)}(m) \beta_m^{(j)} + \beta_m B^{(i,j)}(m) \\ &\quad + \frac{2\alpha_m B(m)}{[1 - 2\alpha_m B(m)]} \left[\gamma_m^{(i)} \gamma_m^{(j)} + (\gamma_m - s) \gamma_m^{(i,j)} \right] \\ &\quad + \frac{2(\gamma_m - s)}{[1 - 2\alpha_m B(m)]^2} \left[\left(\alpha_m^{(i)} B(m) + \alpha_m B^{(i)}(m) \right) \gamma_m^{(j)} + \gamma_m^{(i)} \left(\alpha_m^{(j)} B(m) + \alpha_m B^{(j)}(m) \right) \right] \\ &\quad + \frac{(s - \gamma_m)^2}{[1 - 2\alpha_m B(m)]^2} \left(\alpha_m^{(i,j)} B(m) + \alpha_m^{(i)} B^{(j)}(m) + B^{(i)}(m) \alpha_m^{(j)} + \alpha_m B^{(i,j)}(m) \right) \\ &\quad + \frac{4(s - \gamma_m)^2}{[1 - 2\alpha_m B(m)]^3} \left(\alpha_m^{(i)} B(m) + \alpha_m B^{(i)}(m) \right) \left(\alpha_m^{(j)} B(m) + \alpha_m B^{(j)}(m) \right), \end{aligned}$$

with $A^{(i,j)}(1) = B^{(i,j)}(1) = 0$ and

$$\begin{aligned} \omega_m^{(i)} &= \begin{cases} \omega_m & \text{for } i = M - m, \\ 0 & \text{otherwise,} \end{cases} \quad \alpha_m^{(i)} = \begin{cases} \alpha_m & \text{for } i = M - m, M - m - 1, \\ 0 & \text{otherwise,} \end{cases}, \\ \beta_m^{(i)} &= \begin{cases} \beta_m & \text{for } i = M - m \\ -\beta_m & \text{for } i = M - m - 1, \\ 0 & \text{otherwise,} \end{cases} \quad \gamma_m^{(i)} = \begin{cases} \frac{1}{2} - \gamma_m & \text{for } i = M - m - 1, \\ 0 & \text{otherwise,} \end{cases}, \\ \omega_m^{(i,j)} &= \begin{cases} \omega_m & \text{for } i = j = M - m \\ 0 & \text{otherwise,} \end{cases}, \quad \alpha_m^{(i,j)} = \begin{cases} \alpha_m & \text{for } i, j = M - m, M - m - 1, \\ 0 & \text{otherwise,} \end{cases}, \end{aligned}$$

$$\beta_m^{(i,j)} = \begin{cases} \beta_m & \text{for } i = j \in \{M - m, M - m - 1\} \\ -\beta_m & \text{for } i \neq j \in \{M - m, M - m - 1\}, \\ 0 & \text{otherwise,} \end{cases} \quad \gamma_m^{(i,j)} = \begin{cases} \gamma_m - \frac{1}{2} & \text{for } i = j = M - m - 1 \\ 0 & \text{otherwise.} \end{cases}$$

Finally, the scaled Hessian matrix presented in Theorem 3 is defined by $H_{t,M}(s) = \frac{1}{g_{t,M}(s|\bar{\eta}_{t,M}^e)} \tilde{H}_{t,M}(s)$.

We adopt his formulation because it simplifies the expression.

A.6 Proof of Theorem 4

Next we prove Theorem 4 that enables us to computing moments from the moment-generating function. The k -th moment of cumulative returns can be expressed as

$$\mathbb{E}(R^k) = \int_{-\infty}^{+\infty} R^k f(R) dR = \underbrace{\int_{-\infty}^0 R^k f(R) dR}_{(*)} + \underbrace{\int_0^{+\infty} R^k f(R) dR}_{(**)}$$

where $f(R)$ is the conditional density of cumulated returns under \mathbb{Q} . By the Fourier inverse transform (FIT), $f(R)$ can be expressed as

$$f(R) = \frac{1}{\pi} \int_0^{\infty} \operatorname{Re} \left[e^{-uR} \phi(u) \right] du_I, \quad \phi(u) \equiv \mathbb{E} \left[e^{uR} \right],$$

where $u = u_R + iu_I \in \mathbb{C}$, with $u_R = \operatorname{Re}[u]$ being the real part of u , and $\phi(u)$ is the MGF of cumulated returns. Note that different from traditional Fourier inverse transform based on characteristic function, such form FIT requires the existence of MGF.

Then after changing the order of integration by Fubini's theorem, we find

$$\begin{aligned} (*) &= \frac{1}{\pi} \int_0^{\infty} \operatorname{Re} \left[\left(\int_{-\infty}^0 R^k e^{-uR} dR \right) \phi(u) \right] du_I, \\ (**) &= \frac{1}{\pi} \int_0^{\infty} \operatorname{Re} \left[\left(\int_0^{+\infty} R^k e^{-vR} dR \right) \phi(v) \right] dv_I. \end{aligned}$$

We have here used the following Laplace transformations for R^k :

$$\begin{aligned} \int_{-\infty}^0 R^k e^{-uR} dR &= -\frac{k!}{u^{k+1}}, \quad u_R < 0, \\ \int_0^{+\infty} R^k e^{-vR} dR &= \frac{k!}{v^{k+1}}, \quad v_R > 0. \end{aligned}$$

Thus, it follows that

$$\begin{aligned} (*) &= \frac{1}{\pi} \int_0^\infty \operatorname{Re} \left[-\frac{k!}{u^{k+1}} \phi(u) \right] du_I, \\ (**) &= \frac{1}{\pi} \int_0^\infty \operatorname{Re} \left[\frac{k!}{v^{k+1}} \phi(v) \right] dv_I. \end{aligned}$$

More general results for moment deduced by integrating the moment-generating function can be found in [Hansen and Tong \(2024\)](#).

A.7 Proof of Theorem 5

We observe N_t derivative prices at time t , resulting in the vector of pricing error, $e_t \in \mathbb{R}^{N_t \times 1}$.

So, the derivative with respect to $\log \eta_t$ is

$$\begin{aligned} \nabla_t &\equiv \frac{\partial \ell(X_t | \mathcal{G}_t)}{\partial \log \eta_t} = -\frac{1}{2\sigma_e^2} \frac{\partial (e_t' \Omega_{N_t}^{-1} e_t)}{\partial \log \eta_t} = -\frac{1}{2\sigma_e^2} \frac{\partial (e_t' \Omega_{N_t}^{-1} e_t)}{\partial e_t'} \frac{\partial e_t}{\partial \log \eta_t} \\ &= -\frac{1}{\sigma_e^2} e_t' \Omega_{N_t}^{-1} \frac{\partial e_t}{\partial \log \eta_t} = \frac{1}{\sigma_e^2} \left(\frac{\partial X_t^m}{\partial \log \eta_t} \right)' \Omega_{N_t}^{-1} e_t, \end{aligned}$$

such that

$$\mathbb{E}^{\mathbb{P}}[\nabla_t^2 | \mathcal{G}_t] = \frac{1}{\sigma_e^2} \left(\frac{\partial X_t^m}{\partial \log \eta_t} \right)' \Omega_{N_t}^{-1} \left(\frac{\partial X_t^m}{\partial \log \eta_t} \right).$$

In the special case with a single derivative price, $N_t = 1$, our expressions simplify to

$$\nabla_t = \frac{1}{\sigma_e^2} (X_t - X_t^m) \frac{\partial X_t^m}{\partial \log \eta_t} \quad \text{and} \quad \mathbb{E}^{\mathbb{P}}[\nabla_t^2 | \mathcal{G}_t] = \frac{1}{\sigma_e^2} \left(\frac{\partial X_t^m}{\partial \log \eta_t} \right)^2,$$

such that $s_t = \frac{1}{\sigma_e} (X_t - X_t^m) \operatorname{sign} \left(\frac{\partial X_t^m}{\partial \log \eta_t} \right)$.

A.7.1 The Distribution of the Score

Define

$$\psi_t' = \frac{1}{\sigma_e^2} \left(\frac{\partial X_t^m}{\partial \log \eta_t} \right)' \Omega_{N_t}^{-1}, \quad \Sigma_{N_t} = \sigma_e^2 \Omega_{N_t}.$$

Recall that ψ_t' is \mathcal{G}_t -measurable, then under Assumption 4 where $e_t | \mathcal{G}_t \sim iid N(0, \Sigma_{N_t})$, the conditional MGF of score s_t can be expressed as

$$\mathbb{E}_t^{\mathbb{P}}[\exp(us_t)] = \mathbb{E}_t^{\mathbb{P}} \left[\exp \left(u \frac{\psi_t' e_t}{\sqrt{\psi_t' \Sigma_{N_t} \psi_t}} \right) \right] = \exp \left(\frac{1}{2} \frac{u \psi_t'}{\sqrt{\psi_t' \Sigma_{N_t} \psi_t}} \Sigma_{N_t} \frac{u \psi_t}{\sqrt{\psi_t' \Sigma_{N_t} \psi_t}} \right) = \exp \left(\frac{1}{2} u^2 \right).$$

Therefore, the scaled score, s_t , is iid with a standard normal distribution under \mathbb{P} .

To derive the distribution under \mathbb{Q} , we first obtain,

$$\begin{aligned}
& \mathbb{E}_t^{\mathbb{P}} [\exp (us_t + \phi_t R_{t+1} + \xi_t h_{t+2})] \\
&= \mathbb{E}_t^{\mathbb{P}} \left\{ \mathbb{E}_t^{\mathbb{P}} [\exp (us_t + \phi_t R_{t+1} + \xi_t h_{t+2}) | \phi_t R_{t+1}, \xi_t h_{t+2}] \right\} \\
&= \mathbb{E}_t^{\mathbb{P}} \left\{ \mathbb{E}_t^{\mathbb{P}} \left[\exp \left(\frac{1}{2} u^2 + \phi_t R_{t+1} + \xi_t h_{t+2} \right) | \phi_t R_{t+1}, \xi_t h_{t+2} \right] \right\} \\
&= \exp \left(\frac{1}{2} u^2 \right) \mathbb{E}_t^{\mathbb{P}} [\exp (\phi_t R_{t+1} + \xi_t h_{t+2})],
\end{aligned}$$

where the last equality is a consequence of e_t being assumed to be independent of any return shock. Then, we directly have

$$\mathbb{E}_t^{\mathbb{Q}} (\exp (us_t)) = \frac{\mathbb{E}_t^{\mathbb{P}} [\exp (us_t + \phi_t R_{t+1} + \xi_t h_{t+2})]}{\mathbb{E}_t^{\mathbb{P}} [\exp (\phi_t R_{t+1} + \xi_t h_{t+2})]} = \exp \left(\frac{1}{2} u^2 \right),$$

which shows that the score, s_t , is also iid and distributed as a standard normal under \mathbb{Q} .

A.8 The Scores for Derivatives

A.8.1 Score for VIX

The simplest case to drive the score for is $X_t = \log \text{VIX}_t$, where $N_t = 1$. The log-likelihood function for $\ell(\text{VIX}_t | \mathcal{G}_t)$ is here given by

$$\ell(\text{VIX}_t | \mathcal{G}_t) = -\frac{1}{2\sigma_e^2} (\log \text{VIX}_t - \log \text{VIX}_t^m)^2,$$

and its first derivative is,

$$\nabla_t = \frac{1}{\sigma_e^2} (\log \text{VIX}_t - \log \text{VIX}_t^m) \left(\frac{\partial \log \text{VIX}_t^m}{\partial \log \eta_t} \right).$$

The conditional variance of ∇_t is

$$\mathbb{E}^{\mathbb{P}} [\nabla_t^2 | \mathcal{G}_t] = \frac{1}{\sigma_e^2} \left(\frac{\partial \log \text{VIX}_t^m}{\partial \log \eta_t} \right)^2,$$

and it follows that

$$s_t = \frac{1}{\sigma_e} (\log \text{VIX}_t - \log \text{VIX}_t^m) \text{sign} \left(\frac{\partial \log \text{VIX}_t^m}{\partial \log \eta_t} \right).$$

For the last term, we recall the expression, $\text{VIX}_t^m = \sqrt{a_1 (M, \sigma^2) + a_2 (M, \sigma^2) h_{t+1}^*}$, which leads to

$$\frac{\partial \log \text{VIX}_t^m}{\partial \log \eta_t} = \frac{1}{2 (\text{VIX}_t^m)^2} \left[\frac{\partial a_{1,t}}{\partial \log \eta_t} + \left(\frac{\partial a_{2,t}}{\partial \log \eta_t} + a_{2,t} \right) h_{t+1}^* \right]$$

with

$$\frac{\partial a_1(M, \sigma^2)}{\partial \log \eta_t} = \frac{A^2}{M} \sum_{k=2}^M \sum_{i=2}^k \tilde{\beta}^{k-i} \left[\omega \mathbb{E}_t^{\mathbb{Q}}(\eta_{t+k-1}) B_{k-1,1} + \alpha \mathbb{E}_t^{\mathbb{Q}}(\eta_{t+k-1} \eta_{t+i-2}) (B_{k-1,1} + B_{i-2,1}) \right]$$

and

$$\frac{\partial a_2(M, \sigma^2)}{\partial \log \eta_t} + a_2(M, \sigma^2) = \frac{A^2}{M} \sum_{k=1}^M \tilde{\beta}^{k-1} \mathbb{E}_t^{\mathbb{Q}} \left(\frac{\eta_{t+k-1}}{\eta_t} \right) B_{k-1,1}$$

Therefore, according to recursive formula for $B_{k,i}$ in (A.6), they are all positive if all φ_i are positive for $i = 1, \dots, p$. The term, $\text{sign} \left(\frac{\partial \log \text{VIX}_t^m}{\partial \log \eta_t} \right)$, is therefore redundant and we arrived at the simple expression,

$$s_t = \frac{1}{\sigma_e} (\log \text{VIX}_t - \log \text{VIX}_t^m).$$

By Assumption 4 it follows that s_t is iid standard normally distributed.

A.8.2 Score for Option Prices

When the model is estimated with option prices, the elements of $X_t \in \mathbb{R}^{N_t \times 1}$ are given by $\log(\text{IV}_{bs}(C_t, S_t, M, K, r))$, for the N_t options selected at time t . The logarithm of Black-Scholes implied volatility makes this variable comparable to $\log \text{VIX}_t$, which is used when the model is estimated with VIX data.

Let X_t^m denote the logarithm of model-based implied volatility for a particular option. We seek an expression for

$$\frac{\partial X_t^m}{\partial \log \eta_t} = \frac{\partial \log(\text{IV}_{bs}^m)}{\partial \text{IV}_{bs}^m} \frac{\partial \text{IV}_{bs}^m}{\partial C_t^m} \frac{\partial C_t^m}{\partial \log \eta_t} = \frac{1}{\text{IV}_{bs}^m \cdot \text{Vega}_{bs}^m} \frac{\partial C_t^m}{\partial \log \eta_t},$$

where

$$\text{Vega}_{bs} = \frac{1}{\sqrt{2\pi}} \exp\left(-\frac{1}{2}d_t^2\right) S_t \sqrt{M},$$

is the Black-Scholes implied Vega and

$$d_t = \frac{1}{\text{IV}_{bs} \sqrt{M}} \left[\log\left(\frac{S_t}{K}\right) + \left(r + \frac{\text{IV}_{bs}^2}{2}\right) M \right].$$

For $\partial \hat{C}^m / \partial \log \eta_t$, we find

$$\frac{\partial \hat{C}^m(S_t, M, K, r; h_{t+1}^*)}{\partial \log \eta_t} = S_t \frac{\partial P_{1,t}}{\partial \log \eta_t} - K \exp(-rM) \frac{\partial P_{2,t}}{\partial \log \eta_t},$$

where

$$\begin{aligned} \frac{\partial P_{1,t}}{\partial \log \eta_t} &= \frac{\exp(-rM)}{\pi} \int_0^\infty \operatorname{Re} \left[\frac{K^{-iu}}{iu S_t} \frac{\partial \hat{g}_{t,M}(iu+1)}{\partial \log \eta_t} \right] du, \\ \frac{\partial P_{2,t}}{\partial \log \eta_t} &= \frac{1}{\pi} \int_0^\infty \operatorname{Re} \left[\frac{K^{-iu}}{iu} \frac{\partial \hat{g}_{t,M}(iu)}{\partial \log \eta_t} \right] du, \end{aligned}$$

with

$$\hat{g}_{t,M}(s) = g_{t,M}(s | \bar{\boldsymbol{\eta}}_{t,M}^e) \left[1 + \frac{1}{2} \operatorname{tr} (H_{t,M}(s) \Sigma_M) \right].$$

Using the simplified notations in Section A.5.1, we have

$$\frac{\partial \hat{g}_{t,M}(s)}{\partial \log \eta_t} = \hat{g}_{t,M}(s) \left(A^{(0)}(M) + \left(B^{(0)}(M) + B(M) \right) h_{t+1}^* \right) + \frac{1}{2} g_{t,M} \left(s | \bar{\boldsymbol{\eta}}_{t,M}^e \right) \operatorname{tr} \left(\dot{H}_{t,M}(s) \Sigma_M \right), \quad (\text{A.12})$$

which is the expression we use to price options with the second-order approximation. Pricing options with first-order approximation, amounts to dropping the last term in (A.12). With a first-order approximation, we simply need to compute $A^{(0)}(m)$ and $B^{(0)}(m)$, that are given recursively from (A.10) and (A.11), with initial condition $\dot{A}(1) = \dot{B}(1) = 0$, and use

$$\begin{aligned} \omega_m &= \omega \Psi_t(M - m + 1), \\ \alpha_m &= \alpha \Psi_t(M - m + 1) \Psi_t(M - m), \\ \beta_m &= \beta \Psi_t(M - m + 1) / \Psi_t(M - m), \\ \gamma_m &= (\gamma + \lambda - \frac{1}{2}) / \Psi_t(M - m) + \frac{1}{2}, \end{aligned}$$

where $\Psi_t(k)$ is defined as

$$\Psi_t(k) = \exp \{ \mathbb{E}_t (\log \eta_{t+k-1}) \} = \exp \left\{ \left(1 - \varphi^{k-1} \right) \zeta + \varphi^{k-1} \log \eta_t \right\}.$$

The corresponding first derivatives (with respect to $\log \eta_t$) are given by

$$\begin{aligned}\dot{\omega}_m &= \omega_m \varphi^{M-m}, \\ \dot{\alpha}_m &= \alpha_m \left(\varphi^{M-m} + \varphi^{M-m-1} \right), \\ \dot{\beta}_m &= \beta_m \left(\varphi^{M-m} - \varphi^{M-m-1} \right), \\ \dot{\gamma}_m &= \left(\frac{1}{2} - \gamma_m \right) \varphi^{M-m-1}.\end{aligned}$$

For the second-order approximation in (A.12), we need to evaluate $\dot{H}_{t,M}(s) = \partial H_{t,M}(s) / \partial \log \eta_t$, for which we have

$$\begin{aligned}\dot{H}_{i,j} &= \left(A^{(i,0)}(M) + B^{(i,0)}(M) h_{t+1}^* \right) \left(A^{(j)}(M) + B^{(j)}(M) h_{t+1}^* \right) \\ &+ \left(A^{(i)}(M) + B^{(i)}(M) h_{t+1}^* \right) \left(\dot{A}^{(j)}(M) + \dot{B}^{(j)}(M) h_{t+1}^* \right) \\ &+ \left(A^{(i,j,0)}(M) + B^{(i,j,0)}(M) h_{t+1}^* \right).\end{aligned}$$

The expressions for the third derivatives, $A^{(i,j,0)}(m) = \partial A^{(i,j,0)}(m) / \partial \log \eta_t$ and $B^{(i,j,0)}(m) = \partial B^{(i,j,0)}(m) / \partial \log \eta_t$ are relatively cumbersome, and are omitted to conserve space.

We now have all the terms needed for the analytical formula for $\partial C^m / \partial \log \eta_t$. In practice, however, it may be more convenient to compute this derivative with numerical methods, i.e.

$$\frac{\partial C_t^m}{\partial \log \eta_t} \approx \frac{1}{\Delta} [C_t^m(\log \eta_t + \Delta) - C_t^m(\log \eta_t)],$$

for a very small value of Δ , because this simplifies the calculation of score with respect to option prices, and is very fast.

When the number of daily available option prices, N_t , is large, computing the derivatives $\partial \log IV_{t,i}^m / \partial \log \eta_t$ for $i = 1, 2, \dots, N_t$ becomes very time-consuming. In this case, one could assume that $\partial \log IV_{t,i}^m / \partial \log \eta_t \approx \chi_t > 0$ (which is only t -dependent), such that the scaled score s_t , defined by (9) and Theorem 5, is approximated by

$$s_t^{\text{appro}} = \frac{1}{\sigma_e} \frac{\iota'_{N_t} \Omega_{N_t}^{-1} e_t}{\sqrt{\iota'_{N_t} \Omega_{N_t}^{-1} \iota_{N_t}}}$$

where ι_{N_t} is a $N_t \times 1$ vector of ones. With this approximation, there is no need to compute any derivatives. In our empirical analysis, we find the correlation between s_t^{appro} and the true s_t reaches up to 99.11%, such that the correlation between η_t^{appro} and the true η_t is 99.98%.

A.9 Computation of Option Prices by Numerical Integrations

Our expression for option prices in Theorem 2 requires the evaluation of integrals of the type, $\int_0^\infty f(x)dx$, for the computation of $P_1(t)$ and $P_2(t)$. For this, we use the Gauss-Laguerre quadrature method, which is an extension of the Gaussian quadrature method for approximating the value of integrals of the following kind:

$$\int_0^\infty e^{-x}g(x)dx \approx \sum_{i=1}^L w(x_i)g(x_i).$$

The Gauss-Laguerre quadrature method is also based the abscissae x_1, \dots, x_L and their associated weights $w(x_i)$ with $i = 1, \dots, L$, leading to the following numerical approximation,

$$\int_0^\infty f(x)dx = \int_0^\infty e^{-x}[e^x f(x)]dx \approx \sum_{i=1}^L w(x_i)e^{x_i} f(x_i).$$

In our implementation we use $L = 32$.

Online Appendix

S.1 Alternative RMSE Measure

An alternative metric for evaluation the derivative pricing is to compute the RMSE in volatility levels. For the VIX this is defined by

$$\text{RMSE}_{\text{VIX}} = \sqrt{\frac{1}{T} \sum_{t=1}^T [\text{VIX}_t^m - \text{VIX}_t]^2}, \quad (\text{S.1})$$

and for option prices it is defined by

$$\text{RMSE}_{\text{IV}} = \sqrt{\frac{1}{\sum_{t=1}^T N_t} \sum_{t=1}^T \sum_{i=1}^{N_t} [\text{IV}_{t,i}^m - \text{IV}_{t,i}]^2} \times 100. \quad (\text{S.2})$$

The results for the RMSE in volatility levels are reported in Tables S.1 and S.2, where the former is analogous to Table 4 and the latter is analogous to the out-of-sample results in Table 5. The results are qualitatively very similar to the RMSE for logarithmically transformed volatilities in Tables 4 and 5.

S.2 A Variance Risk Ratio based on Model-Free Realized Variances

As a robustness check, we compute an alternative monthly measure of the VRR, $\tilde{\eta} = \frac{\text{VIX}^2}{\sigma_{\mathbb{P}}^2}$, where $\sigma_{\mathbb{P}}^2$ is an empirical measure of the expected variance under \mathbb{P} , deduced from monthly realized variances. So, $\sigma_{\mathbb{P}}^2$ does not rely on the Heston-Nandi GARCH model. The monthly realized variance for the S&P 500 index is computed as the sum of the squared daily close-to-close log returns within the same month. This quantity is multiplied by 12×100^2 to bring it to the same scale as the VIX^2 (squared annualized percentage). Finally, $\sigma_{\mathbb{P}}^2$ is defined to be the one-month ahead prediction of the monthly realized variance using a AR(1) model.

This time-series of this empirical VRR is presented in Figure S.1, and it is very similar to the model-based time-series presented in Figure 5.

Figure S.2 contains scatterplots of one-month-ahead volatility prediction errors under \mathbb{P} and the level of $\log \eta$. The former is defined as the difference between the ex-post model-implied variance and the ex-ante model-based one-month ahead volatility prediction. The scatterplots indicate some positive correlation, but we do not find that a large proportion of overpredictions of volatility occurs when $\log \eta_t$ is relatively small, nor that a large proportion

Table S.1: VIX and Option Pricing Performance (RMSE)

Model	CHNG [VIX]	CHNG [Opt]	DHNG [VIX]	DHNG [Opt]
<i>A: RMSE for VIX Pricing</i>				
Full Sample	4.117	4.143	1.024	1.795
<i>B: RMSE for Option Pricing</i>				
Full Sample	4.277	4.151	2.327	1.746
<i>Partitioned by moneyness</i>				
Delta<0.3	4.500	4.149	3.108	1.947
0.3≤Delta<0.4	4.069	3.985	2.830	1.859
0.4≤Delta<0.5	3.743	3.862	2.415	1.639
0.5≤Delta<0.6	3.798	3.999	2.033	1.444
0.6≤Delta<0.7	4.017	4.062	1.876	1.455
0.7≤Delta	4.771	4.417	2.098	1.949
<i>Partitioned by maturity</i>				
DTM<30	4.649	4.110	2.385	2.252
30≤DTM<60	4.235	4.058	2.061	1.475
60≤DTM<90	4.065	4.086	2.156	1.311
90≤DTM<120	4.059	4.234	2.492	1.598
120≤DTM<150	4.073	4.212	2.623	1.781
150≤DTM	4.192	4.537	2.757	1.819
<i>Partitioned by the level of VIX</i>				
VIX<15	3.726	3.727	1.821	1.155
15≤VIX<20	2.980	3.252	2.051	1.438
20≤VIX<25	3.711	3.808	2.265	1.718
25≤VIX<30	4.525	4.266	2.703	2.126
30≤VIX<35	5.460	5.227	3.071	2.444
35≤VIX	10.68	9.164	4.727	4.089

Note: This table reports the in-sample VIX and option pricing performance for each model in Table 3. We evaluate the model's option pricing ability through the root of mean square errors of implied volatility ($RMSE_{IV}$). We summarize the results by option moneyness, maturity and market VIX level. Moneyness is measured by Delta computed from the Black-Scholes model. DTM denotes the number of calendar days to maturity.

Table S.2: Out-of-sample VIX and Option Pricing (RMSE)

Model	CHNG [VIX]	CHNG [Opt]	DHNG [VIX]	DHNG [Opt]
<i>A: RMSE for VIX Pricing</i>				
Full Sample	5.083	4.660	1.278	2.067
<i>B: RMSE for Option Pricing</i>				
Full Sample	4.710	4.043	2.724	1.932
<i>Partitioned by moneyness</i>				
Delta<0.3	4.973	4.068	3.839	2.108
0.3≤Delta<0.4	4.622	3.910	3.467	2.018
0.4≤Delta<0.5	4.255	3.709	2.849	1.701
0.5≤Delta<0.6	4.339	3.907	2.281	1.508
0.6≤Delta<0.7	4.696	4.108	2.021	1.635
0.7≤Delta	4.934	4.213	2.202	2.195
<i>Partitioned by maturity</i>				
DTM<30	5.276	4.243	2.858	2.301
30≤DTM<60	4.692	3.968	2.526	1.591
60≤DTM<90	4.217	3.794	2.547	1.524
90≤DTM<120	4.317	4.013	2.758	1.818
120≤DTM<150	4.133	3.870	2.941	2.157
150≤DTM	4.263	4.182	2.965	2.117
<i>Partitioned by the level of VIX</i>				
VIX<15	4.062	3.121	2.003	1.257
15≤VIX<20	3.081	3.060	2.403	1.531
20≤VIX<25	3.026	3.537	2.615	1.714
25≤VIX<30	4.073	3.902	3.169	2.287
30≤VIX<35	5.352	4.856	3.688	2.719
35≤VIX	12.05	9.423	5.199	4.376

Note: This table reports the out-of-sample option pricing performance for each model. We conduct our out-of-sample performance evaluation by splitting our original dataset into two subsamples: the in-sample data consists of the years before 2008 and the out-of-sample consists of the years 2008–2021, which spans a 14-year period. The estimation for each model is done only once for the in-sample data, and then price the out-of-sample data by the estimated parameters. Therefore, the in-sample data is 1990–2007. We evaluate the model’s option pricing ability through the root of mean square errors of implied volatility (IVRMSE). We summarize the results by option moneyness, maturity and market VIX level. Moneyness is measured by Delta computed from the Black-Scholes model. DTM denotes the number of calendar days to maturity.

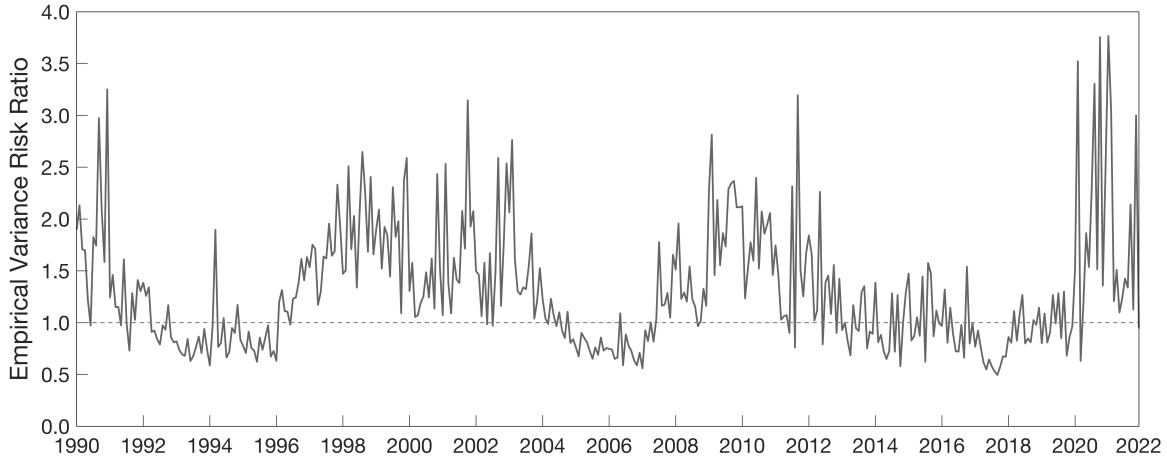


Figure S.1: An empirical monthly variance risk ratio, defined as the ratio of VIX_t^2 and the predicted value of the monthly realized variance using an AR(1) model.

Alt text: Time series of the empirical monthly variance risk ratio, calculated as the ratio of VIX squared to the predicted monthly realized variance, where the prediction is based on a simple first-order autoregressive model.

of underpredictions of volatility occurs when $\log \eta_t$ is large.

S.3 Empirical Results for Auxiliary Structure (Predetermined VRR)

While the Auxiliary structure does not constitute a coherent option pricing model, we can estimate the parameters. We should not expect all parameters to be consistent, because the auxiliary structure employs an option pricing that poorly approximates the true formula, as shown in Table 1. The parameter estimates of the Auxiliary structure are shown in Table S.3, where we also include those of the DHNG model, for comparison. Most parameter estimates are very similar, with the important exception with the intercept in the score-driven model for $\log \eta_t$. This can be seen from the estimate of $\zeta = \mathbb{E}(\log \eta_t)$, which is substantially larger for the Auxiliary structure than the DHNG model. The reason is simple that the Auxiliary structure needs an upwards biased value of η_t to compensate for the shortcomings of its option pricing formula, that neglects the random variations in η_t . So, by inflating the model-implied value of η_t , the Auxiliary structure is able to reduce option pricing errors, which is part of the objective in the estimation problem.

The option pricing performance for the Auxiliary structure is shown in Table S.4, where

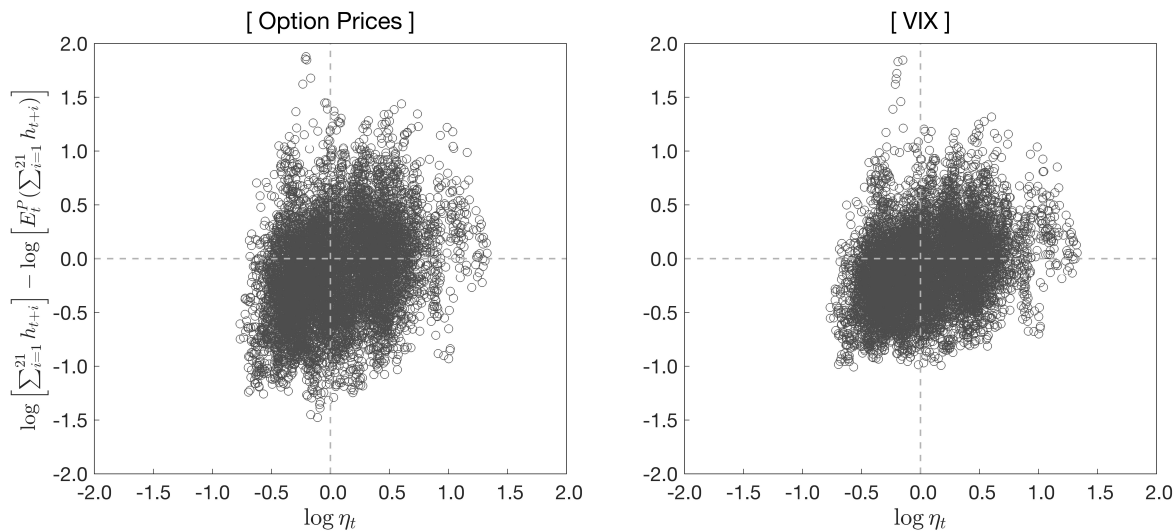


Figure S.2: Volatility prediction errors for one-month ahead predictions plotted against the variance risk ratio. Based on the DHNG model estimated with option prices (left panel) and VIX (right panel).

Alt text: Volatility prediction errors for one-month-ahead forecasts plotted against the variance risk ratio. Predictions are based on the DHNG model estimated using either option prices or VIX data.

we, for the sake of comparison, include the results for the DHNG model. We evaluate the derivative pricing in terms of the RMSE for both the logarithmically transformed implied volatility (the first two columns) and the level of implied volatility (the last two columns). Interestingly, the Auxiliary structure only results in slightly larger pricing errors than the DHNG model. This can be ascribed to the adaptive nature of the score-driven model, which shifts $\log \eta_t$ to a higher level to compensate for errors embedded in the Auxiliary pricing formulae. Thus, while the first-order approximation is insufficient, the estimated score-drive model “rescues” the Auxiliary structure, by inflating the variance risk ratio above its true value.

S.4 Supplementary Material for Table 6

Table S.3: Estimation Results for Auxiliary and DHNG

Model	Auxiliary (1st-order) [Opt]	DHNG (2nd-order) [Opt]
λ	3.080 (0.588)	3.088 (0.644)
β	0.587 (0.023)	0.570 (0.015)
$\alpha(\times 10^{-6})$	5.783 (0.389)	5.833 (0.256)
γ	248.08 (12.52)	249.59 (10.28)
ζ	0.227 (0.012)	0.102 (0.011)
φ	0.994 (0.003)	0.994 (0.001)
σ	0.046 (0.008)	0.042 (0.010)
ρ	0.114 (0.015)	0.087 (0.010)
σ_e	0.090 (0.006)	0.091 (0.006)
$\mathbb{E}\eta$	1.362	1.190
$\widehat{\text{var}}(s_t)$	1.010	1.007
$\pi^{\mathbb{P}}$	0.945	0.934
$\pi^{\mathbb{Q}}$	0.956	0.944
LogL		
$\ell(\text{R})$	26,413	26,419
$\ell(\text{VIX})$	7,828	7,932
$\ell(\text{Opt})$	36,534	36,682
$\ell(\text{R}, \text{VIX})$	34,241	34,351
$\ell(\text{R}, \text{Opt})$	62,947	63,101

Note: Estimation results based on option prices for the Auxiliary structure and the DHNG model using the full sample period, January 1990 to December 2021. Estimates are reported with robust standard errors (in parentheses), and $\pi^{\mathbb{P}}$ and $\pi^{\mathbb{Q}}$ refer to the persistence of volatility under \mathbb{P} and \mathbb{Q} , respectively. The last five rows report the components of the maximized log-likelihood function.

Table S.4: Pricing Performance for Auxiliary and DHNG

Model	Errors in Log-Difference		Errors in Level-Difference	
	Auxiliary (1st-order) [Opt]	DHNG (2nd-order) [Opt]	Auxiliary (1st-order) [Opt]	DHNG (2nd-order) [Opt]
<i>A: RMSE for VIX Pricing</i>				
Full Sample	9.164	9.049	1.804	1.795
<i>B: RMSE for Option Pricing</i>				
Full Sample	9.241	9.191	1.767	1.746
<i>Partitioned by moneyness</i>				
Delta<0.3	12.63	12.77	1.961	1.947
0.3≤Delta<0.4	11.33	11.28	1.880	1.859
0.4≤Delta<0.5	9.496	9.375	1.670	1.639
0.5≤Delta<0.6	7.385	7.271	1.467	1.444
0.6≤Delta<0.7	6.925	6.859	1.468	1.455
0.7≤Delta	8.746	8.634	1.981	1.949
<i>Partitioned by maturity</i>				
DTM<30	12.30	12.19	2.284	2.252
30≤DTM<60	7.969	7.848	1.500	1.475
60≤DTM<90	6.892	6.914	1.312	1.311
90≤DTM<120	7.898	7.963	1.604	1.598
120≤DTM<150	8.556	8.622	1.792	1.781
150≤DTM	9.265	9.226	1.862	1.819
<i>Partitioned by the level of VIX</i>				
VIX<15	10.04	10.02	1.160	1.155
15≤VIX<20	9.062	9.021	1.450	1.438
20≤VIX<25	8.288	8.224	1.739	1.718
25≤VIX<30	8.613	8.518	2.155	2.126
30≤VIX<35	8.593	8.542	2.464	2.444
35≤VIX	9.661	9.508	4.172	4.089

Note: This table reports the in-sample VIX and option pricing performance for the Auxiliary structure and DHNG. The pricing performance is evaluated in terms of the RMSEs of logarithmically transformed VIX/implied volatility (the first two columns) and the levels of VIX/implied volatilities (last two columns). For option pricing the performance is also show for different ranges of moneyness, DTM, and the level of VIX level.

